UAB

Universitat Autònoma de Barcelona

Development and application of innovative point-of-care biosensing platforms

Amadeo Sena Torralba

PhD Thesis

PhD in Biotechnology

Directors:

Prof. Arben Merkoçi and Dr. Ruslan Álvarez

Department of Chemical, Biological and Environmental Engineering

Chemical Engineering Faculty

2020

The present work entitled "Development and application of innovative point-of-care biosensing platforms", presented by Amadeo Sena Torralba to obtain the degree of doctor by the Universitat Autònoma de Barcelona, was performed at the Nanobioelectronics and Biosensors Group at the Institut Català de Nanociencia i Nanotecnología (ICN2), under the supervision of Prof. Arben Merkoçi, ICREA Professor and Group Leader, and Dr. Ruslan Álvarez.

Bellaterra, July 2020

The supervisors

Prof. Arben Merkoçi Hyka   Dr. Ruslan Álvarez Diduk

The present Thesis was performed also under the doctoral program studies "Doctorado en Biotecnología" at the Faculty of Chemical Engineering, Universitat Autònoma de Barcelona, under the tutorship of Professor Francesc Godia.

The University tutor

Prof. Francesc Godia Casablancas

"I am among those who think that science has great beauty. A scientist in his laboratory is not only a technician: he is also a child placed before natural phenomena which impress him like a fairy tale."

— **Marie Skłodowska-Curie**

The research work accomplished, resulted in several publications and manuscripts that were submitted to international peer-reviewed scientific journals.

The state-of-the art studies carried out resulted in two reviews not yet published:

Parolo, C.; Sena-Torralba, A.; Bergua, J.F.; *et al.* "Development of a nanoparticle-based lateral flow immunoassay: detection of Human Immunoglobulin G as model target." *Accepted in Nature Protocols* (2020).

Sena-Torralba, A.; Álvarez-Diduk, R.; Merkoçi, A. "Towards next generation lateral flow biosensors." *In preparation* (2020).

The experimental work performed conducted to one patent submission, one publication and two articles not yet published:

Sena-Torralba, A.; Álvarez-Diduk, R.; Merkoçi, A. "Bioensayo lateral-electroforético." European patent request nº EP19382648.4 (2019) – work related to Chapter 3.

Sena-Torralba, A.; Álvarez-Diduk, R.; Torné-Morató, H.; *et al.* "Paper-based Electrophoretic Bioassay: biosensing in whole blood operating via smartphone." *Submitted to Science Advances* (2020) – work related to Chapter 3.

Sena-Torralba, A.; Ba Ngo, D.; Parolo, C.; *et al.* "Lateral flow assay modified with time-delay wax barriers as a sensitivity and signal enhancement strategy." *Re-submitted to Biosensors and bioelectronics* (2020) – work related to Chapter 4.

Amin, N.; Sena-Torralba, A.; Álvarez-Diduk, R.; *et al.* "Lab in a Tube: Point-of-Care detection of *Escherichia coli*." *Anal. Chem.* 92(6), 4209-4216 (2020) – work related to Chapter 5.

In this section I would like to thank all the people that has accompanied me during the PhD. Those who have served as inspiration. Those who have helped to achieve my goals. Those, who always trusted my abilities as a researcher. Above all, those who have made me enjoy this very vibrant stage of my life, the one I will never forget.

No podría empezar esta sección si no fuera hablando de ella, mi confidente, mi compañera de viaje, Natalia. Las palabras se quedan cortas para expresar lo que siento por ti. Tú has vivido el día a día de mi doctorado, sufriendo igual que yo cuando las cosas no iban bien y alegrándote con cada uno de mis logros. Gracias por ese continuo apoyo moral, vivir contigo durante estos últimos años me ha hecho sentir que tenía una vida plena. Nos esperan por delante los años más bonitos de nuestras vidas, sigamos creciendo juntos y disfrutando el uno del otro.

Qué decir de vosotros, Papá y Mamá. Me habéis dado todos los recursos para llegar a ser la persona que soy ahora. Si tengo valores es gracias a vosotros, si tengo ambición es gracias a vosotros. No solo me habéis ayudado a dedicarme a lo que más me gusta, sino que me habéis empujado a querer ser el mejor. Sentir que estáis tan orgullosos de mí me da la vida. Muchas gracias también a mi hermana. Nos hemos cuidado mutuamente durante esta etapa en Barcelona. Siento que tenemos un vínculo muy especial. Espero que volvamos a estar muy cerca el uno del otro. Dale duro a la carrera que lo bueno está por llegar.

Seguidamente quiero dar las gracias al Prof. Merkoçi mi co-director de tesis, para mi Arben, porque considero que eres un jefe cercano. Siempre estas preocupándote por los miembros de tu grupo; creas un ambiente muy familiar y eso hace que la gente se sienta como en casa. Te tengo mucho cariño porque siempre me has dado alas para probar mis ideas, para disfrutar de la ciencia y eso me ha hecho ser muy feliz. Me has protegido y comprendido cuando más lo necesitaba y lo más importante, me has hecho sentirme especial, valioso. Si alguna vez tengo la oportunidad de dirigir un grupo, seguiré todo lo que he aprendido de ti durante estos años, ya que sin lugar a duda esa la clave del éxito. Espero que nuestros caminos se vuelvan a encontrar, ya que aún me queda mucho por aprender.

También quiero agradecer al Dr. Ruslan Álvarez-Diduk, mi co-director de tesis. Cuánto me has enseñado estos años…te debo tanto. Mijo, te tengo un cariño inmenso, este camino no hubiera sido ni por asomo igual sin ti. Qué agradecido estoy de que hayamos

trabajado juntos para sacar los proyectos adelante. Vales por las ideas tan increíbles que tienes, y es que no miento si digo que con cada idea tuya el grupo saca un paper y/o una patente. Vales mucho, aprovecha esa capacidad que tienes de innovar para hacer cosas grandes.

Y si hay alguien al que también se le caen las ideas de los bolsillos, ese no es otro que el Dr. Claudio Parolo. Tienes alma de líder, tienes ideas brillantes y tienes un corazón que no te cabe en el pecho. Eres un gran científico, espero verte dirigiendo un grupo pronto, porque vales para eso y porque te lo has ganado a pulso. He disfrutado mucho trabajando contigo y sobre todo me has enseñado muchísimo.

Además quiero agradecer profundamente al Dr. Alfredo de la Escosura, la persona que me hizo mi primera "entrevista de trabajo", quien me fichó para entrar en el grupo del Prof. Merkoçi. Pues no ha llovido desde entonces…. Has sido partícipe de uno de los momentos más alegres de mi vida, cuando después de meses esperando, me llamaste para proponerme hacer el doctorado en vuestro grupo. Siempre tendré la espinita de no haber podido disfrutar de ti más tiempo. Me alegra que hayamos mantenido el contacto, tengo la sensación de que algún día volveremos a trabajar juntos.

Jose Fran, Enric y Dani, que bien nos lo hemos pasado estos años. Me pasan por la cabeza mil anécdotas al escribir estos agradecimientos, la mayoría de ellas no serian apropiadas de explicar aquí. Jose Fran, tú y yo empezamos este camino juntos. Hemos trabajado muy duro durante el doctorado, con presión, cargados de responsabilidades. Hemos pasado por momentos difíciles juntos y siempre hemos demostrado tener agallas y mucha fortaleza mental. También hemos sabido disfrutar de la experiencia, nos hemos dejado llevar y lo hemos dado todo. Gracias por todos los consejos que me has ido dando, creo que hemos aprendido mucho el uno del otro. Siempre guardaré buen recuerdo de nuestras peripecias por Taiwán y Huesca, que por cierto con razón puedes sentirte orgulloso de una tierra tan bonita y con tanto encanto. Volveré siempre que pueda. Enric, mi compañero de despacho, mi buen amigo. No te imaginas cuanto de menos te estoy echando. Hemos conectado muchísimo. Contigo me he llegado a reír tanto que me ha acabado doliendo la tripa. Tenemos una forma muy parecida de ver la vida. Ojalá seas feliz por muchos años junto a esa persona tan especial. Los dos sois un tesoro. Siempre nos quedará Barry White y Pluto. Mi querido Dani, no he conocido a persona tan buena como tú. Si me pude adaptar tan rápido al grupo fue gracias a ti.

Fuiste un padre para Jose Fran y para mí, nos inculcaste los valores del grupo, sin duda has sido un escalón fundamental para mi desarrollo como investigador y como persona. También nos lo hemos pasado genial en el lab y en el despacho. Mi primer artículo publicado es contigo, es algo que nos va a unir para siempre. Alex, sabes que te quiero mucho a pesar de ser un madridista empedernido. Al igual que con Enric, eres alguien con el que he conectado mucho durante estos años. Tenemos infinidad de historias y anécdotas juntos. Ese viaje a Granada marcó un antes y un después en nuestra relación. Siento que si últimamente nos veíamos poco, ahora nos veremos menos aún. Pero espero y deseo que hagamos el esfuerzo por mantener la relación. Anna, podría decir que eres el pilar que sostiene al grupo, pero para mí eres mucho más que todo eso. Me he reído muchísimo contigo, también "lloramos" juntos la despedida de Alfredo. Estos años han dado para muchas vivencias compartidas, como el viaje a Valencia, Asturias o las partidas de Básquet. Xavi, Guillem y tú formáis una familia preciosa. Estáis más que invitados a Valencia. Marc, ets un moniato valencià o que? Muchas gracias por los buenos momentos vividos. Te deseo la mejor de las suertes con tus tintas. Espero que nos podamos seguir viendo.

I'm thankful for all the people I've meet in Nanobioelectronics and Biosensors group. To Luis Pires, for helping me so much as co-supervisor of my Master's thesis. You are a really special guy. Pablo Guardia, pasamos momentos muy divertidos en el ICN2. Me quedo con todos los consejos que me diste, la mayoría ya han sido muy útiles durante la tesis. Hassan, I really enjoyed playing football with you. You are an excellent person and probably the most motivated Liverpool supporter. Jie Liu, Nopchulee and Dee you are completely crazy! Thank you so much for those funny moments in Barcelona and Taiwan. You are both doing an excellent job as assistant professors. Hope we can meet soon. Denise and Maddalena, the first Italians I meet in the group. I enjoyed spending time with you in the lab and taking some beers. Denise I always remember your beautiful smile, Maddalena, I will never forget Alfredo's farewell party where we laughed and danced a lot. Gina, que momentos más buenos pasamos juntos en el lab. Siempre que voy a cenar al pendejo me acuerdo de ti. Compartimos la pasión por la ciencia y por Luis Miguel. Juan, también he compartido momentos únicos contigo. Ese viaje a Granada se quedará por muchos años en nuestra memoría. Espero que el PhD te esté yendo de lujo, eres un tío muy inteligente, aprovéchalo. Alba, mi primera alumna

de TFG. Fue un gran reto supervisor a alguien en mi primer año de doctorado, pero he decir que me lo pusiste fácil, con tus ganas de trabajar y tu felicidad.

My dear friends Bernardo, Alex Müller, Anna T., Caterina, I spent with you the one of the best years in my life. Bernardo, we worked very hard together in our experiments and we also had time to talk and laugh. Hope to see you this summer in Palermo. Alex Müller, you are a really special person, I would need two more lives in order to meet again someone like you. You were the push that I required to start developing the paper-electrophoretic bioassay. We had a lot of fun together with Enric in the lab. Your song, Pluto, still serves as inspiration for Enric and me when things go wrong. Anna T. we share the passion for Reggaeton music and we had a lot of fun with Caterina at Copetin club. Caterina you are a super sweet girl, thank you so much for the nice time we spent together. Mohga and Niloufar, my two girls. We did a very nice team working together. I learnt a lot from both of you, I really hope that I can meet you again. Duy, Oguz and Mr. *sex symbol* Panácek, I spent very nice moments with you during these last months. Duy, something sure is that I will see you again soon. You are an excellent person; I want people like you in my life. We worked super hard till the last day and finally we achieved to finish the work. Señor Salvador, you are a gentleman. We had lot of fun in the office.

I'm also really thankful to my Chinese team, Lei, Qiuyue and Liming. You are the next generation of PhD students after Jose Fran and me. Keep fighting hard to achieve your objectives. Lei, it has been a pleasure to support you during your recovery. You are a very nice man. Qiuyue, I'm really in love with your name's meaning. Thank you for always coming to work with a big smile. Liming, you are a very disciplined PhD student and very hard worker. I'm sure that you will achieve excellent publications. Celia, me hizo mucha ilusión saber que harías el PhD en el grupo. Desde que empezaste no has parado de trabajar, eres una curranta cómo yo. Disfruta mucho de esta etapa, me ha encantado conocerte. Marrugo, que lástima que has llegado justo cuando me iba, nos lo hubiéramos pasado genial. ¡Eres mi parse! Disfruta mucho de la compañía de Enric en el despacho y mucho ánimo con la tesis. Queda pendiente salir a bailar bachata por Barna. Andrea, you are a super nice guy, an excellent researcher and above all an outstanding calciatore. It's a shame we haven't had time to work together. Enjoy your stay in the group. Lourdes, Dani siempre me habló maravillas de ti, de cómo le apadrinaste en el grupo. Es una lástima no haber podido coincidir más tiempo. Me

pierdo la oportunidad de trabajar junto a una gran científica y persona. Giulio, since you arrived you are doing great things for the group. You are with no doubts a great researcher. Thank you for helping me with my projects and I wish you a great future in Barcelona. Emily, I also wish you a great future, hope you can achieve great publications in the group. You are a very nice person.

I should also thank all the support from the NACANCELL Project partners. Starting with Carlos, who is an extremely good guy and has been an excellent colleague during the project. We spent very nice moments in the project meetings. Hope I can see you again soon. Eivind, Jean-Jacques and Ronan, you have proved to be the best hosts. I will never forget the trip along the fiords or the beautiful bus trip through Bordeaux. You have done an excellent work for the project and hope we can continue this nice collaboration for many years. Moreover, this thesis is dedicated to the memory of Prof. Carmen de Torres and Dag Bremnes, who passed away during the project period. Science has lost two great scientists and people. We will always remember you.

Finally, I will like to thank the support and hospitality of Prof. Akon Higuchi, Sophie and his lovely group members, Vito, Kevin, and Didi. I spent an amazing summer in Taiwan. Please come to visit Jose and me in Spain. We will be eternally grateful for the love with which you treated us. Durante mi estancia en Taiwán, conocí a una persona muy especial, con un gran corazón, que me ha ayudado mucho a superarme cómo persona. Vero, gracias por haberte esforzado en mantener el contacto conmigo. Me acuerdo muchas veces de las conversaciones que teníamos, fuiste un gran apoyo esos dos meses.

Por último, no quiero acabar esta sección sin agradecer a mi familia, tanto a la de mi padre como a la de mi madre, todo el cariño incondicional que me tienen. Ahora que vuelvo a Valencia me gustaría disfrutar más tiempo con vosotros. Durante esta etapa fuera de casa, he aprendido que la familia lo es todo. También quiero agradecer a mi familia de Castellón, la cual lleva ocho años cuidándome y queriéndome como uno más. Alex y Cris, me abristeis las puertas de vuestra casa de par en par, eso ya dice mucho de la clase de personas que sois. Paqui y Tica, os he cogido un cariño…gracias por cuidarme tanto. Por último Vicente, que orgulloso debes estar de mí. Gracias por preguntarme siempre a cerca de mis proyectos, hubiera sido capaz de traducirte toda la

tesis al castellano para que la hubieses leído. Me encantaba escuchar las historias de tu vida. Nos volveremos a encontrar allá donde estés. Protégenos y cuídanos, te queremos.

ALP	Alkaline Phosphatase
AgNPs	Silver Nanoparticles
A.U.	Arbitrary Units
AuNCs	Gold Nanoclusters
AuNPs	Gold Nanoparticles
BSA	Bovine Serum Albumin
BB	Borate Buffer
BWAs	Biowarfare Agents
CdSe@ZnS QDs	Cadmium Selenide/Zinc Sulfide Quantum Dots
CEA	Carcinoembryonic Antigen
CFU	Colony-forming Unit
CL	Control Line
CdTe QDs	Cadmium Telluride Quantum Dots
CNTs	Carbon-nanotubes
DC	Direct Current
DNA	Deoxyribonucleic Acid
DTNB	5,5'-dithiobis-(2-nitrobenzoic acid)
E	Electric Field Strength
E. coli	*Escherichia coli*
ELISA	Enzyme-linked Immunosorbent Assay
et al.	*et alia* (and others)
FDA	Food and Drug Administration
Fig.	Figure
FOBS	Fiber-optic Biosensors

FRET	Förster Resonance Energy Transfer
GAT	Gold Aggregation Test
GMP	Good Manufacturing Practices
G-QDs	Graphene Quantum Dots
$HAuCl_4$	Tetrachloroauric (III) Acid
H_3BO_3	Boric Acid
hCG	human Chorionic Gonadotropin
HIgG	Human Immunoglobulin G
HRP	Horseradish Peroxidase
ICP	Inductively Coupled Plasma
IgG	Immunoglobulin G
ISO	International Organization of Standardization
ITP	Isotachophoresis
IUPAC	International Union of Pure and Applied Chemistry
KCl	Potassium Chloride
KDa	Kilodaltons (molecular weight)
LDW	Laser Direct Writing
LED	Light-emitting Diode
LFAs	Lateral Flow Assays
LFIA	Lateral Flow Immunoassay
LOD	Limit of Detection
LOQ	Limit of Quantification
μ	Particle Mobility
miRNAs	micro-RNA

MPQ	Magnetic particle quantification
MWCNTs	Multi-walled Carbon Nanotubes
MWCO	Molecular Weight Cut-off
NaCl	Sodium Chloride
NaOH	Sodium Hydroxide
NaH_2PO_4	Sodium Phosphate
NIR	Near-Infrared Radiation
NPs	Nanoparticles
N-S-doped	Nitrogen and Sulfur Doped
OD	Optical Density
OTG	On The Go
OVA	Ovalbumin
PA	Photoacoustic
PB	Phosphate Buffer Non-saline
PBS	Phosphate Buffer Saline
PCL	Polycaprolactone
PCR	Polymerase Chain Reaction
PEB	Paper-based Electrophoretic Bioassay
PES	Polyester
pH	Power of Hydrogen
P.L.	Photoluminescence
PoC	Point-of-Care
POCTs	Point-of-Care Tests
PSA	Prostate Specific Antigen

PVDF	Polyvinylidene Fluoride
QCM	Quartz Crystal Microbalance
QDs	Quantum Dots
r	Correlation Coefficient
R&D	Research and Development
RNA	Ribonucleic Acid
RPA	Recombinase Polymerase Amplification
SAW	Surface Acoustic wave
SB	Sodium Borate
SD	Standard Deviation
SDS	Sodium Dodecyl Sulfate
SELEX	Systematic Evolution of Ligands by Exponential Enrichment
SEM	Scanning Electron Microscopy
SERS	Surface-enhanced Raman Scattering
SPR	Surface Plasmon Resonance
SSC	Saline-Sodium Citrate
ssDNA	Single-stranded DNA
TCA	Trichloroacetic Acid
TCA	Thermal Contrast Amplification
TEM	Transmission Electron Microscopy
TL	Test Line
TMB	3,3',5,5'-tetramethylbenzidine
UCNPs	Upconverting Nanoparticles

USD	United States Dollar
UV	Ultraviolet
WHO	World Health Organization
Ø	Diameter
2D	2-dimensional
3D	3-dimensional

THESIS OVERVIEW

This thesis is divided in five chapters followed by a general conclusions section. A brief explanation of each chapter is given below:

Chapter 1. Introduction. This chapter starts with a general introduction to the concepts of biosensors and point-of-care biosensing. Then, the focus is given to one of the most successful point-of-care tests: the lateral flow assay. Key aspects of the assay such as components and reagents, fabrication and operation procedures are deeply covered (Fig. 0.1). The chapter continues with an analysis of the challenges that LFA has been facing, concluding with a review of the most relevant LFA improvements reported within the last years.
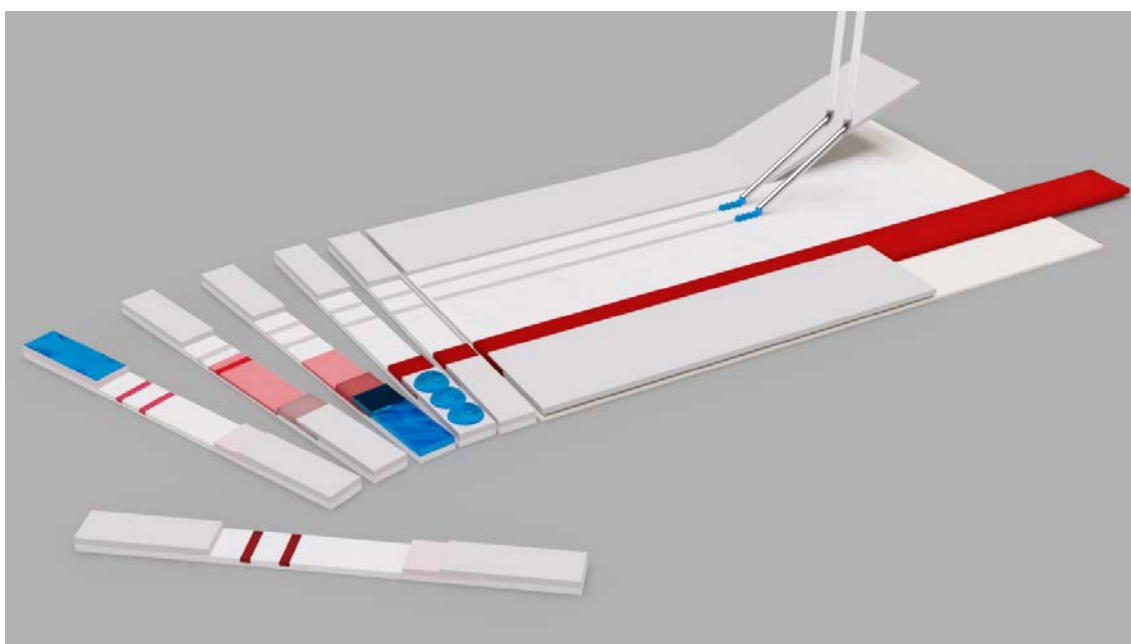
Fig. 0.1. Graphical abstract of the work: Parolo, C.; Sena-Torralba, A.; Bergua, J.F.; et al. "Development of a nanoparticle-based lateral flow immunoassay: detection of Human Immunoglobulin G as model target." Accepted in *Nature Protocols* (2020). Figure courtesy of PhD. Ruslan Álvarez-Diduk.

Chapter 2. Objectives of the thesis. This chapter briefly describes the objectives that motivated this work.

Chapter 3. Paper-based Electrophoretic Bioassay (PEB): biosensing in whole blood operating via smartphone. This chapter presents a new sensing platform that combines the key characteristics of a lateral flow assay (LFA), the most widely used point-of-care

test, with the sample treatment capabilities of electrophoresis. In particular, the ability of PEB to separate different types of particles and to detect human antibodies in untreated blood samples is demonstrated. Finally, in order to make the platform deployable at the point of care, PEB is coupled with a smartphone that controls the electrophoresis and reads the optical signal generated (Fig. 0.2).
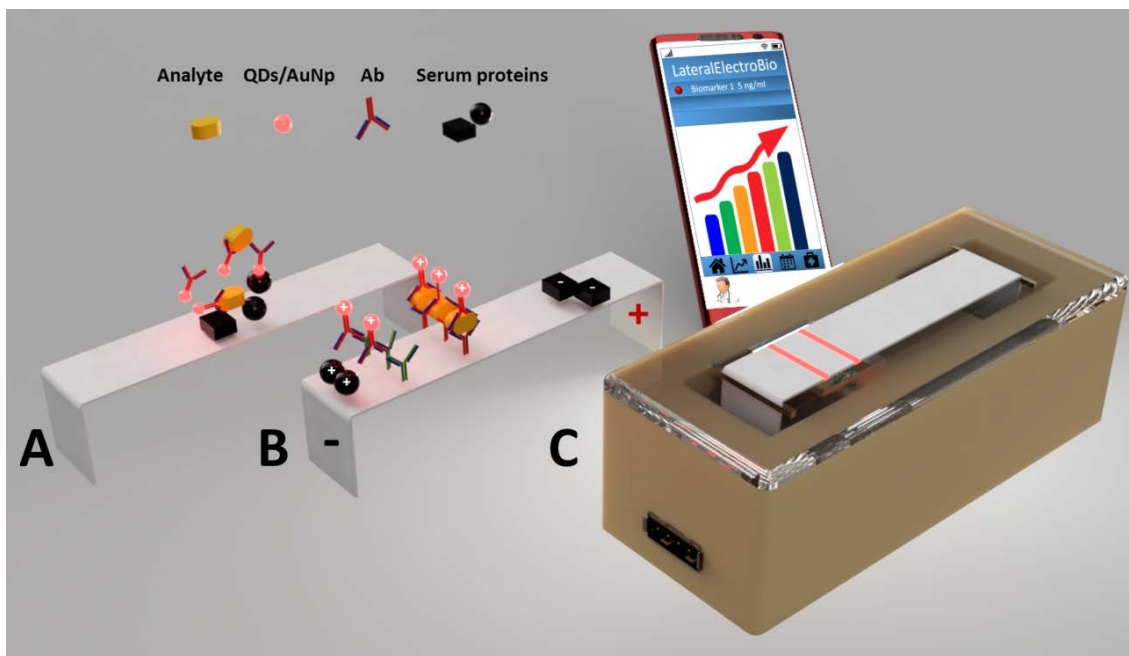
Fig. 0.2. Graphical abstract of the work: Sena-Torralba, A.; Álvarez-Diduk, R.; Parolo, C.; *et al.* "Paper-based Electrophoretic Bioassay: biosensing in whole blood operating via smartphone." Submitted to *Science Advances* (2020) and Sena-Torralba, A.; Álvarez-Diduk, R.; Merkoçi, A. "Bioensayo lateral-electroforético." European patent request nᵒ EP19382648.4 (2019). Figure courtesy of PhD. Ruslan Álvarez-Diduk.

Chapter 4. Lateral flow assay modified with time-delay wax barriers as a sensitivity and signal enhancement strategy. In this chapter is shown a simple and low-cost strategy to improve the analytical performance of LFAs. By the use of soluble wax barriers, the target and label nanoparticles are temporarily accumulated on top of the test line (TL). This extended internal incubation step promotes the formation of the immune-complex, generating a 2.8-fold sensitivity enhancement and up to 96% signal enhancement compared to the conventional LFA for Human IgG (H-IgG) detection (Fig. 0.3).
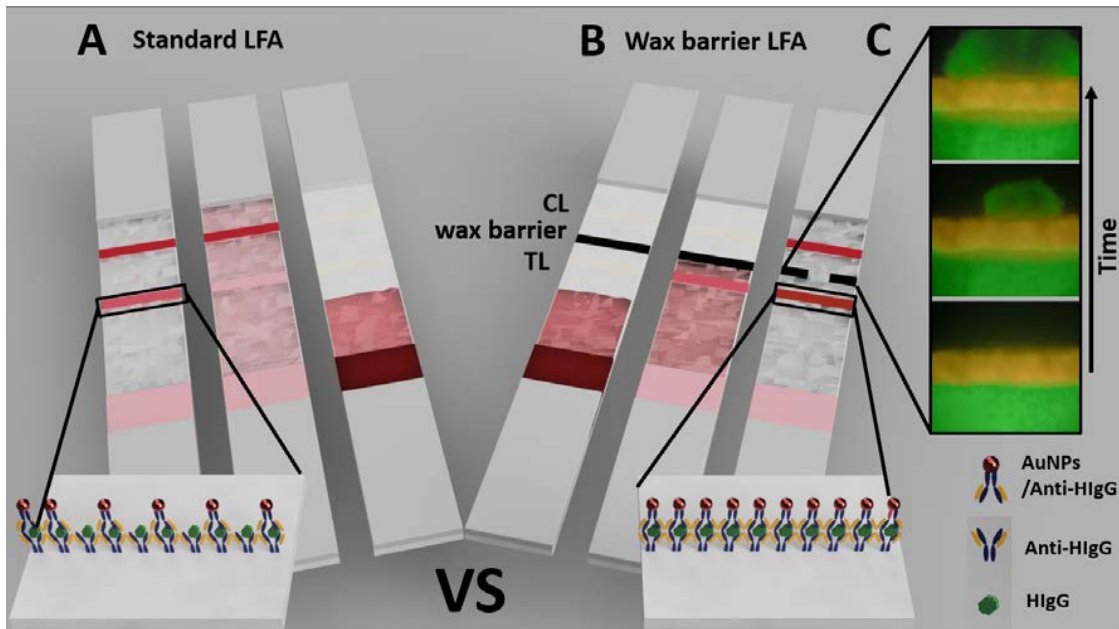
Fig. 0.3. Graphical abstract of the work: Sena-Torralba, A.; Ba Ngo, D.; Parolo, C.; et al. "Lateral flow assay modified with time-delay wax barriers as a sensitivity and signal enhancement strategy." Re-submitted to *Biosensors and bioelectronics* (2020). Figure courtesy of PhD. Ruslan Álvarez-Diduk.

Chapter 5. Lab in a Tube: Point-of-Care detection of Escherichia coli. This chapter presents a sensitive point-of-care sensing platform consisting in a microtube and two pieces of glass fiber (commonly used as conjugate pad in lateral flow assay). The detection principle is based on Förster Resonance Energy Transfer using gold nanoclusters as signal reporter and gold nanoparticles conjugated with antibodies as a quencher (Fig. 0.4). The platform has been validated for the detection of Escherichia coli O157:H7 in river and tap water, proving a limit of detection as low as 4.0 CFU mL[1].
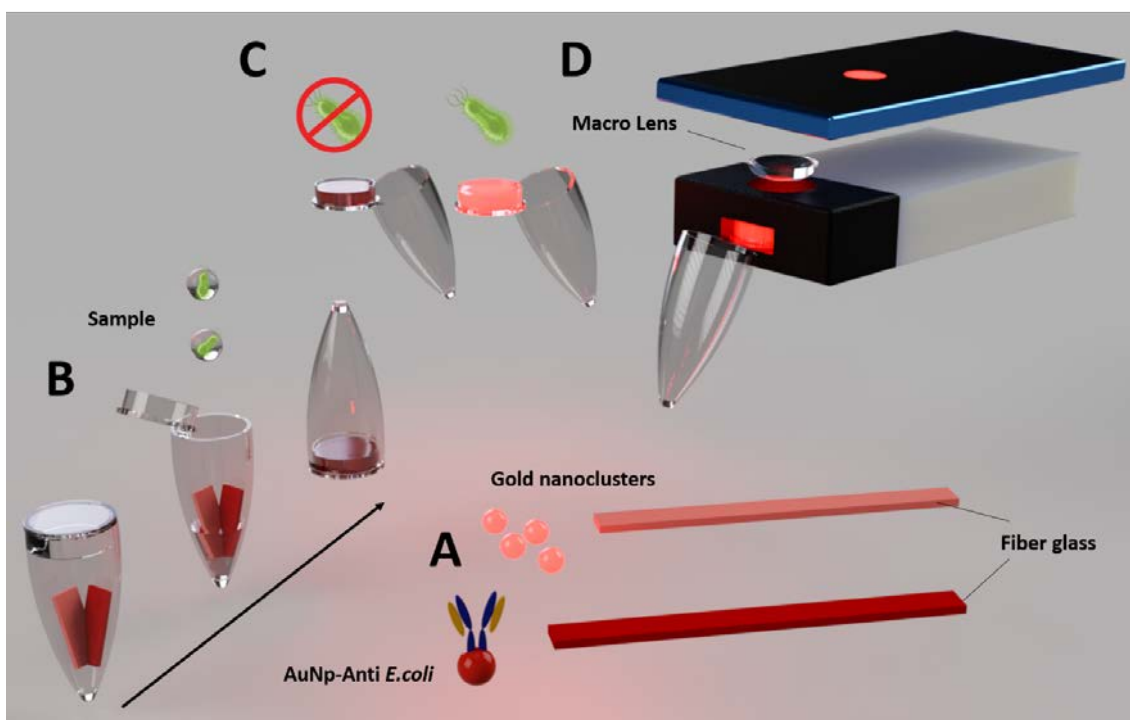
Fig. 0.4. Graphical abstract of the work: Amin, N.; Sena-Torralba, A.; Álvarez-Diduk, R.; et al. "Lab in a Tube: Point-of-Care detection of Escherichia coli." *Anal. Chem.* 92 (6), 4209-4216 (2020) – work related to Chapter 5.

General conclusions. Summary of objectives achieved, conclusion remarks, future perspectives and work to be done are given in this section.

CHAPTER 1. INTRODUCTION

1.1. Biosensors

1.1.1. Definition and historical background of biosensors

It is imperative to start this thesis by defining the term biosensors and clarify the difference between chemical sensors and biosensors. As defined by the IUPAC biosensors are devices that use specific biochemical reactions mediated by isolated enzymes, immunosystems, tissues, organelles or whole cells to detect chemical compounds usually by electrical, thermal or optical signals.[1] On the other hand, chemical sensors are defined as devices that transform chemical information, ranging from the concentration of a specific sample component to total composition analysis, into an analytically useful signal. Sensors are based on two basic components connected in series, a receptor and a transducer. In chemical sensors the receptor is a chemical (molecular) recognition system whereas in biosensors the receptor is of biological nature and the recognition system utilizes a biochemical mechanism.[2,3]
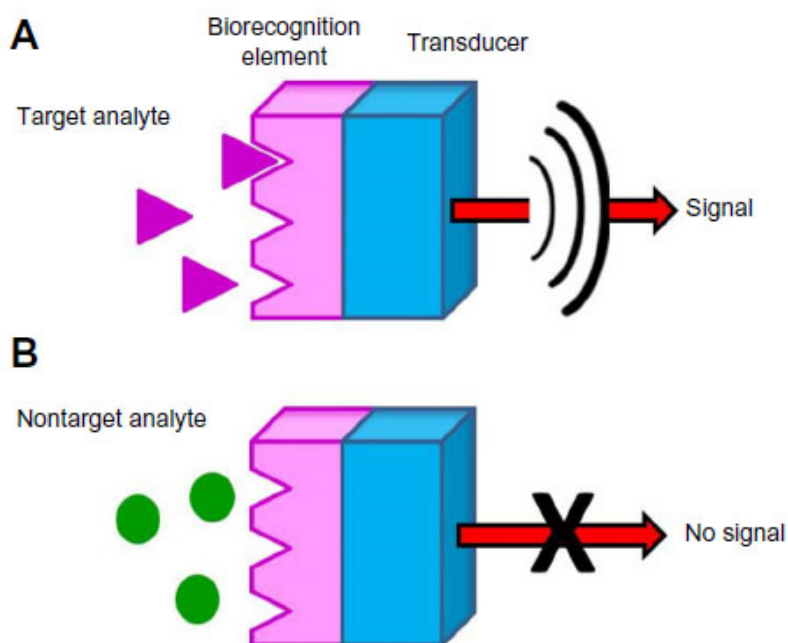
Figure. 1.1. Schematic representation of the components in a biosensor. The bioreceptor is able to specifically recognize the target analyte. The transducer transfers the signal from the recognition system to an analytical signal. Reprinted (adapted) with permission from Krejcova, L., Michalek, P., Merlos, R.M. *et al.* Nanoscale virus biosensors: state of the art. ***Nanobiosensors in Disease Diagnosis.* 4**, 47-66 (2015).

Importantly, chemical sensors used for monitoring of biological processes can't be defined as biosensors if the receptor doesn't incorporate a biological specificity-conferring part.[4]

Biosensors have been consequently developed after the discovery of novel functional materials and advances in biotechnology-related fields.[5] The discovery of the enzyme immobilization in 1916 lead to the development of the first biosensor for glucose detection by Leland Clark Jr. in 1962. This technology enabled the development of the first commercial biosensor, which was developed by Yellow Spring instruments in 1975.[6,7] Moreover, the ability of labelling antibodies with enzymes (discovered in 1966) together with the development of functionalizable mictrotiter plates (in 1967) and the creation of the DU spectrophotometer (in 1940), triggered the elaboration of the enzyme-linked immunosorbent assay (ELISA) (in 1971).[8-10]

Similarly, paper has been applied in analytical chemistry since 1800 with the development of litmus paper as a pH sensor by J.L. Gay Lussac.[11] However, the use of paper for diagnostic applications started to emerge after the invention of paper chromatography by Martin and Synge in 1943.[12] This was one more step towards the development of the first immunochromatographic assay for the detection of glucose in urine in 1956. Twenty years later, the FDA approved the early pregnancy test designed by Warner-Chilcott.[13] In 2007 more complex microfluidic approaches were developed after the emergence of the patterning technology in paper.[14] Since then, paper has become a promising platform for point-of-care applications due to its portable and on-site-real time detection capabilities.[15] In turn, nanotechnology has been growing exponentially since Norio Taniguchi first used its term in 1974. In the late 1990s almost all developed countries created nanotechnology initiatives, leading to the fabrication and discovery of novel nanomaterials and properties.[16] The unique physico-chemical properties of the nanomaterials are of great interest in various fields including biosensing. Many kinds of nanomaterials have been gradually applied to biosensors so as to enhance the analytical sensitivity. Well known examples are the ultrasensitive plasmonic ELISA[17] and the nanoparticle-based lateral flow assays.[18,19]

1.1.2. Properties and Types of biosensors

The properties of a biosensor define its quality and ability to perform its function. These properties must be optimized during the development of the biosensors until achieving the best performance for the detection of the target analyte in the required environment. Selectivity is the most important feature of a biosensor, as it is the ability of a bioreceptor to detect a specific analyte in a complex sample.[20] In this sense, the selection of a bioreceptor with the highest specificity is fundamental when designing a biosensor. Besides, sensitivity refers to the change of the response with regard to a change in the analyte concentration.[21] A biosensor is expected to have a high sensitivity, which is high signal change related to the detection of low concentration of the target analyte. Differently to the selectivity, the sensitivity is mainly influenced by the transducer. In relation to the sensitivity, the biosensor's resolution is the smallest detectable incremental change of an input parameter that can be detected in the output signal.[22] Another important property of biosensors is the reproducibility, which is defined by the IUPAC as "the closeness of agreement between independent results obtained with the same method on identical test material under different conditions (different operators, different apparatus, different laboratories and/or after different intervals of time)".[23] The reproducibility of a biosensor is given by the precision and accuracy of its transducer and signal readout system. Moreover, the stability of a biosensor is an important feature to consider during its design as it can highly affect the precision and accuracy of the measure. Biosensors instability is defined as the signal drift caused by the ambient disturbance during a measurement.[21] The instability of the biosensor can be influenced by the storage shelf life of the bioreceptor or other materials, the affinity of the bioreceptor or the matrix interferences after long incubation steps or continuous monitoring. Finally, linearity is the difference between the measured curve of a biosensor and the ideal curve.[22]

1.1.2.1 Types of biosensors based upon the biorecognition mechanism

Biosensors are commonly classified according to the biorecognition mechanism (enzymes, antibodies, nucleic acids, cells).[24,25] Briefly, enzyme-based biosensors take advantage of enzymes as bioreceptors that catalyse the generation of a product upon the recognition of the desired molecule. The product is measured using a suitable transducer. The thickness of the enzyme layer, the enzyme immobilization method, pH

value, temperature and cofactor requirements can influence the performance of these types of biosensors.[26] Biosensors that use antibodies as bioreceptors are known as immunosensors. They have as main attractive feature a high selectivity for the target antigen. Heterogeneous formats (also known as solid-phase immunoassays) in which the antibodies or antigens are immobilized in a solid support have been the most studied and reported.[27,28] Nucleic acids-based biosensores take advantage of the strong base pair affinity between complementary nucleotide strands to use DNA and RNA as highly specific bioreceptors. The complementary sequence of the target is synthesized, labelled and used as probe for the detection of the target molecule. Furthermore, the use of aptamers as bioreceptors provides outstanding properties to the biosensors such as higher stability than antibodies and low cost fabrication. Aptamers are single-stranded DNA or RNA oligonucleotides that have the ability to fold into unique 3D structures upon the detection of a specific molecule. Aptamers are selected from randomized oligonucleotide libraries by SELEX (systematic evolution of ligands by exponential enrichment).[29,30] Finally, the application of whole cells as bioreceptors in biosensing is of interest not only for the acquisition of analytical information but for the determination of functional information, such as the effect of a stimulus on a living organism. Cell's can be employed as biosensors by the use of their membrane receptors as ligand recognisers. Also, bacteria bioluminescence has been widely applied as a detection method for toxic compounds. The main challenge of these type of biosensors is the handling and lifetime of the living organisms.[31,32]

1.1.2.2 Types of biosensors based upon the signal transduction mode

Biosensors can be classified according to the signal transduction mode, which can be optical, electrochemical, mass, magnetic, calorimetric or micromechanical. The electrochemical and the optical transduction methods are the most frequently used.

1.1.2.2.1 Optical detection

In optical detection the transduced signal is light. The measured signal can be either generated directly by the interaction of the target analyte with the transducer (label-free biosensors) or by the use of labels coupled to the bioreceptor (label-based biosensors).[33] Optical detection methods can be classified upon the signal response such as absorption, reflection, refraction, dispersion, colorimetry, fluorescence, chemiluminiscence and

phosphorescence.[34] Surface Plasmon Resonance **(SPR)** is one of the most reported optical biosensors. It is a label-free detection method based upon the generation of plasmon waves on a dielectric surface interface. Bioreceptors are immobilized in the surface interface and the detection of the target analyte is recorded by variations in the propagation constant of the plasmon wave (interface refractive index). SPR provides fast, label-free and real-time biosensing, however it is noteworthy that any physical change that alters the refractive index will induce a response.[26,35] Colorimetric biosensors are particularly attractive for its easy operation and rapid reading. The transduction method is based on the colour change related to the biorecognition of the target analyte. This can be visualized directly by naked eye or using dedicated readout systems. AuNPs are the most investigated colorimetric labels due to its low-cost, fast synthesis and simple functionalization either with protein-based or oligonucleotide bioreceptors.[36] Chemiluminiscence biosensors are based on light emission resulting from a chemical reaction, most often an enzymatic reaction, although living organisms as in the case of bioluminescence can produce it naturally. In this type of biosensors the light emitted is correlated to the analyte concentration, however a photomultiplier is usually required for highly sensitive detections. Fluorescence biosensors consist in coupling fluorescence responsive molecule to the bioreceptor. Fluorescence is based on small and rapid photon emission after light absorption; therefore a short-wavelength light source is required to initiate the electronic transition in the molecule. This photo-excitation source usually generates non-specific signal, contrary to chemiluminiscence in which the photons are produced in the dark. In this sense, chemiluminiscence provides a higher signal-to-noise ratio.[34] Finally, fiber-optic biosensors use optical fibers for signal transduction, in which the light is transmitted from the fiber to the detector by total internal reflection. The bioreceptors are integrated in the optical fiber and recognize the target analyte. The concentration of target analyte is correlated to the absorbance at a given wavelength of light. Fiber-optic biosensors (FOBS) have as main advantages a superior light transmission delivery and resistance to electromagnetic disturbances.[38]

1.1.2.2.2 Electrochemical detection

Electrochemical biosensors are a class of biosensors that work using an electrochemical transducer. The principle of this detection method is a production or consumption of ions or electrons upon the recognition of the target analyte by the immobilized bioreceptors. Consequently, a change in the electric current or potential can be recorded.[39] The most common electrochemical transduction modes are amperometry or potentiometry. Amperometric biosensors are based on the measurement of current resulting from the oxidation or reduction of an electroactive species, maintaining a constant potential. Conversely, potentiometric biosensores measure the potential difference across an interface at zero-current flow. Amperometric biosensors are more suitable for mass production than potentiometric ones. Voltammetric biosensors use another type of electrochemical mode in which the current is measured as a function of the potential. Common voltammetry techniques include cyclic voltammetry, squarewave voltammetry and stripping voltammetry.[4] Impedance spectroscopy is an electrochemical method in which the resistive and capacitive properties of a material are measured. It can be used in biosensing to monitor the binding event on an electrode avoiding interferences and with no mediator requirements.[40]

1.1.2.2.3 Mechanical biosensors

Mechanical biosensors employ mechanical methods for signal transduction. According to the physical processes involved in their operation, they can be categorized into surface-stress sensors and dynamic-mode sensors. The former measures the quasistatic deflection caused by the biorecognition of the target analyte in the cantilever. The latter is based on the non-quasistatic frequency oscillation when the biomolecules land on the cantilever.[41] Another type of mechanical biosensors is mass-based or gravimetric biosensors, which produce a signal response related to a change in mass. They are commonly based on piezoelectric quartz crystals in the form of quartz crystal microbalance (QCM) or surface acoustic wave (SAW) devices. They are label-free, simple, fast and low-cost biosensing systems.[42] Besides, calorimetric biosensors are based on the changes in the temperature of the sensing site due to biochemical reactions. Specificity is achieved by the immobilization of bioreceptors on the calorimeter. The biochemical reaction begins upon the detection of the target analyte, in which the amount of generated heat is proportional to the concentration of reactants and constant

rate of reaction.[43] The temperature is recorded with a dedicated thermistor. The key advantages of calorimetric biosensors are that they don't require frequent recalibration and avoid optical and electrochemical interferences of the sample.[26] Moreover, magnetic biosensors use magnetic nanoparticles as signal transducers. This transduction mode presents several advantages as extremely high sensitivity, stability (compared to optical transducers) and low background noise.[44]

1.1.3. Impact of nanotechnology in biosensors

As defined by the European commission, nanotechnology is the term given to those areas of science and engineering where phenomena that take place at dimensions in the nanometre scale are utilised in the design, characterisation, production and application of materials, structures, devices and systems.[45] The application of nanotechnology in biosensing has been beneficial for two main reasons; it has enabled size reduction of biosensors to the micro- or the nano- scale and it has led to the use of nanomaterials as signal transducers. The former makes possible the use of smaller sample volumes, lower assay costs and better signal-to-noise ratio, while the latter provides multi detection, enhanced sensitivities and detection limits for single molecule detection.[46,47] Nanomaterials are materials with dimensions between 1-100 nanometres. Their physicochemical properties are totally different from the same materials in the big scale. Various nanomaterials has been implemented as signal transducers, receptors or both.[48] Nanomaterials can be classified based on the number of dimensions reduced to the nanometer scale. These are thin films (one-dimension), carbon nanotubes, nanorods, silicon nanowires (two-dimensions), quantum dots, nanoparticles and liposomes (three-dimensions). Their size, shape and other physicochemical properties can be modified in order to provide the biosensor with the required absorptive, emissive, and light-scattering properties.[49] Nanomaterials also stand out for their high surface-to-volume ratio that enables the immobilization of an enhanced amount of bioreceptor units. Also, the great disparity of immobilization methods available, provide the nanomaterials with versatile functionalizations.[50] All in all, the implementation of nanotechnology opened along time ago new frontiers in biosensors.

1.1.4. Biosensors applications

Biosensors have been applied in a wide range of fields due to their great versatility in terms of bioreceptors, materials and transduction modes. In the food processing industry, biosensors have emerged as an alternative to the laborious, expensive and time-consuming spectroscopy and chromatography assays used for food authentication and safety monitoring. Biosensors have been developed for the detection of pathogens, pesticides and additives in food.[51–53] In the food industry, biosensors have also been applied to monitor fermentation processes due to their simple instrumentation and easy automation. For instance, the glucose biosensor has been successfully implemented in the saccharification process as an alternative to the traditional Fehiing's method.[24,54] In the medical field, biosensors have been applied for the precise control on blood glucose levels[55], for the fast diagnosis of infectious diseases[56,57] for the monitoring of disease biomarkers such as Prostate Specific Antigen (PSA) or Carcinoembryonic Antigen (CEA) for prostate and multiple cancer diseases, respectively.[58,59] Biosensors are of interest also in the biodefense field so as to identify biowarfare agents (BWAs). BWAs are infectious microorganisms or toxins with the capability to harm or kill humans, common diseases caused by BWAs are anthrax, Smallpox and haemorrhagic fever.[60] Biosensors have also been applied for pollution monitoring in the environment.[61,62]

1.1.4.1 Biosensors for nanotheranostic applications

Theranostics (or theragnostics) refers to comprehensive effort that integrates diagnostic and therapy in a single system/platform.[63] With the emergence of nanotechnology and nanomaterials, the concept of nanotheranostics was then introduced. Nanotheranostics is able to provide non-invasive imaging, targeting and therapy at the disease sites, without affecting surrounding healthy cells.[63,64] Hence, the use of empirical treatment can be avoided (therapy given based on experience, usually without a prior definitive medical diagnosis and likely to cause infectious disease), greatly improve the prognoses and subsequently expedite clinician's therapeutic decisions. Therefore, early diagnosis will increase the patient's survival rate, and the optimized treatment will contribute to high therapeutic efficiency along with best safety profile.[63,65] Furthermore, over-dosing of drugs and cost of treatment can be effectively reduced. Nanotheranostics will also enable real-time monitoring of the drug release and its biodistribution in patients.[66]

Generally, theranostic nanomaterials can be made up of different chemical constructs: targeting moiety (for specific cellular binding), therapeutic agents (for drug delivery), diagnostic agents (for non-invasive imaging), and polymer coating or matrix that imparts colloidal stability and provide functional groups for bio-conjugation.[63,65] Some of the important advantages of nanomaterials are undoubtedly their small size and large functional surface area to volume ratio, in addition to interesting optical and electrical properties. These properties allow the diagnostic and therapeutic agent to be adsorbed, dissolved or covalently attached to the surface, to form nanoparticle-drug/imaging/targeting complexes.[67] The complex can subsequently signal (diagnostics) and deliver the agents to the cancer cells or other targeted sites to perform the therapy.[68,69] Ideally, after the controlled release of encapsulated drug molecules, the residual nanoparticle will be safely degraded and excreted from the body.[67] Recently, the application of nanomaterials with multiple physical imaging modalities and therapeutic capabilities has received increasing attention. There are several excellent review papers with similar topics made.[70–75] The comprehensive comparison of the nanomaterials for theranostics of cancer, neurodegenerative, autoimmune and cardiovascular diseases has also been interestingly reported.

1.2. Biosensors at the point-of-care and impact in society

Point-of-care testing (POCT or bedside testing) is defined as medical diagnostic testing at or near the point of care, that is at the time and place of patient care.[76,77] Settings where POCT is intended to be performed are the physician's offices or other hospital units, ambulance stations, workplaces in general and homes, although it is also of interest for military purposes[78] and space missions.[79,80] Common clinical scenarios for the application of POCT is in family medicine as a support for decision making upon the best suited approach to follow or emergency units where the immediate diagnosis of stroke or sepsis is vital.[81] In this sense POCT provides a fast diagnostic result at the time of patient consultation.[82] Besides, POCT is highly intended for home applications in which the patient is the end-user. Governments expect POCT to reduce in the next years the costs related to health service and minimise the did-not-attend issues occurring in the health check programme.[83] There are two well-known POC tests that have already been integrated into our daily lives, the pregnancy test[84] and the blood glucose meter.[85] The most important factor that defines the success of these two POC tests is economic

efficiency, which is basically high-throughput fabrication at extremely low costs. This is achieved by combining a disposable sensing unit and a portable and inexpensive dedicated readout device. Crucially, apart from the cost requirements, the delivered results must be precise and in accordance with the international quality standards.[5] In this sense, the world health organization (WHO) has established an acronym for the selection of POC tests, which must follow the ASSURED (affordable, sensitive, specific, user-friendly, rapid and robust, equipment-free and deliverable to end-users) criteria.[86] Table 1.1. provides an example of the expected ASSURED specifications for a HIV POC test.

Table 1.1. ASSURED characteristics and specifications for HIV point-of-care diagnostic devices.[87]

Characteristic	Target Specification
Affordable	Less than US$ 500 per machine, less than US$ 10 per test.
Sensitivity, specificity	Lower limit of detection: 500 HIV RNA copies per mL, 350 CD4+ T-cells per µL.
User-friendly	1-2 days of training, easy to use.
Rapid and robust	< 30 minutes for diagnosis, >1 year at room temperature, high throughput.
Equipment-free	Compact, battery powered, on-site data analysis, easy disposal, easy sample handling, no cold chain.
Deliverable	Portable, hand-held.

Furthermore, there are some challenges, mainly technical (sensitivity, multi-analyte detection, real samples) and social barriers (acceptance in daily practice) that need to be overcome.[5,88]

The global biosensors market was valued at approximately USD 21.2 billion in 2019 and is estimated to grow up to USD 31.5 billion by 2024. This is due in part by continuous technological advances such as the biosensors miniaturization and the increasing demand of point-of-care tests. In fact, point-of-care tests are the fastest-growing biosensors, with special interest in their application for cardiac biomarkers

detection as there is an expected growth demand of rapid diagnostic tests for cardiovascular diseases.[89]

1.3. Nanoparticles-based lateral flow assay

1.3.1. Introduction

For the past 70 years the field of point-of-care biosensing has always had an undisputed leader: The lateral flow assays (LFAs),[77,90] which has been employed for both, diagnostic[91–95] and environmental applications.[96,97] For the former ones, LFAs provide ASSURED (affordable, specific, sensitive, user-friendly, rapid and robust, equipment-free, deliverable to end user) solutions[98,86] for both, over-saturated healthcare systems in developed countries, and systems with limited resources in developing countries.[99] For the latter ones, LFAs represent the ideal portable sensors for measurements of contaminants in the field.[100,101] The concept at the base of any LFA is the capillary movement of the sample through different areas (pads) of the sensor (Figure 1.2).[102]
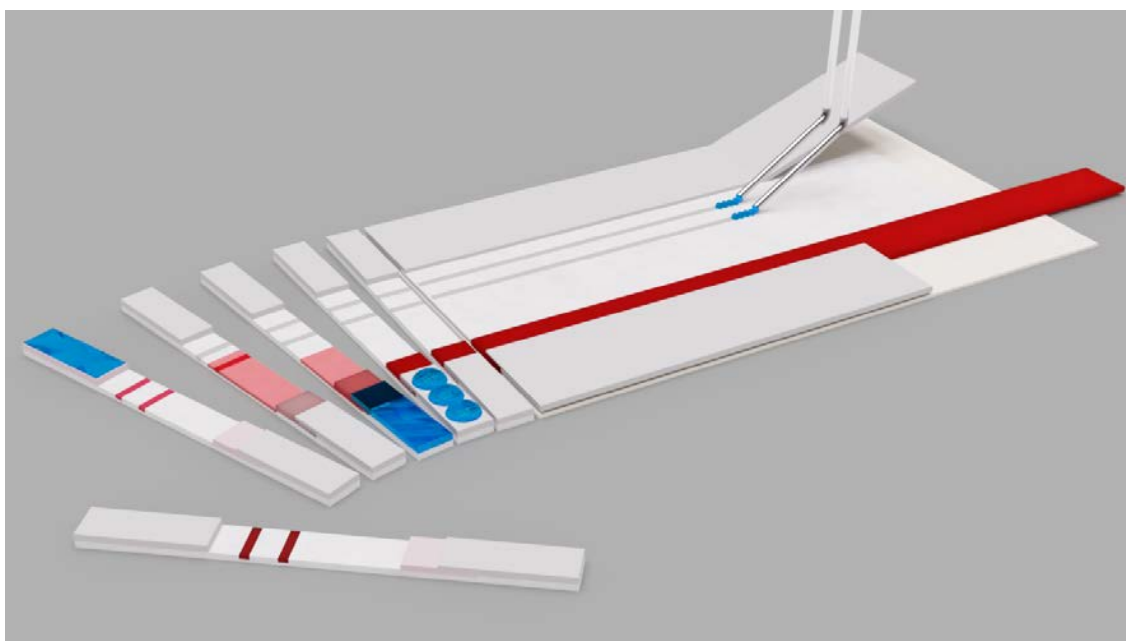
Figure 1.2. Schematic representation of lateral flow strips fabrication and assay operation. The strips are prepared by first attaching the pads onto the backing card, then depositing the bioreceptors in test line (TL) and control line (CL) and finally cutting the backing card into strips. The assay is performed by drop casting of sample solution onto sample pad, which favors the release of the conjugate solution from conjugate pad and enables the generation of optical-based signal in TL and CL. Figure courtesy of PhD. Ruslan Álvarez-Diduk.

Thanks to the specific functions of each pad, the sample receives all the required treatments to finally produce a clear optical signal related to the presence or absence of the analyte of interest.[103] This extremely simple sensor operation (one step) comes to the price of a complex fabrication optimization. This has become even more relevant in the last years, when the widespread of nanotechnology provided LFA developers with a big variety of possible optical labels (plasmonic nanoparticles, fluorescent nanoparticles, 2D materials)[104–106]

1.3.2. Lateral flow assay operation

Before going into fabrication details and specific considerations for different types of LFAs, it is important to describe how LFAs work (Figure 1.3). The classical LFA (also called immunochromatographic assay, dipstick assay or lateral flow strip) consists of four pads: sample, conjugate, detection and absorbent, which are attached to a sticky supporting card.[107,102] In most cases the final user has just to add the sample and wait for the signal generation, although sometimes the addition of a washing buffer is also required. Having a look at what happens to the sample after its application, it is observed that it first encounters the sample pad, which assures that the characteristics of the sample match those required for an optimal detection (pH, ionic strength, purity and concentration of blocking agents). Secondly, the sample reaches the conjugate pad that releases upon wetting the labelled bioreceptor and allows for a first analyte/bioreceptor interaction. Thirdly, the sample goes through the detection pad, where the capture bioreceptor adsorbed on the pad binds to the now labelled analyte generating the classical coloured lines. In most LFAs there is a minimum of two lines: the test line, which indicates the presence or absence of the analyte; and the control line, which assures the correct operation of the LFA (by selectively capture of the labelled bioreceptor). Finally, the sample reaches the absorbent pad, which provides enough bed volume for the complete flow of the sample.
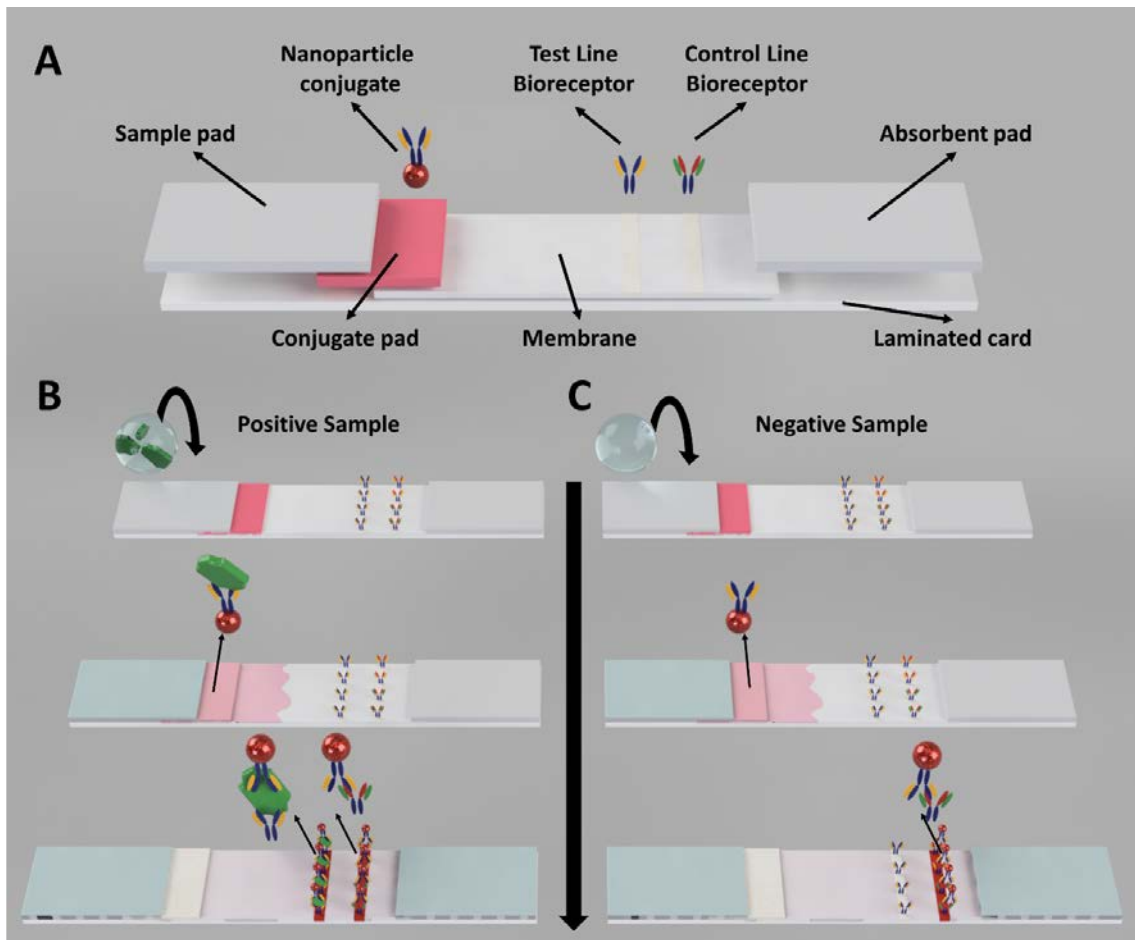
Figure 1.3. Schematic of the main components and operation of a typical LFA. A) A LFA is made of four main parts: the sample pad, the conjugate pad, the membrane and the absorbent pad. They are mounted on a laminated card. The membrane contains the bioreceptors with the printed test and control lines. The bottom part shows the operation of a LFA based on an immunosandwich recognition. B) The presence of the target in the sample produces the accumulation of nanoparticles on the test and control lines making the classical two red lines to appear. C) Instead the absence of the target makes the nanoparticles to accumulate just on the control line, giving a single coloured line output. Figure courtesy of PhD. Ruslan Álvarez-Diduk.

Thus, in summary, a LFA strip is actually composed of six main components: sample pad, conjugate pad, membrane, absorbent pad, labels and bioreceptors. In the next sections, we will examine in detail the effects that each component has on the LFA, and discuss the key characteristics developers should consider when choosing the best materials and reagents.

1.3.3. Lateral flow assay fabrication

In order to provide the final user with a single-step sensor, the developer of a LFA has to optimize and coordinate all the different components (pads, bioreceptors and label) to achieve the best possible sensing operation. In this section we will describe the standard procedures for the fabrication of the different pads, as well as important considerations to take into account for an appropriate optimization.

1.3.3.1. Sample pad

The main function of the sample pad is to prepare the sample for the optimal detection of the target further down the LFA strip. In order to achieve this, the sample pad has three main roles: filtering, buffering and controlling of the flow (Figure 1.4.). Depending on the type of sample, the sample pad can directly act as a filter (i.e. for dirty environmental samples that need the removal of big particles/detriments) or it may require dedicated filters to be attached on top of it (i.e. for biological fluids that require the separation of cells from the media).[102,108,109] For the buffering of the sample, during the fabrication process, the sample pad is loaded with the appropriate buffer that get re-solubilized as soon as the sample wet the pad. Finally, the sample pad also controls the initial flow of the sample conferring the appropriate speed and homogenous wetting of the conjugate pad.

Overall the most used material for sample pads is cellulose, because of its low-price and high-volume loading capacity that allows the storage of an adequate amount of buffer. Other materials are: glass fiber (useful for unifying sample and conjugate pads), polyester (it can retain cells and proteins from whole blood)[110] and other type of woven meshes (for an even distribution of the sample on the conjugate pad),[111] but they are generally more expensive and/or have a smaller volume loading capacity, which decreases the buffering capabilities of the pad.

During the fabrication process the sample pad first gets soaked in the desired buffer, then dried and finally mounted on the backing card. The drying temperature depends on the material and the composition of the buffer, overall we aim for a fast drying, which speeds up the fabrication process (around 60 °C), but if the buffer contains delicate biological materials it may require a lower temperature. Although the buffer

composition is highly dependent on the type of sample and analyte, we can find common types of reagents in the buffer recipe,[112,113] such as salts to control the ionic strength (e.g. KCl, NaCl), acids/bases to control the pH (e.g. H_3BO_3, NaH_2PO_4), surfactants to facilitate the release and running of the label particles (e.g. Tween 20, Triton X-100) and blocking agents to assure a specific signal (e.g. BSA, OVA).

1.3.3.2. Conjugate pad

The main functions of the conjugate pad are to efficiently label the analyte and consistently transfer it to the detection pad. In order to achieve these goals, an ideal conjugate pad needs to comply with several requirements (Figure 1.4.). First, it should provide a consistent flow of the sample, meaning that it gets homogenously wetted (so all the label/bioreceptor conjugate is efficiently used) and it deposits the sample uniformly onto the detection pad. Second, it should have enough and consistent volume to contain the amount of conjugate required to achieve the desired sensing performance. Failing in complying with these two requirements would generate non-reproducible and non-sensitive LFA. Third, it should not modify the sample composition besides the incorporation of the conjugate. This means that it must not bind to the analyte of interest (which would affect the sensor sensitivity) and it must not contain any loosen materials that can contaminate the sample (chemicals or particles, which could produce non-specific results).
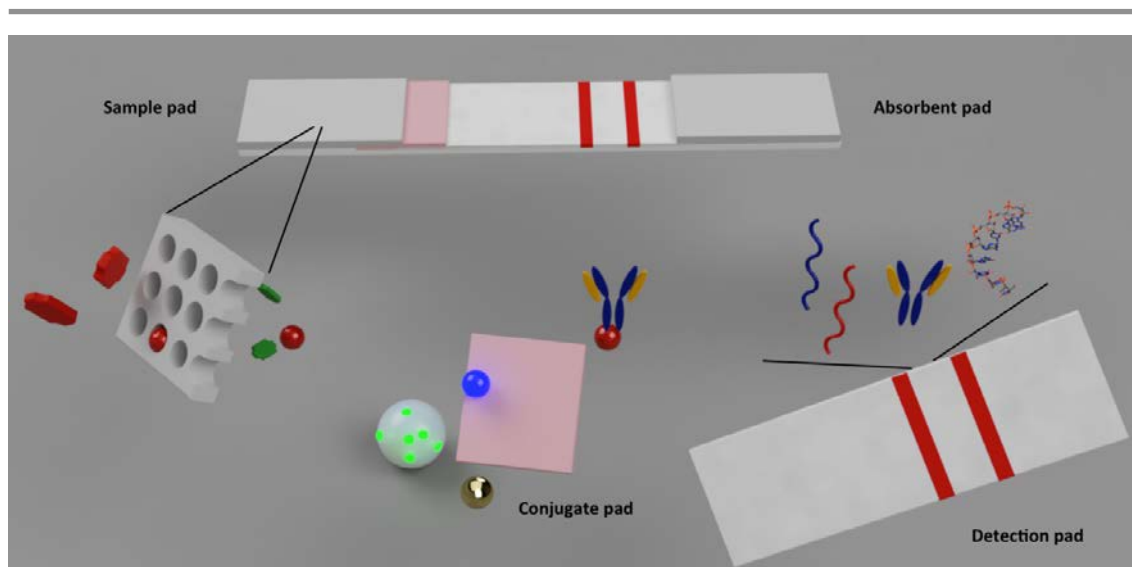
Figure 1.4. Lateral Flow assay pads. Sample pad, conjugate pad, detection pad and absorbent pad. Figure courtesy of PhD. Ruslan Álvarez-Diduk.

Finally, it should also have enough tensile strength to be easily handled during the fabrication process, as well as once incorporated in the final sensor.[114]

There are three main materials commonly used as conjugate pads: glass-fiber, cellulose and polyester. While the three of them have good low nonspecific binding, they differ mainly on the hold-up volume (minimum volume required to re-suspend all the content of the pad) they provide and their textile properties.[115] Conjugate pads made of cellulose have a thickness varying between 300 and 1000 μm making them particularly weak when wet and having a very high hold-up volume. Instead, the most robust of the three materials, polyester conjugate pads, have the smallest and less consistent hold-up volume (due to a thickness of 100-300 μm). Finally, glass fiber conjugate pads with a thickness between 100 and 500 μm provide a good and consistent hold-up volume and; although weaker than polyester, can still provide decent handling, making them the most used type.[114]

The optimization of the conjugate pad is probably the most delicate step in the all LFA production. It starts with the choice of the right label/bioreceptor conjugate solution, which must provide: i) enough label to produce a strong signal, ii) the appropriate buffer conditions to stabilize the conjugate during the fabrication and allow for the bioreceptor to recognize the analyte and iii) a fast conjugate re-solubilization to maximize the interaction time between bioreceptor and analyte before reaching the test line. This is generally achieved with a low ionic strength buffer[114] (for the nanoparticle stabilization) containing high concentrations of sucrose (approx. 10%), which acts as a soluble linker between the nanoparticles and the conjugate pad.[116] The application of the label/bioreceptor conjugate solution into the pad can be achieved by dipping, dropping or spraying. In automatized facilities the spraying is generally the most effective way, but in small laboratories dipping/dropping are viable alternatives. In any case, it is really important to obtain a uniform dispersion of the conjugate throughout the whole conjugate pad surface, in order to achieve reproducible results from sensor to sensor, as well as a uniform signal in the same LFA (if the pad has different conjugate densities it could produce a striped line).[114,116] Another key step in the fabrication is the drying of the conjugate pad. Given the presence of bioreceptor and possibly unstable nanoparticles, the conjugate pad is generally dried in a vacuum chamber that ensures the preservation of the label/bioreceptor conjugate. Fundamental is also assuring the

complete drying, since failing in this could produce a syrup-like solution that would prevent the flow of the sample through the pad. If a vacuum chamber is not available, the conjugate pad could also be dried at 37 °C.

1.3.3.2.1. Nanomaterials used as labels

The most common detection method is optical, and this is subdivided into colorimetric, fluorescent and luminescent. The label most widely used in diagnostic laboratories is gold nanoparticles (AuNPs), their high popularity is related to their biocompatibility and ease of conjugation to protein-based bioreceptors. This can be attached to the surface of the AuNPs by electrostatic absorption after incubation for at least 30 minutes under constant agitation conditions. However, this type of conjugation can only be achieved if the AuNPs are stabilized with citrate following the simple, fast and well-established Turkevich method.[117] Therefore, AuNPs are convenient labels for the preliminary development of a LFA, where the first thing to be checked is the binding ability of the biorecognition elements to the target analyte. They are also suitable in cases where cost-effectiveness is a critical issue or conditions in which high sensitivity is not required. Besides, highly fluorescent quantum dots (QDs) can be applied in order to achieve an enhancement in the sensitivity.[118–121] QDs are characterized by their broad adsorption, narrow photoluminescence spectra, size-tunable emission and strong luminescence.[122] However, QDs usually present photostability and high background signal issues which can be avoided by the use of upconverting nanoparticles (UCNPs). These are nanomaterials doped with lanthanide ions that present a unique anti-stokes optical property,[123] which confers them a longer lifetime and high resistance to photobleaching. Moreover, the fact that this type of luminescence is not common in other nanomaterials, the detection based on UCNPs is characterized by a high signal-to-noise ratio.[124] Something to take into account when developing an UCNPs-based LFA is that they requiere a near-infrared (NIR) excitation wavelength, so a diode-laser can be used for the evaluation of the strips.

1.3.3.3. Detection pad

The function of the detection pad is to generate a signal specific and sensitive enough to address the purpose of the sensor. In order to achieve it, the detection pad has to provide: i) a homogenous/constant flow of the sample (this includes enough porosity to enable the flow of big analytes, like cells),[125] ii) binding properties that assure the localization and functionality of the capture bioreceptor,[126] and iii) minimum background noise.[127] A homogenous constant flow is essential for the reproducibility of the test. Detection pads that do not provide these properties can generate different levels of signal in the same strip (i.e. striped lines) or from sensor to sensor, besides increasing the background noise (the label could accumulate non-specifically in the areas with a slower flow). The binding properties of the detection pad define the type of capture reagents that can be used and play an important role in the sensitivity and specificity of the test. Overall there are two main types of binding mechanisms to attach the capture probe to the detection pad: electrostatic and hydrophobic. Electrostatic interactions can be found in nitrocellulose and charged-modified nylon membranes,[128] while hydrophobic interactions are typical of polyvinylidene fluoride (PVDF) and polyethersulfone (PES).[129] Independently on the mechanism, the binding between the membrane and the capture molecule must be irreversible and possibly oriented. The irreversibility of the binding is essential to generate a stable signal, since once the flow passes the bioreceptor/analyte/conjugate complex must stay in place to allow for the accumulation of the label.[114] The orientation of the bioreceptor on the strip is also particularly important, given that the binding portion must be easily accessible to the moving target. Although there is generally not much room to play to orientate the capture molecules, generally the screening of different deposition pH or the use of spacer molecules could help to maximize the binding efficacy. Finally, the background noise that the membrane itself can generate must also be considered, especially for fluorescent applications.[130] In fact, depending on the reagents used for the membrane fabrication or possible additives used post-fabrication (i.e. wax structures), the membrane itself can have a fluorescent signal, which can interfere with the signal coming from the label.

Detection pads are generally classified depending on their flow speed since it plays a major role in the sensitivity of the test: the slower is the flow speed and the higher is the

sensitivity.[131] In fact, a slower flow allows for a longer time for the immunoreaction between the target and the capture probe on the pad to happen, making a higher number of immune-complexes. We must point out though that a slower flow also makes the whole sensing slower (which could be a burden for applications that require a result as fast as possible) and a higher chance of background noise (a slower flow facilitate also non-specific interactions). The flow is also the defining characteristics of the names of commercial membranes. In fact, since the pore size is generally not homogenous (especially for nitrocellulose membranes), companies tend to define the membrane with a capillary flow rate that defines the time the liquid requires to cross 4 cm of nitrocellulose membrane.[132,133] So for example a 180s/4cm membrane requires 180 seconds for the liquid to cross a section of 4 cm.

The fabrication of the detection pad must assure that the capture bioreceptor is homogenously distributed on the test line preserving its function and it could also involve a blocking step. The application of the capture bioreceptor onto the membrane can be achieved using contact or non-contact techniques. The former ones are generally cheaper and easier to optimize but can damage the membrane if the contact is too harsh; while the latter can provide higher precision and may require less amount of capture bioreceptor, but are more expensive and more difficult to optimize.[134] The general rule is to deposit the capture bioreceptor in the smallest possible area, in order to achieve the maximum signal resolution. The capture bioreceptor solution must provide the conditions for an optimal binding and the maintaining of the bioreceptor functionality. This is generally achieved using a low ionic strength (especially for nitrocellulose membrane) and keeping the bioreceptor concentration high (in the case of expensive antibodies it is possible to add a second protein, such as BSA, to raise the overall protein concentration, in order to keep its structural integrity and preventing the adsorption of the antibodies onto the membrane). Some LFAs may require the use of additional blocking that can be achieved by dipping/spraying the detection pad in a solution with blocking agents (BSA, milk, etc), followed by their proper removal using one or more washing steps (they may include some detergents)[135]. As for the conjugate pad, the drying of the detection pad is very important since it must be done at a temperature that does not affect the functionality of the capture bioreceptor (not more than 37-40 °C).

1.3.3.4. Bioreceptor selection

A bioreceptor (typically proteins, antibody, DNA, RNA) to be effective in a LFA has to comply with three main characteristics: i) being stable, ii) having fast association kinetics and iii) having strong binding affinities. In LFA, the stability of the bioreceptor means that it has to keep its structure and functionality in a variety of environments (different temperatures, humidity %, pressures)[136] and, above all, it has to maintain its function after a cycle of drying and rewetting. In regards to this, fast binding kinetics are essential as there are practically no incubation steps on the LFA and the bioreceptors have to bind to the target within seconds. These two are important characteristics to be considered when choosing antibodies as bioreceptors in LFA (Table 1.2.). In fact, most commercial antibodies are characterized with techniques such as Enzyme Linked Immunosorbent Assay (ELISA) and western blot, which include long incubation steps, typically in the order of hours. Finally, the binding between the bioreceptor and the target must also be strong to obtain a stable signal. In practice, most of the labelled target will pass through and travel to the detection zone in matter of seconds. Meanwhile, the flow still continues for minutes and acts as an internal washing step. If the binding was weak, signal losses are obtained over time once the concentration of the labelled-analyte in solution decreases.

The choice of the proper bioreceptors is probably the most important step to achieving the required analytical sensitivity and specificity in a LFA. This is particularly challenging for the detection of protein targets given the large variety of possible bioreceptors (Table 3). Ideally, during the initial phases of a LFA development, several bioreceptors are screened using a combinatorial approach, where a single bioreceptor is tested both in the test line and conjugated to the label particle. Depending on the resources and facilities available, the use of standard techniques (such as ELISA, Surface Plasmon Resonance (SPR), Biolayer interferometry (BLI)[137] and Isothermal Titration Calorimetry (ITC)) could speed up the screening of multiple bioreceptors. For example, ELISA can be used to evaluate dozens of antibody/antigen combinations to find those producing the most sensitive result in a relatively short amount of time. In this respect, the developer could minimize the duration of the incubation steps in order to eliminate the bioreceptors with slow binding kinetics. Moreover, SPR, BLI and ITC can provide useful information about the association and dissociation binding kinetics,

although they are more expensive techniques than ELISAs. Indeed, these techniques can help to identify and shortlist the most promising bioreceptors, however, they must be finally tested in a real LFA, in order to choose those that will be used in the final assay.

Table 1.2. Common bioreceptors used in LFA for the detection of protein targets.

BIORECEPTOR	ADVANTAGES	DISADVANTAGES	CONSIDERATIONS
Polyclonal antibodies	• Cost-effective • Fast production • Multiple binding sites	• Low specificity • Cross-reactivity • Variability between different batches	Affinity purification of the serum required to minimize cross-reactivity.
Monoclonal antibodies	• High specificity • Low batch-to-batch variability.	• Expensive • Long development process.	For immune-sandwich assays antibodies binding to different epitopes must be chosen.
Fragments	• Less nonspecific binding • Cheaper than full length antibodies • Easier production • Low batch-to-batch variability	• Less stable than full length antibodies since they lack of Fc region	Antibody against IgG Fc region cannot be used in control line. BSA should not be used as blocking agent, given its higher molecular weight (66 kDa) compared to the fragments (<50 kDa).
Nanobodies	• Less nonspecific binding • Cheaper than full length antibodies • Easier production • Low batch-to-batch variability	• Production limited to *Camelidae* and *Sharks* species.	BSA should not be used as blocking agent, given its higher molecular weight (66 kDa) compared to nanobodies (15 kDa).

Table 1.2. Cont. Common bioreceptors used in LFA for the detection of protein targets.

BIORECEPTOR	ADVANTAGES	DISADVANTAGES	CONSIDERATIONS
Aptamers[138]	• Cheaper than antibodies. • Ability to recognize any type of target analyte. • High stability • High batch-to-batch reproducibility	Their binding activity is highly dependent on the ionic strength of the buffer.	It is recommended to perform a denaturation and refold step before fabricating the LFA.

1.3.3.5. Absorbent pad

The absorbent pad is generally the less considered section of a LFA, although it plays a crucial role in its operation, such as controlling the volume of sample we can use.[114] In the absence of the absorbent pad, once the liquid reaches the end of the detection pad, the flow stops and the liquid evaporates homogenously along the strip. This means that all the labels that did not reach the last part of the detection pad accumulate on the strip increasing the background noise. On contrary, the presence of an absorbent pad assures that all the label reaches the end of the strip.[102] In fact, it is important to note that the label is not homogenously distributed in the whole sample volume, but just in the first part of the sample that reaches the conjugate pad and in the amount required for the complete release of the label-conjugate. Keeping this in mind, using an absorbent pad in a LFA allows for the use of more sample than the one required for the release of the label from the conjugate pad.[139] This will allow that the final part of the sample acts as an inner washing step, removing non-specifically bound labels and thus decreasing the background noise. The absorbent pad does not require any special handling during the fabrication, and although its use is generally recommended, considerations such as its cost and its implementation in the sensor geometry should be done by the developer.

1.3.4. Types of lateral flow assays

As any other biosensors LFA can integrate the three main types of sensing strategies: direct, competitive and non-competitive assays (Figure 1.5.). Their successful use in LFA requires the developer to consider important factors during the sensor design, fabrication and optimization.

1.3.4.1. Direct assay

A direct assay is the simplest one and consists in the use of a labelled bioreceptor that directly binds the target, which is generally attached to the detection pad (it can also work with a labelled target and the bioreceptor on the detection pad). This type of assay has none or very limited applications in real life situations, since the target needs to be labelled or adsorbed on the detection pad first (it is not feasible for a point-of-care sensor that the final user does it). Nonetheless it can still be useful for preliminary optimizations such bioreceptor/target binding studies or optimization of the competitor or bioreceptor deposition concentrations, especially for a competitive assay (see next paragraph).

1.3.4.2. Competitive assay

A competitive assay can be considered an evolution of a direct assay but with a use for real-life applications. We can find two main types of competitive formats: i) the target in the sample and a labelled-target (alternatively a molecule with less affinity for the bioreceptor than the target itself) in the strip compete for the capture bioreceptor on the test line,[140,141] and ii) the target in the sample and the target on the test line compete for the labelled bioreceptor.[100,142,143] A key characteristic of competitive assays is that to a higher target concentration corresponds a lower signal. Competitive assays are generally used for small target molecules that cannot be efficiently recognized by more than one bioreceptor (such as drugs and toxins), but they could also be adapted for big analytes. Since competitive assay are not affected by the hook effect (the detection and capture bioreceptors have all their binding sites occupied by single targets, preventing the sandwich formation), they are particularly useful for the detection of targets with extremely high concentrations.[144] The development of competitive assays is quite long since it requires the optimization of labelled- and capture molecules concentrations. In

fact, a high concentration of labelled-molecule would produce a worse limit of detection (a higher concentration of target would be required to decrease the signal), while a low concentration could produce a very low signal (a faint line that could be mis-interpreted as no line).[102,114] Similar situations happen for the concentration of the capture molecule, where a too low concentration would result in faint bands, while a too high concentration would decrease the sensitivity of the test. Another important consideration to do is that the developer of a competitive assay must verify that the bioreceptor can recognize the competitor molecule even after it is labelled or adsorbed on the detection pad (the use of a spacer-molecule could improve such recognition).

1.3.4.3. Non-competitive assay

A non-competitive (sandwich) assay is probably the most used strategy for the detection of mid-and big-size analytes (such as proteins, bacteria, cells) in LFAs. It consists in capturing the target molecule between a capture bioreceptor and a labelled-bioreceptor, producing a signal that increases proportionally with the amount of target in the sample.[94,145,146] One key aspect for the development of this type of assays is the availability of bioreceptors that bind different portions of the target. For example, two different monoclonal antibodies or a labelled monoclonal antibody and a capture polyclonal antibody are the most secure ways to ensure the sandwich formation. In the case of particularly big targets, such as bacteria or cells, where the same antigen is repeated many times in the same target, the use of the same antibody (better if polyclonal) would also be a feasible option. As previously mentioned, sandwich assays are subjected to possible Hook effects in the case of extremely high target concentrations. If this happens, a simple solution would be to dilute the sample.[144] The optimization of a sandwich assay is considerable easier than the one of a competitive one, since overall we aim for the highest capture bioreceptor concentration and the highest amount of labelled-bioreceptor (obviously keeping in mind the cost of both reagents).
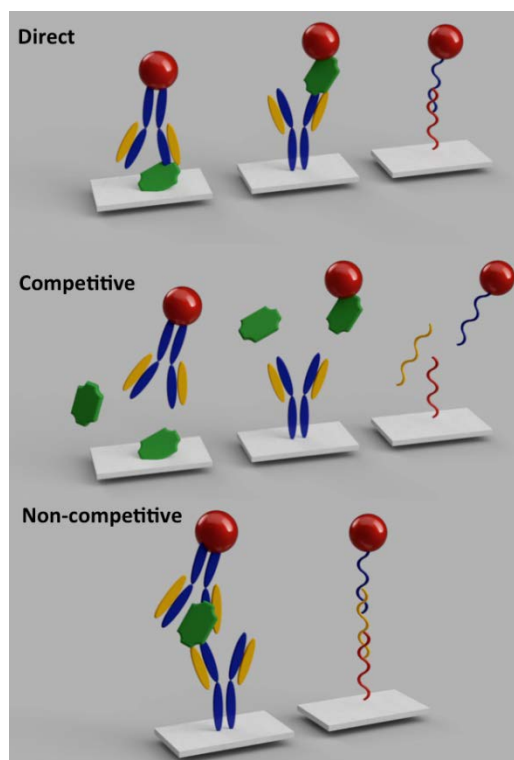
Figure 1.5. Types of lateral flow assay. Direct, competitive and non-competitive. Figure courtesy of PhD. Ruslan Álvarez-Diduk.

1.3.5. Assay Evaluation

When thinking of LFA the first thing that comes to mind is the presence or absence of the line in a pregnancy test. This intuitive and qualitative analysis done by naked eye is the reason of LFA popularity. This type of sensing is ideal for the discrimination between the presence or absence of a particular condition, such as pregnancy.[107] Reading a LFA by naked eye would also allow for a semi-quantitative analysis in highly reproducible strips. This can be of use in two main scenarios: i) during the fabrication process when two or more analyte concentrations needs to be compared (so the colour of the corresponding lines should differ), and ii) for the detection of a defined target concentration threshold (a measurable line appears just if the concentration of analyte is at least at the threshold value). This last scenario is useful for the detection of biomarkers which are of interest just above a defined concentration, such as *E. coli* in urine. In the recent years the development of dedicated readers and then smartphones have permitted the quantitative analysis of LFA (Figure 1.6.).[147–149]
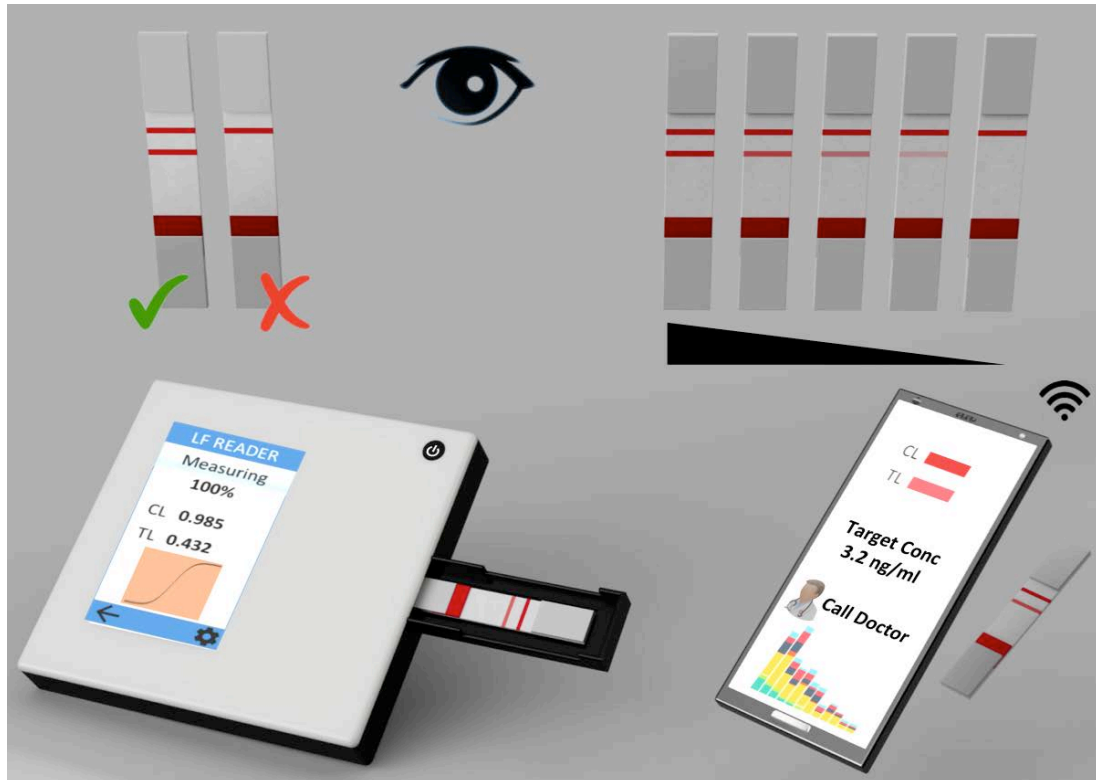
Figure 1.6. Lateral flow assay evaluation. The strips can be evaluated qualitatively by naked eye or and/or quantitatively using a lateral flow reader or a smartphone camera. Figure courtesy of PhD. Ruslan Álvarez-Diduk.

In order to achieve quantification, the fabrication process must provide highly reproducible sensors (from batch to batch) and an accurate calibration curve to be used as standard. The use of a dedicated reader is still preferred to obtain accurate measurements, since it minimizes the effect of ambient light on the signal intensity (to obtain a proper quantitative result the measurement should be done using the same light conditions as the original calibrate, from here the need of a fully closed box with integrated light sources). Hybrid systems where a smartphone is coupled to a special support also provide excellent performances.[135,150–152]

1.3.6. Other considerations

In this section we will discuss two important aspects that any LFA developer should keep in mind during the design and fabrication of a new sensor.

1.3.6.1. Storage

Being LFAs sensors to be deployed in the field (i.e. doctor office, countryside, home) their storage must ensure that their analytical performance remains intact over-time and in different environments.[153] There are three main components that can affect the stability of a LFA: the detection pad, the bioreceptors and the label. First of all, nitrocellulose (the most used type of detection pad) has an expiration date, and this is as far as a LFA should be used. Deteriorated nitrocellulose shows a yellowish colour, produces a sourly smell and might generate faint lines after performing the assay. To maximize its life-time, nitrocellulose should be stored in dry conditions protected from direct light (i.e. at least in a zipper bag with drying pearls).[114,154] Regarding the stability of bioreceptors we need to distinguish between the stable DNA molecules (which includes also aptamers) from the delicate proteins (including antibodies). While the former do not require any special storage, the latter prefer dry and cool conditions (better if refrigerated but at least under 37-40 °C).[155] Particularly delicate bioreceptors could require also the addition of stabilizers, such as sugars, proteins, agars and gelatins.[156,157] Finally, the label stability also depends on the nature of the label itself: properly modified and dried particles in the glass fiber should not have any stability issues, while enzyme-based or dye-loaded particles labels may require refrigeration to preserve their activity.[158] Overall LFA should not be frozen.

1.3.6.3. Cost

The estimation of the cost of a LFA depends on the development phase of that particular test: Research and development (R&D), factory, market. During the R&D phase most of the costs come from the bioreceptors used in the LFA. Generally, we can estimate the cost of a single LFA to be less than 1 USD. For instance, we can estimate the cost of the fabrication of a LF strip for the detection of the model protein Human Immunoglobulin G, using our group's previous work as reference.[159] This estimation is based on the product prices provided by Millipore (pads), Abcam (bioreceptors) and Sigma Aldrich (chemical reagents). Considering a 6 mm wide strip the pads and the backing card would cost: backing card $0.0080, nitrocellulose membrane $0.0204, glass fiber 0.0044 $, cellulose (for both sample and absorbent pad) $0.0046. The printing of test and control bioreceptors at a concentration of 1 mg/mL using a dispense rate of 0.05 μL/mm would cost $0.0450. The cost of the gold nanoparticle/bioreceptor conjugate can be

divided into: gold salt $0.0621, salts for the synthesis and modification $0.0007, pad pretreatment $0.0031 and antibodies $0.1416. Finally, the pretreatment of the sample pad with the sample buffer cost $0.0047. Adding all up the cost of a single LFA costed us $0.3576 (excluding the dispenser, around 20000.00 $ the cheapest models, and of course the salary of personnel). It must be highlighted that from the final cost, approximately 19 cents are for the bioreceptors (54.29 %), 6 cents for the nanomaterial (17.14 %) and the rest for the paper and treatments (28.56 %).

It is noteworthy that during the mass production in a factory the cost decreases to several LF strips for 0.01 USD, although this does not include equipment and its maintenance, the employees, insurances, taxes, quality controls and many other indirect costs. Finally, the market cost is the toughest one to estimate[160]. For the sake of comparison, we will use the cost of "Clearblue Rapid Detection Pregnancy Test", which we can purchase for approximately 6 USD per test[161]. Although it could seem that there is a great benefit for the company and the seller, there are also even more indirect costs such as: wrapping (cassettes, bags, desiccants) and storage of the product, shipping, marketing, taxes, additional reagents and tools, plus the cost of R&D and clinical validation that need to be refunded.

1.4. Towards next generation lateral flow assay

1.4.1. Challenges to be solved

The success of LFA comes from their simplicity, effectiveness and cost. For this reason, any improvement aiming to make them better should still keep those three characteristics. Taking this into account, we found three main areas that are trying to bring LFA to their next generation: boosting sensitivity, multiplexing and interfacing with smartphones.

The use of smartphones for the analysis of LFA should not be limited to obtain quantitative results; instead thanks to their imaging, processing, storing and connectivity tools they should allow LFA to be defined as REASSURED sensors.[98,86] This means that they will have/be: Real-time connectivity, Ease of specimen collection, Affordable by the end user, Sensitive with very few false-negatives, Specific with very few false-positives, User-friendly possibly being single-step, Rapid/Robust to provide an accurate

diagnosis within the time of a doctor visit, Equipment-free not requiring dedicated equipment (smartphone are already widespread within the general population) and Delivered to those who need it.

The multiplexing of lateral flow assays comes from a need that the current healthcare systems have, which is the simultaneous detection of different biomarkers. With the field moving towards precision and personalized medicine, the detection of a single biomarker is not enough anymore to give an accurate diagnosis.[162,163] Nonetheless improving the number of analytes for a single LFA is not always as straightforward as increasing the number of test lines.[164,165] This approach could work for limited multiplexing requirements, such as <5-10 analytes, in which case the amount of reagents and the ease of read-out would still be reasonable. We envisage that the use of single dots[166] (instead of lines) per analyte and/or the use of multicolour nanoparticles[167,168] in combination with smartphone readers could provide the high level of multiplexing required by personalized and precision medicine.

Finally, improving the sensitivity of LFA would spread its use to many different applications, which are still relying in laboratory-based techniques.[107] For protein targets, this could include the integration of more efficient pre-concentration pads[170,171,131] or the use of nanoparticles with stronger plasmonic[172] or fluorescent properties[173,174] than those currently in use. For nucleic acid targets the development of an amplification pad based on isothermal amplification strategies[175,176] would be a ground-breaking achievement in the field of point-of-care biosensors, if this can maintain the REASSURED standards.

1.4.1.1. Sensitivity enhancement

The reported strategies for sensitivity enhancement in LFA can be categorized according to improvements in the affinity of the bioreceptors, modulation of the flow dynamics or selection of superior signal transducers. This section is devoted to review the most relevant approaches within each category, emphasizing in their limitations and its feasibility.[177]

The main reason for the poor sensitivity in LFA compared to other analytical techniques is the low binding rate between the capture reagents immobilized in TL and the labelled reagents. This is due to the capillary action that makes the binding reaction be transient.

In this sense, much research has been focused in changing the geometry of the strip or performing architecture modifications to the objective of increasing the reaction time between the bioreceptors and the target analyte. In this sense, Asiaei *et al.* have developed a strategy to enhance the sensitivity up to 40% for the detection of human chorionic gonadotropin (hCG) pregnancy biomarker by displacing the TL 12 mm from the LFA strip origin. They observed that both, bed volume and flow velocity decrease by increasing the distance of the TL from the beginning of the strip. The former directly controls the amount of antibody and antigen that can participate in the binding reaction in TL. The latter controls the biorecognition efficiency. [178] This approach outstands by its simplicity and substantial cost saving, as no extra reagents or further steps are required. However, further experiments should be performed in order to demonstrate the adequacy of the strategy with bigger target analytes such as bacteria, which its poor mobility along the detection membrane is highly reported.

Another method to enhance the sensitivity by reducing the flow rate in LFA has been reported by the group of Prof. Pingguan-Murphy. They electrospun a 10% solution of Polycaprolactone (PCL) nanofibers onto the nitrocellulose membrane for 60 seconds in order to increase the flow time up to 17 seconds. The incorporation of PCL increases the hydrophobicity at the coated region, which in turn provides a flow rate reduction and an enhanced interaction of the biomolecules.[179] Although this strategy proves a 10-fold sensitivity enhancement for the detection of synthetic zika virus oligonucleotide, the cost of the electrospinning system and the reagents required should be taken into consideration. Moreover, a stability study of the electrospun nanofibers should be performed to determine the expiration time of the test, which is mainly due to the bioreceptors instability over time but also to the materials degradation. In this regard, Katis *et al.* reports a sensitivity enhancement strategy that enables the maintenance of the same materials in LFA, favouring the scale up manufacturing. They reduce the detection area (TL and CL zone) from 5 mm to 1 mm width by laser direct writing (LDW) a polymerised pattern on the nitrocellulose membrane. By narrowing the flow path, they achieve both, an increase in the flow time and a reagents concentration. This enables a 30-fold sensitivity enhancement for the detection of C-reactive protein compared to the assay with no constrictions. As suggested by the authors, LDW has the advantages of being low-cost and non-special laboratory requirements compared to other patterning techniques such as photolithography.[180] However, this fabrication

method still requires extra equipment. In this sense, Prof. Feng Xu and co-workers have developed a non-complicated physical-chemical coupling method based on the addition of a dissolvable saline barrier on the nitrocellulose membrane, as a sensitivity enhancement strategy (Figure 1.7.).
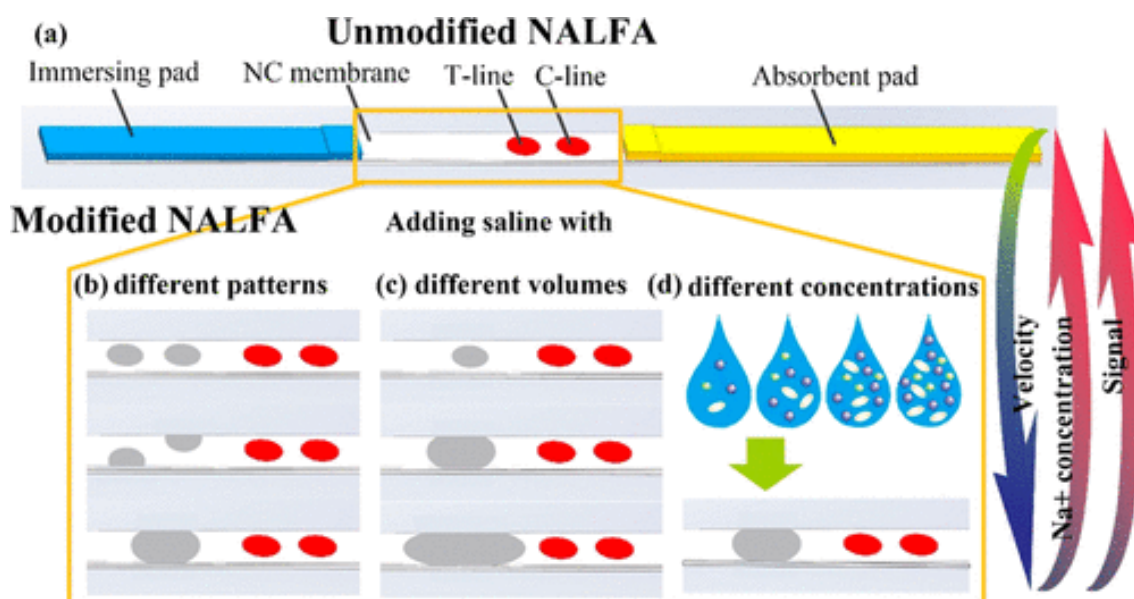
Figure 1.7. (A) Schematic representation of a sensitivity enhancement approach based on the introduction of dissolvable saline barriers in the nitrocellulose membrane. The barriers slow the flow rate and enhance the DNA hybridization efficiency due to the increment in Na^+. Different **(B)** salt barrier patterns, **(C)** salt barrier sizes and **(D)** salt concentrations were evaluated in order to optimize the nucleotide-based LFA (NALFA). Reprinted (adapted) with permission from He, X. *et al.* Sensitivity Enhancement of Nucleic Acid Lateral Flow Assays through a Physical-Chemical Coupling Method: Dissoluble Saline Barriers. *ACS Sensors* **4**, 1691–1700 (2019). Copyright (2019) American Chemical Society.

The salt barrier allows a decrease of the flow velocity and an increase in the Na^+ concentration during the binding reaction. It is extensively reported that the increase in salt concentration improves the association rate constant for the hybridization of nucleic acids. They report a 10-fold sensitivity enhancement for the detection of Hepatitis B virus when introducing a saline barrier based on SSC buffer 16X.[181] This approach is simple and low-cost and doesn't sacrifice much the assay time, however it is only useful for nucleic acid-based LFA since the change of the ionic strength of the assay buffers have a dramatic effect on the binding capabilities of protein-based bioreceptors. Shen

and colleagues have reported another approach based on flow rate modulation for sensitivity enhancement in LFA. Similarly, Rivas *et al.* have proposed the introduction of wax pillars on the beginning of the nitrocellulose membrane to produce a flow delay and generate pseudo-turbulences in the capillary flow. With this simple and low-cost strategy they achieve a 3-fold sensitivity enhancement for H-IgG detection compared to the free-barrier LFA.[146] Contrary to other laborious fluid control methods, the wax patterning of the nitrocellulose membrane requires a fast printing extra step.

Alternatively to the introduction of barriers or spatial constrictions, Shen and colleagues have developed a paper-based assay in which the flow rate is controlled by centrifugal forces instead of by capillary action of the absorbent pad (Figure 1.8.). The authors claim that in the conventional LFA the sample pad absorbs and retains the sample, reducing the effective volume up to 40 μL. Also the capillary force generated by the absorbent pad governs the flow rate.
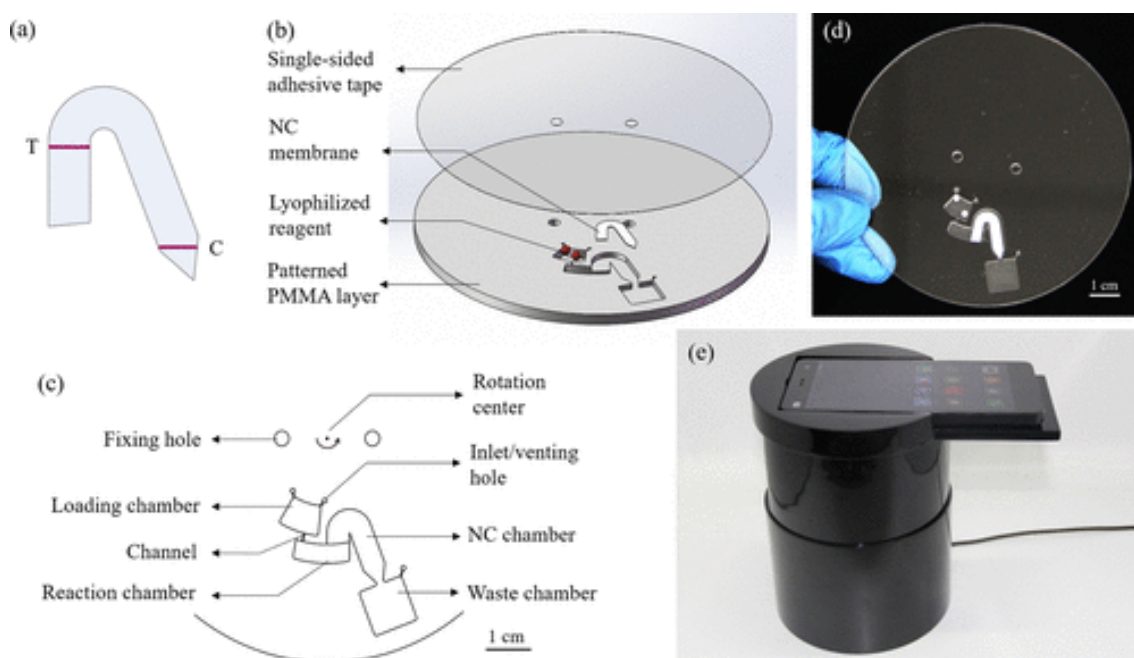
Figure 1.8. Sensitivity enhancement approach based on the flow rate control by centrifugal forces. Schematic representation of **(A)** LFA strip, **(B)** centrifugal disc components and **(C)** disc chambers. Picture of **(D)** centrifugal assisted-LFA platform **(E)** set-up for smartphone-based quantification. Reprinted (adapted) with permission from Shen, M., Chen, Y., Zhu, Y., Zhao, M. & Xu, Y. Enhancing the Sensitivity of Lateral Flow Immunoassay by Centrifugation-Assisted Flow Control. ***Anal. Chem.*** **91**, 4814–4820 (2019). Copyright (2019) American Chemical Society.

Conversely, in the centrifugal assisted LFA a constant rotation speed is adjusted by a portable dedicated device. In this regard, 1500 rpm and 120 μL of sample where used for the detection of prostate specific antigen (PSA) in diluted human serum, showing a 6.2-fold sensitivity enhancement compared to the conventional LFA.[182] This innovative approach shows an interesting and simple way of modulating the physical parameters of the test, however the lack of a dedicated sample pad acting as a filter can limit its application with more complex samples such as whole blood. Also, the assay time (45 minutes) is not adequate for POC applications, in which the results are expected in less than 30 minutes.

Another way to enhance the sensitivity in LFA is by performing sample pre-concentration strategies by using ultrafiltration, solid-phase extraction or isotachophoresis **(ITP)** within others. However, additional steps and extra reagents are usually required, which increase the time, costs and simplicity of the assay. In this context, Prof. Lee and co-workers have developed a LFA with a nafion-based an ICP pre-concentrator integrated in the conjugate pad. They have proved a 26% sensitivity enhancement for the detection of β-hCG by pre-concentrating the sample 15-fold for 8 minutes using a portable 9 V battery.[183] More effectively has been the pre-concentration approach reported by Ren and colleagues in which they achieved a 4000-times sensitivity enhancement for the detection of valosin-containing protein by applying magnetic focusing (Figure 1.9.).
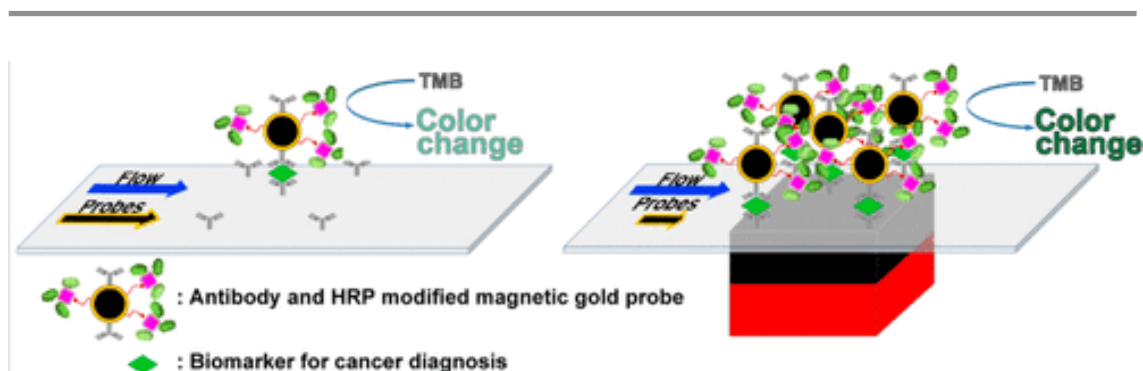
Figure 1.9. Schematic representation of a sensitivity enhancement approach based on sample pre-concentration by magnetic focusing. Reprinted (adapted) with permission from Ren, W., Mohammed, S. I., Wereley, S. & Irudayaraj, J. Magnetic Focus Lateral Flow Sensor for Detection of Cervical Cancer Biomarkers. *Anal. Chem.* **91**, 2876–2884 (2019). Copyright (2019) American Chemical Society.

The application of a magnetic field increases the number of magnetic particles up to 10-fold in the detection zone. The higher concentration of target contributes to enhanced capture efficiency, which in turns improves the assay's sensitivity.[184] This strategy seems ideal apart from the fact that multiple washing steps are required. This makes the assay to be less user-friendly and more prone to error.

Simpler than the pre-concentration strategies, the assay's sensitivity can be improved by increasing the concentration of capture reagents in the TL so as to enhance the binding efficiency. This seems obvious in the first instance, however it is noteworthy that there is a limited protein binding capacity on the nitrocellulose membranes. In order to overcome this limitation, Pan and co-workers devised a way to increase the concentration of antibodies in the TL up to 2.2 mg/mL avoiding the enlargement of the TL area. They took advantage of the high surface-to-volume ratio of the AuNPs to conjugate a great amount of antibodies and fix them in the TL. In this way, they achieved a 100-fold sensitivity enhancement for the detection of *C. sakazakii* compared to the conventional LFA.[185] This approach might seem ideal due to its simplicity, however it has two big limitations. On the one hand, the use of higher amounts of bioreceptors makes the assay more expensive and LFA has as main asset being a low-cost alternative to conventional analytical tests. On the other hand, the signal appearance in TL before performing the assay can definitely hinder the interpretive capacity of the end-user, who is used to relate a signal change with the presence of the target analyte. Similarly, Parolo *et al.* reported a 8-fold limit of quantification enhancement for H-IgG detection by allowing the application of higher amount of sample volume on the strip, which implies more quantity of the target analyte. This was achieved by the enlargement of three times the width of the sample and conjugate pad compared to the conventional LFA. It is noteworthy that the enlargement of the sample pad produces an increase in the flow velocity, which is not beneficial in terms of binding kinetics. Therefore, the enlargement of the conjugate pad provides a bigger amount of conjugated bioreceptors and compensates the consequent increase in the flow speed. This strategy is simple and can be easily implemented for any application without the need of changing the fabrication method.[186] However, it would have been interesting to report the sensitivity enhancement in terms of the curve slope rather than the LoQ improvement, so as to perform a more precise comparison between techniques.

Despite the flow control strategies, much research has been to find alternative signal transducers for the sensitivity enhancement in LFA. This includes carbon-nanotubes (CNTs), fluorescent nanoparticles, quantum dots, up-converting materials, among others. Sun *et al.* reported a 10-fold sensitivity enhancement for methamphetamine detection by using multi-walled carbon nanotubes (MWCNTs) instead of AuNPs. Firstly, CNTs posses more binding sites than AuNPs due to their greater surface area. This enables the functionalization of more bioreceptors per label, which in turn provides enhanced detection sensitivity. Secondly, CNTs provide a black colour signal against the white background. This outstanding signal contrast is more suitable for image analysis.[187] MWCNTs solve the instability limitations characteristic of the single-walled CNTs, however the preparation and conjugation of the MWCNTs remains more challenging than the one for AuNPs. QDs-based LFAs are widely reported as highly sensitive due to the narrow emission peak of the QDs and their elevated quantum yield.[158] However, their use in PoC applications is limited due to the requirement of dedicated fluorescent readers. Nevertheless, portable solutions are being developed, such as the use of a phone-based fluorometer.[188] In this sense, the use of UCNPs as fluorescent reporters in LFA enables ultralow detection limits and simpler reader instruments, as the excitation of the nanoparticles can be done with an affordable infrared laser diode.[189] Although fluorescent-based LFAs are known to be highly sensitive, no reports have been found determining the achieved sensitivity enhancement compared to the common colloidal gold nanoparticles-based LFA. The published works just take into consideration the outstanding LoDs that allow the detection of tracer analytes.[190–192]

Signal amplification is also a well-known strategy for sensitivity enhancement in LFA. There are several ways to perform signal amplification, although the most reported ones are AuNPs enlargement through silver staining and coating the AuNPs with enzymes or catalytic metals.[193] The former has been applied for the detection of Troponin I by the integration of water-soluble hybrid nanofibers between the conjugate pad and the TL. Once the AuNPs bind at the TL, the silver enhancement reagents are released from the nanofibers and are reduced to metallic silver around the AuNPs. The darkening of TL enables a 10-fold sensitivity enhancement.[194] The integration of the signal amplification reagents in the LFA strip is the most interesting of this approach, without sacrificing the assay time and simplicity of the test. The latter has been performed with horseradish

peroxidase (HRP) and alkaline phosphatase (ALP). These are the traditionally used enzymes in ELISA due to their commercial availability, high stability and catalytic properties. Parolo *et al.* achieved one order of magnitude sensitivity enhancement for the detection of H-IgG by the conjugation of the AuNPs with anti-HIgG antibodies and HRP. Different substrates where evaluated, but 3,3',5,5'-tetramethylbenzidine (TMB) resulted the best in terms of sensitivity achieved, low cost and its ready-to-use property.[195] However, multiple washing steps where required, which reduces its applicability at the PoC. Moreover, it is reported that the presence of HRP inhibitors or interfering components in the real sample's matrix reduces the HRP enhancement effectiveness. In this sense, Panferov and co-workers decorated the AuNPs with ALP and obtained a 10-fold sensitivity enhancement for the detection of potato virus X in leaf extracts. The authors claim that the enhanced LFA preserves the major advantages of the conventional LFA; 15 minutes assay-time, no additional equipment is required and no need of assay manipulation, as all the components are in a dry form.[196] However, the substrate addition step is still required to perform the signal amplification. The signal amplification can also be performed by catalytic metals as in the case of conventional AuNPs coated with ultrathin Pt skins. The Pt shells have ultrahigh peroxidase-like catalytic activity and enable the generation of blue colour by the oxidation of TMB. This approach enables a 100 times sensitivity enhancement for the detection of PSA, due to the large molar extinction coefficient of the blue-coloured product generated in TL (Figure 1.10.). The authors also proved the strategy feasibility on human plasma samples, demonstrating that the complex matrix did not hinder the catalytic activity of the Pt shells.[197]
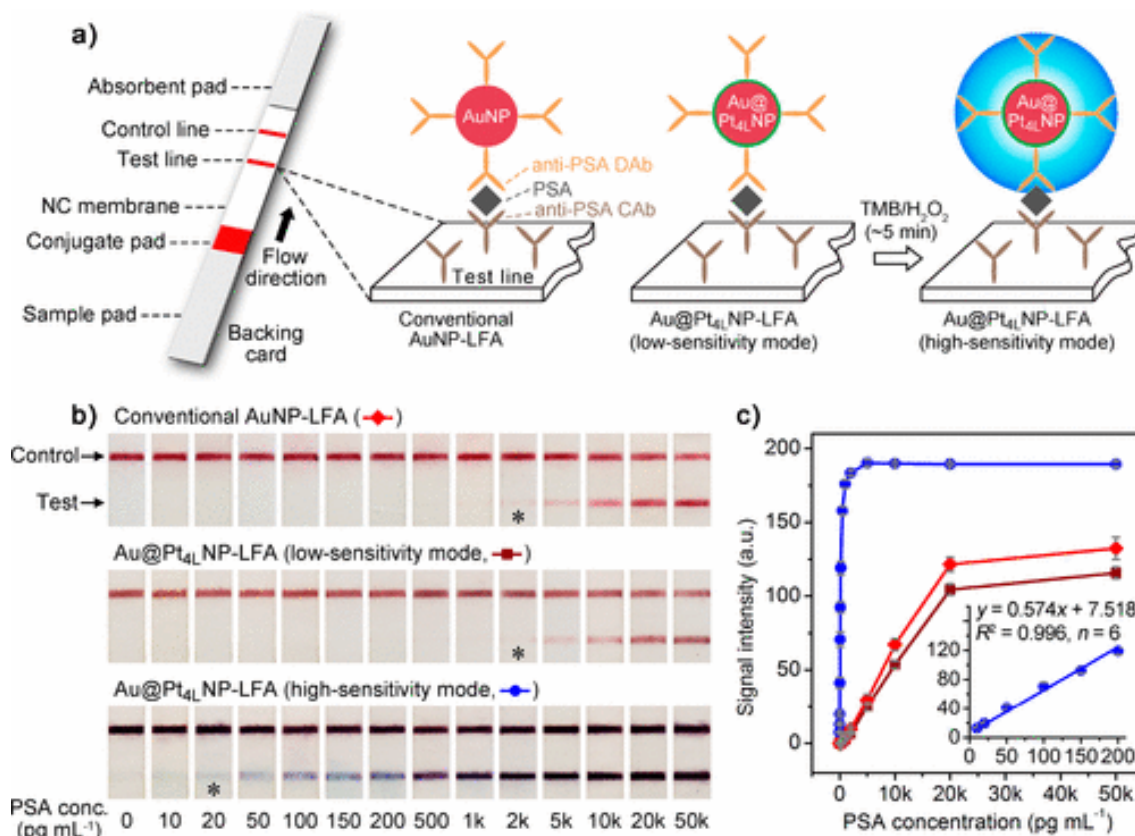
Figure 1.10. (A) Schematic representation of a sensitivity enhancement approach based on signal amplification using AuNPs decorated with ultrathin Pt skins. Blue colour is generated in TL upon oxidation of TMB catalysed by the Pt. **(B)** Picture of LFA strips for detection of PSA using conventional AuNPs, AuNPs decorated with Pt ultrathin skins (Au@Pt$_{4L}$) and Au@Pt$_{4L}$ with TMB substrate. The latter condition enables the highest sensitivity **(C)** Calibration curves for the three conditions: AuNPs (in light red), Au@Pt$_{4L}$ (in dark red) and Au@Pt$_{4L}$ with TMB (in blue). The latter condition provides a curve with the highest slope. Reprinted (adapted) with permission from Gao, Z. *et al.* Platinum-Decorated Gold Nanoparticles with Dual Functionalities for Ultrasensitive Colorimetric in Vitro Diagnostics. ***Nano Lett.*** **17**, 5572–5579 (2017). Copyright (2017) American Chemical Society.

Other researchers have focused in increasing the signal-to-noise ratio as a strategy for sensitivity enhancement in LFA. Prof. Yager and colleagues have developed a simple quantitative framework to select low-fluorescence substrates. It is well known that most commercial porous membranes emit auto-fluorescence in the blue, yellow and green regions of the visible spectrum. They proved that the use of materials with lower auto-fluorescence could help to enhance the sensitivity of the LFA.[198] In addition, Li *et al.*

has reported a 1000-fold sensitivity improvement in the detection of bacteriophage λ-DNA by the integration of a graphene oxide-based purification step in LFA. After the PCR amplification, the graphene oxide immobilized in the stacking pad is capable of removing the residual primers that compete with the amplicons for the binding sites in the TL (Figure 1.11.).
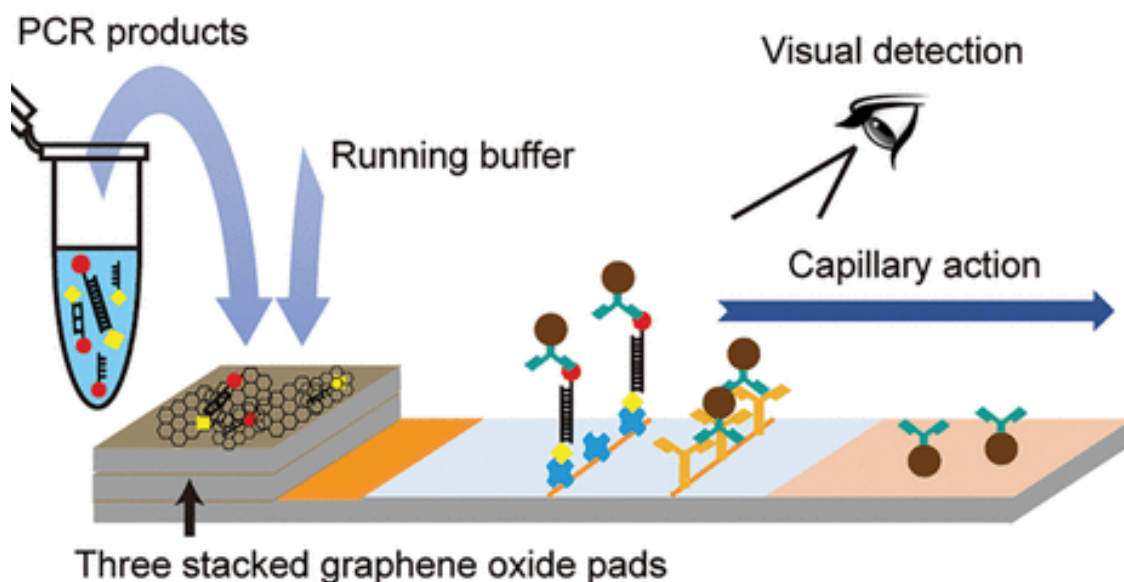
Figure 1.11. Schematic representation of a sensitivity enhancement approach based on the increment of the signal-to-noise ratio. The graphene oxide is able to selectively remove the residual primers, which compete with the amplicons to bind to the TL. Reprinted (adapted) with permission from Li, S., Gu, Y., Lyu, Y., Jiang, Y. & Liu, P. Integrated Graphene Oxide Purification-Lateral Flow Test Strips (iGOP-LFTS) for Direct Detection of PCR Products with Enhanced Sensitivity and Specificity. *Anal Chem.* **89**, 12137–12144 (2017). Copyright (2017) American Chemical Society.

This is achieved due to the adsorption capability of the graphene oxide to single-stranded DNA. Moreover, the possibility of false positive results is reduced due to the selective removal of the primer-dimers. This approach is easy-to-use and inexpensive, however, as suggested by the authors it would be ideal to also integrate the nucleic acid extraction and PCR amplification, so as to resolve the contamination issues of the current "open-tube" detection in the strip.[199]

The use of alternative detection methods has been exploited for the sensitivity enhancement in LFA. For instance, Wang and co-workers have applied thermal contrast amplification (TCA) analysis, proving a 8-fold sensitivity enhancement for the detection

of influenza, malaria and *C. difficile,* compared to gold colorimetric visual signal. Matching the laser wavelength to the AuNPs plasmon resonance peak generates heat that is correlated to the AuNPs concentration in the TL. The main limitations of this approach is the current cost of the TCA reader (around $18000), the influence of the environmental temperature on the assay's signal, which requires careful calibration and the appearance of false positive results (that did not occur with visual contrast).[200] Moreover, Zhao *et al.* have proved that by performing photoacoustic (PA) analysis of the LFA assay the sensitivity could be improved 100-fold in comparison to colorimetric measurements for the detection of Cryptococcal antigen (CrAg). The PA detection method includes three steps: the light absorption by the AuNPs, the conversion of the absorbed energy into heat and the heat-induced thermal expansion of the air that generates pressure oscillations. The advantages of performing PA analysis don't just rely on the outstanding signal generation but also to the noise reduction, due to the different energy domains of the input and output signal. However, as discussed by the authors, this strategy is still limited by the high price of the PA detector and oscilloscope required to perform the PA analysis. They are currently working in the miniaturization and cost-reduction of the detection system, aiming for its application in resource-limited settings.[201] Furthermore, Wang and colleagues have developed a surface-enhanced Raman scattering (SERS)-based LFA as a sensitivity enhancement strategy. They have designed Fe_3O_4@Ag magnetic nanoparticles loaded with DTNB dyes for dual magnetic sample pre-concentration SERS signal generation. With this strategy they have achieved a 2000-fold sensitivity enhancement for the detection of H1N1 and HAdV viruses, compared to the conventional AuNPs-based LFA (Figure 1.12.).[202] Although, the approach is versatile, highly sensitive and the signal quantification is performed with a portable SERS reader, the magnetic concentration step is not user-friendly. Moreover, it would be interesting to determine the sensitivity enhancement obtained individually with the SERS detection and the magnetic concentration, to evaluate the impact of the pre-concentration on the assay's improvement.
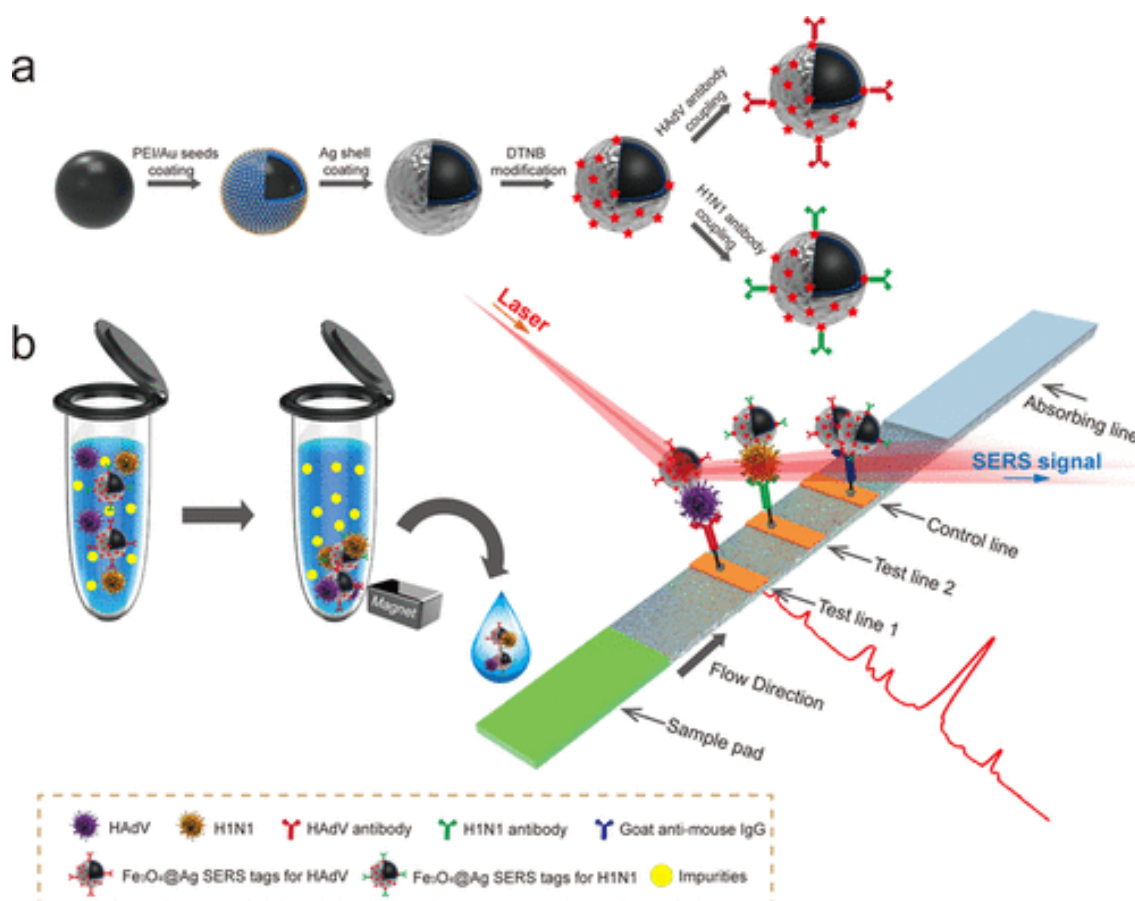
Figure 1.12. Schematic representation of a sensitivity enhancement approach based on **(A)** Fe$_3$O$_4$@Ag magnetic nanoparticles loaded with DTNB dyes and **(B)** dual magnetic sample concentration and SERS detection of two respiratory viruses. Reprinted (adapted) with permission from Wang, C. *et al.* Magnetic SERS Strip for Sensitive and Simultaneous Detection of Respiratory Viruses. ***ACS Appl. Mater. Interfaces*** **11**, 19495–19505 (2019). Copyright (2019) American Chemical Society.

Table 1.3. Comparison of the sensitivity enhancement strategies reported for LFA.

Strategy	Method/material	Detection of	Enhancement	Comp. to	Ref.
Flow rate decrease	Displacing the TL 12 mm from origin	hCG	2.5-fold	Conv. LFA	178
Flow rate decrease	Hydrophobic PCL nanofibers	Synthetic zika virus	10-fold	Conv. LFA	179
Flow rate decrease & reagents concentration	Reduce detection area from 5 mm to 1 mm	C-reactive protein	30-fold	Conv. LFA	180

Table 1.3. Cont. Comparison of the sensitivity enhancement strategies reported for LFA.

Strategy	Method/material	Detection of	Enhancement	Comp. to	Ref.
Flow rate decrease & increase DNA hybrid. effi.	Dissolvable saline barrier	Hepatitis B virus	10-fold	Conv. LFA	181
Flow rate decrease & Pseudo-turbulence generation	Wax pillars	H-IgG	3-fold	Conv. LFA	146
Flow control	Centrifugal forces	PSA	6.2-fold	Conv. LFA	182
Sample pre-concentration	Nafion-based ICP	β-hCG	3.9-fold	No pre-conc.	183
Sample pre-concentration	Magnetic focusing	Valosin-containing protein	4000-fold	No pre-conc.	184
Increase antibodies conc.	Fixing conj. AuNPs in TL	*C. sakazakii*	100-fold	Conv. LFA	185
Increase sample volume	3X width increase of sample and conj. pad	H-IgG	8-fold	Conv. LFA	186
Increase signal contrast	MWCNTs	Meth.	10-fold	AuNPs-LFA	187
Signal amplification	Silver staining of AuNPs	Troponin I	10-fold	AuNPs-LFA	194
Signal amplification	AuNPs coated with HRP	H-IgG	10-fold	AuNPs-LFA	195
Signal amplification	AuNPs coated with ALP	Potato virus X	10-fold	AuNPs-LFA	196
Signal amplification	AuNPs coated with ultrathin Pt skins	PSA	100-fold	AuNPs-LFA	197

Table 1.3. Cont. Comparison of the sensitivity enhancement strategies reported for LFA.

Strategy	Method/material	Detection of	Enhancement	Comp. to	Ref.
Increase signal-to-noise ratio	Integration of a graphene oxide-based purification step	λ-DNA	1000-fold	Conv. LFA	199
Alternative detection methods	Thermal contrast amplification analysis	Influenza, malaria & *C. difficile*	8-fold	AuNPs-LFA	200
Alternative detection methods	Photoacoustic analysis	Cryptococcal antigen	100-fold	AuNPs-LFA	201
Alternative detection methods	Surface-enhanced Raman scattering	H1N1 & HAdV viruses	2000-fold	AuNPs-LFA	202

1.4.1.2. Multiplexing

Multiplexing strategies in LFA include the introduction of multiple test lines, the use of multiple strips, the application of signal transducers with different output signal domains or the combination of these approaches.

1.4.1.2.1. Multiple test lines

The simplest strategies are based on the immobilization of multiple TLs in series, although this limits the number of target analytes that can be detected. Zheng and colleagues have developed a LFA for the simultaneous detection of **micro-RNA-21, -155 and -210** cancer biomarkers in human serum. They have achieved this by the introduction of three TLs on different zones of the nitrocellulose membrane (Figure 1.13.). In order to overcome cross-reactivity issues, the ssDNA probes where carefully designed and optimized for the specific detection of the miRNAs of interest.[203]
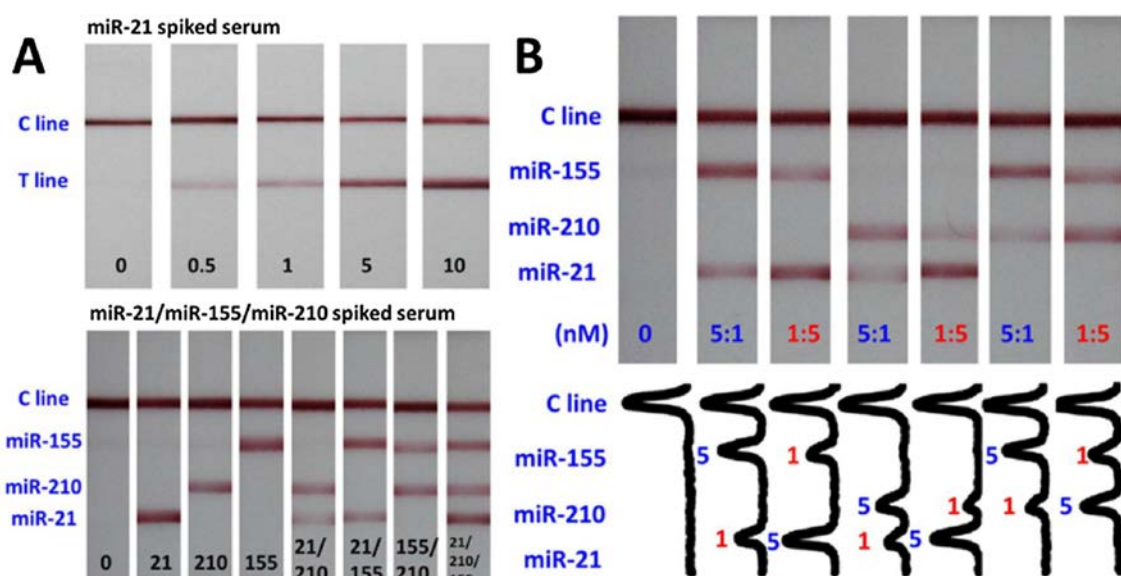
Figure 1.13. Multiplexing strategy based on three TLs in series. **(A)** Pictures of conventional LFA strips for detection of one target analyte (miR-21). **(B)** Pictures of LFA strips for the detection of 3 target analytes (miR-21, miR-210 and miR-155). Reprinted (adapted) with permission from Zheng, W. *et al.* Lateral Flow Test for Visual Detection of Multiple MicroRNAs. ***Sens Actuators B Chem.*** **264**, 320–326 (2018). Copyright (2019) American Chemical Society.

Similarly, Crannell *et at.* have combined a Recombinase Polymerase Amplification (RPA) technique with a triple-TL LFA for the detection of DNA from *Giardia*, *Cryptosporidium* and *Entamoeba* parasites in stool samples. RPA enables the amplification of the different DNA targets, which are present at very low concentrations in real samples. The advantages of using RPA in comparison to other isothermal amplification platforms are that their enzymes don't require refrigeration and that RPA is tolerant to inhibitors present in the sample.[204] However, this strategy is limited by the fact that the RPA step is not integrated in the LFA strip, making the assay less user-friendly and more prone-to-error. Moreover, one of the challenges when performing multiplex detection in LFA is to achieve a broad signal that can encompass concentrations in a wide range, especially when the working ranges of the target analytes differ in orders of magnitude. In this sense, Zhang and colleagues have proposed the use of SERS nanotags as transducers, since they are able to provide ultra-sensitive signals and wide linear dynamic range. They have developed a triple-TL LFA using silver core and gold shell NPs loaded with Nile blue A dye ($Ag^{NBA}@Au$) as

labels, for the detection of Myo, cTnI and CK-MB cardiac biomarkers in human serum. By the use of SERS detection method, the assay was able to effectively cover the concentration of the three markers, which spans 6 orders of magnitude.[205] However, the authors don't give details on the cost and portability of the Raman microscope system used to evaluate the strips. It would be interesting to compare the fabrication procedure complexity and production-related costs of the SERS nanolabels to ones for conventional AuNPs. Furthermore, Lee and colleagues have developed a triple-TL LFA with a 100% clinical sensitivity and specificity for the detection of antibodies specific to HIV, HCV and HAV antigenic peptides in patient sera. They have achieved this by fixing in the TL proteinticle-based 3D probes, which display the antigenic peptides on the surface in a homogeneous orientation and conformation. This is an alternative to the direct fixation of the peptides on the TL that presents limitations such as uncontrolled orientation, clustering, inactivation or instability of the peptides, which can reduce the accuracy of the assay.[206]

The main drawback of the multiplexing strategies based in the incorporation of several TLs in series is the limited length of the test strip, which restricts the amount of TLs and target analytes to be detected. Increasing the length of the test strip would support the fitting of more TLs, however this would make the assay more expensive as more quantity of reagents would be required. Moreover, taking in consideration the theory of Washburn, the assay time would increase exponentially as further is the TL from the sample pad.[207] Therefore it is more reasonable to implement other strategies for the detection of higher amount of analytes without sacrifying the advantages of LFA. In this sense, Xu *et al.* proposes the combination of fluorescence colour and physical position in order to achieve the detection of up to 13 human papillomavirus types (16, 18, 31, 33, 35, 39, 45, 51, 52, 56, 58, 59 & 68) in a single step. They included 7 TLs, each one holding two different capture probes and they used two different labels FAM and ROX (Figure 1.14.). Interestingly, the specificity results showed no cross-reactivity among the different HPV types.[208] Usually, cross-reactivity is one of the reasons of the low sensitivity of the multiplex LFA compared to the single-plex. In this sense, it is imperative to select the bioreceptors that lack of cross-reactivity when developing multiplex LFA, usually monoclonal antibodies, which are more specific than polyclonal antibodies, aptamers or molecular imprinted polymers.
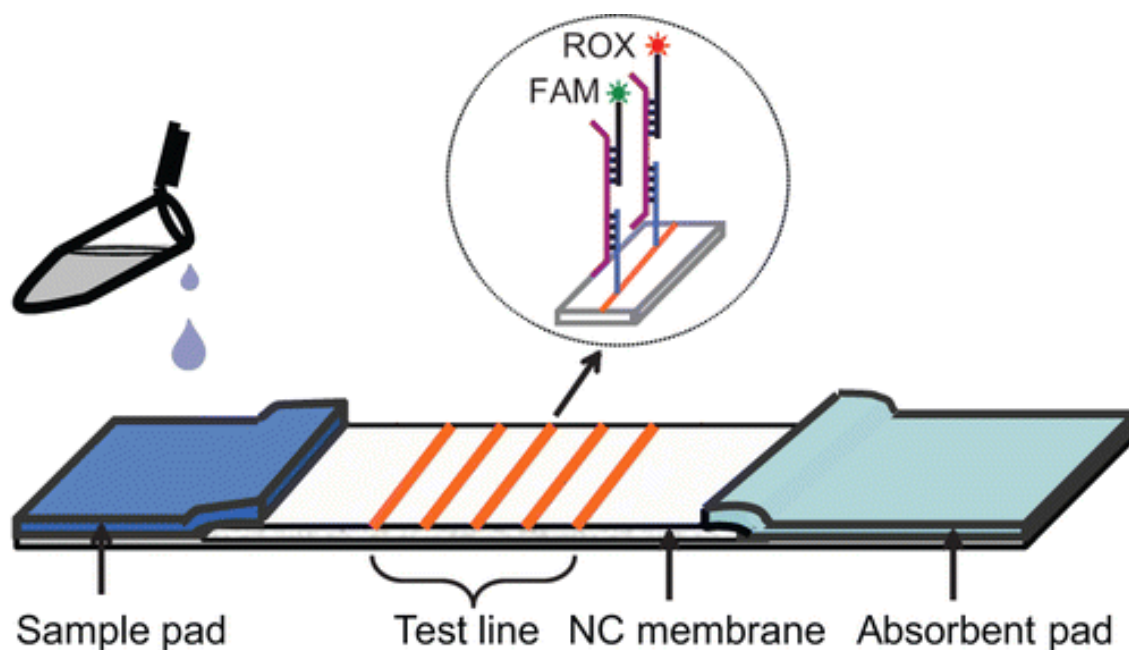
Figure 1.14. Schematic representation of a multiplex LFA based on four TLs in series and two fluorophores (ROX and FAM) as signal transducers. Reprinted (adapted) with permission from Xu, Y. *et al.* Fluorescent probe-based lateral flow assay for multiplex nucleic acid detection. ***Anal Chem.*** **86**, 5611–4 (2014). Copyright (2014) American Chemical Society.

1.4.1.2.2. Multiple dots

Alternatively to the use of detection lines, the capture reagents can be spotted in the nitrocellulose membrane. The reduced area of the spots/dots compared to the lines enables the fixation of more capture reagents and thus the detection of more target analytes in a single step. For instance, Gomez-Martinez and co-workers have developed a multiplex LFA for the detection of 7 DNA alleles (FY*01, FY*02, FY02N.01, GYPB*03, GYPB*04, JK*01 & JK*02) related to four blood group single nucleotide polymorphisms (SNPs). They achieved this by the manual spotting of 8 capture oligonucleotide probes in the nitrocellulose membrane (one spot corresponded to the control zone (Figure 1.15.). The alleles where previously amplified directly from the whole blood samples by LATE-PCR using biotin-labelled primers. Once the PCR product was drop-casted onto the sample pad, the amplified alleles where detected by anti-biotin antibodies conjugated to AuNPs.[209] Although the approach is attractive in terms of direct detection using whole blood samples without the need of DNA extraction, there are two aspects to take into consideration.
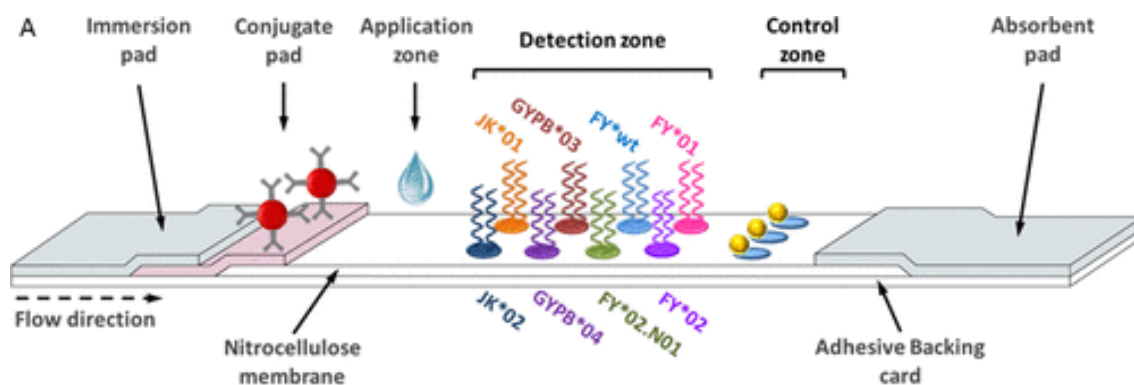
Figure 1.15. Schematic representation of a multiplex LFA based on 8 detection dots and antibody-functionalized AuNPs for the detection of 7 DNA alleles. Reprinted (adapted) with permission from Gomez-Martinez, J. *et al.* Multiplex Lateral Flow Assay for Rapid Visual Blood Group Genotyping. ***Anal Chem.*** **90**, 7502–7509 (2018). Copyright (2018) American Chemical Society.

Firstly, the capture bioreceptors were deposited manually on the detection pad and this might provide lower reproducibility compared to the use of a dedicated reagent dispenser. Secondly, the use of anti-biotin antibodies as bioreceptors for all the 7 amplified alleles might present cross-reactivity issues upon the generation of non-specific biotinylated amplicons (produced by PCR contamination). More effectively, Taranova et al. succeeded in the deposition of up to 32 microarray spots in the nitrocellulose (NC) membrane. The membrane functionalization was performed with a steel pin able to precisely deposit 20 nL of the capture reagent in the NC. However, although 32 spots where deposited, the assay was applied for the detection of just 4 analytes (morphine, amphetamine, methamphetamine and benzoylecgonine) in urine.[210]

1.4.1.2.3. Multiple test lines/dots and labels

The difficulty to interpret multiple spots with variable colour intensities can be overcome by the use of different coloured probes. In this sense, Lee and colleagues have developed a multiplex LFA based on red and blue latex beads for the detection of IgG and IgM related to Dengue (DENV) and Chikungunya (CHIKV). The blue and red latex beads are conjugated with anti-IgG and anti-IgM antibodies, respectively. In order to discriminate the pathogen specificity, two spatially separated TLs associated with DENV and CHIKV are dispensed in the nitrocellulose membrane. Therefore the developed LFA enables a 4-plex detection in which the appearance of purple colour in

either TL indicates the presence of both IgG and IgM pathogen-specific antibodies in the sample. The quantitative evaluation of the strips is performed with smartphone camera and an image analysis software. In this regard, the strips are analysed considering the hue (H) intensities, as this is more precise than RGB values.[211] Similarly, Anfossi *et al.* have employed AgNPs, spherical and desert-rose-like AuNPs with SPR peaks at 420, 525 and 620 nm, respectively, in order to developed a multiplex LFA for detection of casein, ovalbumin and hazelnut allergenic proteins in commercial biscuits. The LFA comprises three lines, each responsive for one allergen. The possible cross-reactivity of the monoclonal antibodies was evaluated by TEM and direct assays. Both confirmed the lack of interference between the selected monoclonal antibodies. Interestingly, the authors where required to increase the concentration of AgNPs in the conjugate pad compared to the used for the AuNPs. The reason was not related to the differences in affinity of the antibodies but to the lower extinction coefficient of the yellow coloured AgNPs. Therefore the optical density of the AgNPs was increased when preparing the mixture of conjugated labels. The most interesting aspect of this approach is the colour code used: cyan/casein, yellow/ovalbumin, magenta/hazelnut proteins, which simplifies the interpretation of the assay's result by the non-experienced end-user.[212] However, it would have been attractive to reduce the test detection areas from three to one by combining the analyte-specific capture reagents in a single TL.

1.4.1.2.4. Multiple labels in single test line

This has been reported by Yen and colleagues, who have took advantage of the size-dependent optical properties of AgNPs to develop a multiplex LFA for the detection of dengue virus dengue virus (DENV) NS1 protein, Yellow fever virus (YFV) NS1 protein and Ebola virus (ZEBOV) glycoprotein. The three monoclonal capture antibodies where mixed at equal concentrations and deposited in a single TL and the conjugated pad was loaded with a mixture or antibody-functionalized orange, red and green AgNPs. In this sense, the presence of the three proteins in sample resulted in a brown colour signal in TL. Quantification analysis was performed using a smartphone camera followed by RGB analysis.[168] The multiplexed detection in a single TL favours the miniaturization of the strip and the possibility to detect a higher amount of analytes by the incorporation of more detection lines or coloured labels. Similarly, Zhang *et al.* have developed a multiplex strategy based on the detection of CK-MB, cTnI and Myo cardiac biomarkers in a single TL. Instead of colorimetric AgNPs they used monoclonal antibodies-

functionalized silver core and gold shell NPs loaded with Methylene blue (MB), Nile blue A (NBA) and Rhodamine 6G (R6 G) Raman dyes (Figure 1.16.). Performing the detection in a single TL resulted in several advantages, such as cost reduction and a 3-fold lower detection time due to the requirement of a single SERS signal acquisition. In addition, the use of SERS detection method provided ultra-high sensitivity detection in clinical serum samples.[213]

Figure 1.16. Schematic representation of a multiplex LFA based on SERS nanotags for the detection of three cardiac biomarkers (CK-MB, cTnI and Myo) in a single TL. Reprinted (adapted) with permission from Zhang, D. *et al.* Quantitative detection of
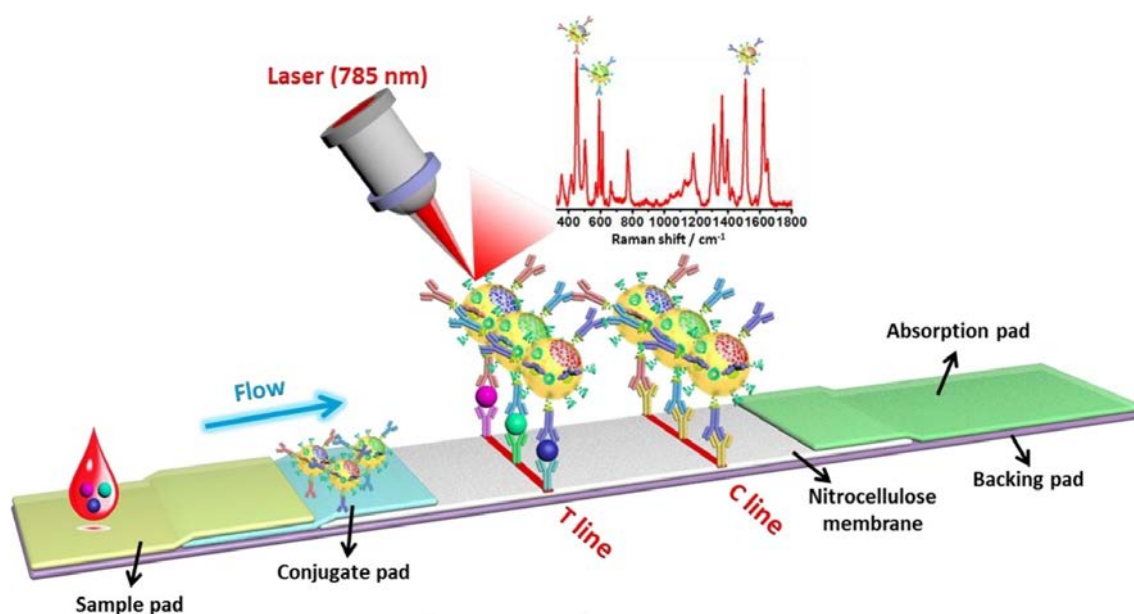
multiplex cardiac biomarkers with encoded SERS nanotags on a single T line in lateral flow assay. *Sensors Actuators B. Chem.* **277**, 502–509 (2018). Copyright (2018) ELSEVIER.

1.4.1.2.5. Multiple strips

Multiplexing can also be extended to the compilation of several test strips within a single sample pad, as reported by Zhao and co-workers, who have developed a multiplex strategy based on 10-channel lateral flow assay for the detection of 10 epidemic foodborne pathogens (E. *coli* O157:H7, S. *paratyphi* A, S. *paratyphi* B, S. *paratyphi* C, S. *typhi*, S. *enteritidis*, S. *choleraesuis*, V. *cholera* O1, V. *cholera* O139 and V. *parahaemolyticus*) in food samples. Each conjugate pad was prepared with bacteria-specific monoclonal antibodies conjugated to up-converting phosphor nanoparticles. Specificity studies where performed, indicating the lack of interference

between the monoclonal antibodies. The approach showed 100% consistency with culture-based detection methods when evaluating 279 real food samples. However, the use of multiple strips for multiplexing assays has an important limitation regarding the requirement of higher sample volumes. In this case the authors drop-casted 700 μl of the sample onto the sample pad, which is more or less 7 times more amount of volume than the required in a single strip of conventional dimensions (6x0.05 cm).[214] In addition, the strategies based on two-dimensional shaping, as the one reported previously, might have challenges when performing quantification. The wide distribution of the test zones is not compatible with the commercially available LFA readers. In this sense, Orlov and colleagues have developed a multiplexing strategy based on the use of three individual LFA strips that were interrogated by a single processor unit. Magnetic nanoparticles functionalized with monoclonal antibodies were used for the detection of botulinum neurotoxin (BoNT) types A, B and E in whole milk and juices (Figure 1.17.).
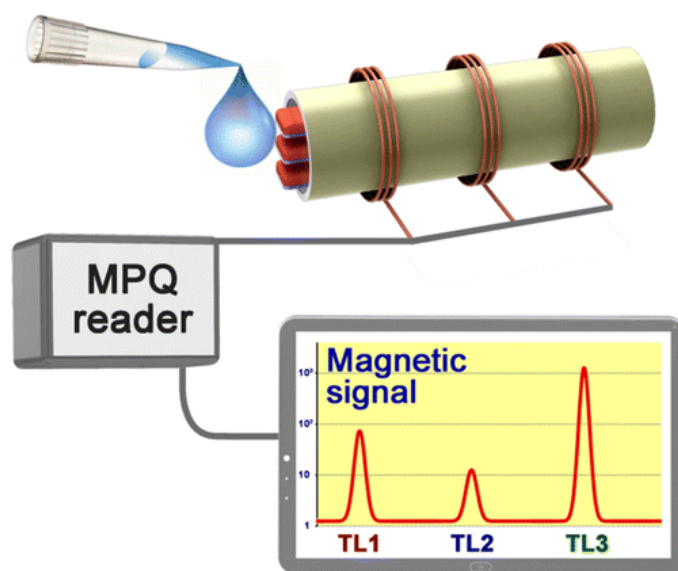
Figure 1.17. Schematic representation of a multiplex LFA based on magnetic particle quantification of three botulinum neurotoxins using three strips interrogated simultaneously by a single processor unit. Reprinted (adapted) with permission from Orlov, A. V., Znoyko, S. L., Cherkasov, V. R., Nikitin, M. P. & Nikitin, P. I. Multiplex Biosensing Based on Highly Sensitive Magnetic Nanolabel Quantification: Rapid Detection of Botulinum Neurotoxins A, B, and E in Liquids. *Anal Chem.* **88**, 10419–10426 (2016). Copyright (2016) American Chemical Society.

The three strips were introduced in a cartridge that enables highly sensitive detection based on magnetic particle quantification (MPQ).[215] The advantages of this technology compared to multiplexing strategies in single strip are the elimination of cross-reactivity issues and the ability to analyse opaque mediums. However, this approach still requires three-times more sample volume than the single-strip assay. Moreover, the price of the MPQ reader and the complexity of the results interpretation by the end-used must also be taken in consideration.

Table 1.4. Comparison of the multiplexing strategies reported for LFA.

Strategy	Transducer	# anal.	Detection of	Sample	Ref.
Multiple TLs	AuNPs	3	miRNA -21, -155 & -210	Human serum	203
Multiple TLs	AuNPs	3	*Giardia, Cryptosporidium & Entamoeba*	Stool	204
Multiple TLs	Ag^{NBA}@Au SERS NPs	3	Myo, cTn1 & CK-MB	Human serum	205
Multiple TLs	AuNPs	3	Anti-HIV, HCV and HAV antibodies	Human serum	206
Multiple TLs & 2 labels	FAM & ROX fluorophores	13	HPV (16, 18, 31, 33, 35, 39, 45, 51, 52, 56, 58, 59 & 68)	Cervical swab	207
Multiple dots	AuNPs	7	DNA alleles (FY*01, FY*02, FY02N.01, GYPB*03, GYPB*04, JK*01 & JK*02) related to four blood group SNPs	Whole blood	208
Multiple dots	AuNPs	4	Morphine, amphetamine, methamphetamine & benzoylecgonine	Urine	209
Multi TLs & 2 labels	Red and blue latex beads	4	IgG and IgM specific to DENV and CHIKV	Whole blood	211
Multi TLs & 3 labels	AgNPs, spherical & desert rose-like AuNPs	3	Casein, ovalbumin & hazelnut allergenic proteins	Biscuits	212

Table 1.4. Cont. Comparison of the multiplexing strategies reported for LFA.

Strategy	Transducer	# anal.	Detection of	Sample	Ref.
Single TL & 3 labels	Orange, red and green AgNPs	3	DENV NS1 protein, YFV NS1 protein & ZEBOV glycoprotein	-	168
Single TL & 3 labels	Ag^{NBA}@Au, Ag^{MB}@Au & Ag^{R6G}@Au SERS nanotags	3	CK-MB, cTnI & Myo cardiac biomarkers	Human serum	213
Multiple strips	UCP nanoparticles	10	*E. coli* O157:H7, *S. paratyphi A, S. paratyphi B, S. paratyphi C, S. typhi, S. enteritidis, S. choleraesuis, V. cholera O1, V. cholera O139 & V. parahaemolyticus*	Food samples	214
Multiple strips	Magnetic nanolabels	3	BoNT-A, -B, & -E	Milk, Apple & Orange juices	215

1.4.1.3. Quantification at the point-of-care

LFA has experienced a progression in the way to perform quantification, from bench top instruments towards point-of-care devices. Cozart Biosciences Ltd. has been one of the first companies to produce a device for LFA quantification, the Cozart RapiScan a hand-held instrument with integral reader and microcontroller. The device uses a complementary metal-oxide semiconductor (CMOS) sensor to capture the light signal from TL and convert it into electrical signal. The imaging array coupled to the microprocessor is able to interpret the shaded variations of the TL and provide an electronic measurement, which is related to the concentration of target analyte in the sample.[101,186,195] However, a self-calibration must be performed using the system test cartridge.[216] Moreover, the position of lines in the strip must not be varied since the image array system is fixed. Qiagen came up with ESE Quant benchtop lateral flow readers, which despite relying on a software PC to carry out the evaluation, it can precisely measure the absorbance at 520 nm for AuNPs-based LFA and the wavelength emission at 650/520 nm when using red and green fluorescent labels.[217] Several

research articles have been published regarding the quantitative evaluation of LFA with ESE Quant reader.[94,118,218]

It has been the development of the smartphone-based lateral flow readers that has allowed the quantitative evaluation of LFA in a point-of-care context.[219] The smartphone has become part of our day-to-day; according to the Global system for Mobile Communications (GSMA) real time intelligence data, 66,53% of the world's population own an smartphone.[220] Smartphones are part of the daily life of citizens; they are taken everywhere and serve as a form of instant communication, breaking the geographical barriers. Currently, smartphones are miniaturized computers, with large random access memory, high speed CPU, sophisticated camera lenses and Wi-Fi network.[149] Thus, it is not strange to think that smartphones can be the key for personalized medicine, particularly the outcome of an assay can quantitatively evaluated at any moment and time. Additionally, the end-user can store the results and eventually transfer them to the doctor for precise diagnosis.[148,149]

In recent years, many reports have been published the possibility to perform quantitative evaluations of LFA with smartphones. For instance, Jung *et al.* have developed a smartphone-based colorimetric reader consisting in a 3D printed smartphone holder and a customized Android app for data analysis. The former contains a smartphone cradle that provides 3X amplification, a reflector that redirects an LED light onto the strip and diffuser used to spread the light all over the strip. The latter processes the image and creates a polynomial fitted curve. For unknown samples, the app estimates the concentration of target analyte by comparing the intensity value in TL to the calibration curve. The high-resolution smartphone camera (with CMOS sensor) together with the constant illumination during image acquisition enabled a consistent and repeatable imaging of the LFA strips. A LoD of 10^4 CFU/mL was achieved for the detection of *E. coli* O157:H7 in grounded beef without sample enrichment.[221] Moreover, Quesada and co-workers have developed a smartphone-based quantification system for the detection of H-IgG using colorimetric LFA. Pictures of the strips were taken with the smartphone camera (Motorola "Moto Z") and a 3D printed support was used to keep constant the distance between the smartphone and the strips. In this case, the light conditions were kept constant by taking the photographs in a controlled light environment. Finally, the images were analysed with Image J software in which the signal in TL was measured in grey scale and transformed into a numerical value.[135] In addition, the same author has

proposed a simple way to improve the smartphone-based quantification in LFA by attaching commercial microscopic lenses to the smartphone camera (Figure 1.18.). The lenses provide high quality image amplification by increasing the number of pixels that can be recorded. In this regard they proved an interesting signal enhancement for H-IgG detection.[159]
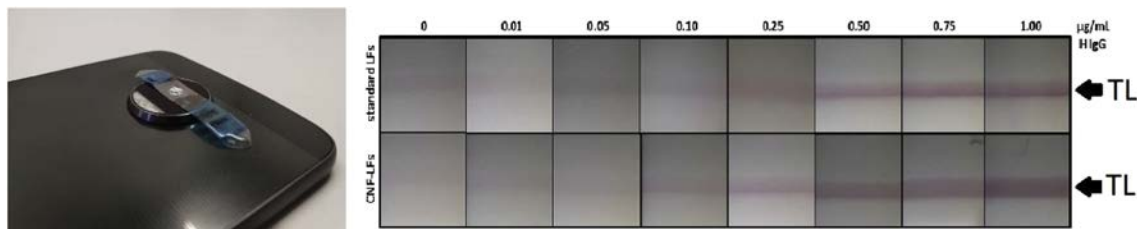
Figure 1.18. Picture of the microscopic lenses attached to the smartphone camera, that were used to photograph the detection are of the colorimetric LFA strips. Reprinted (adapted) with permission from Quesada-González, D. *et al.* Signal enhancement on gold nanoparticle-based lateral flow tests using cellulose nanofibers. ***Biosens. Bioelectron.*** **141**, 111407 (2019). Copyright (2019) ELSEVIER.

Brangel *et al.* have exploited all properties that smartphone-based LFA quantification can provide at the POC. Besides of offering portable and rapid evaluation, the smartphones proved to be an interesting platform for surveillance screening and Ebola-infected patient management in Uganda. They customized an Android app compatible with Samsung Galaxy S4 that enabled patient's detail recording plus geotagging of the collected samples.[91] Moreover, Miller and colleagues have proved that the performance of video analysis with smartphones can be a cost-effective and simple method to calculate the thermodynamic equilibrium dissociation constant K_D of analyte and bioreceptor in LFA. The authors suggest that this strategy can overcome the barriers associated with quantitative analysis on LFA, such as colour inhomogeneity and reproducibility issues. The achieved K_D showed excellent consistency with a reference benchtop interferometer.[137]

Smartphone-based quantification has also been developed for luminescent LFAs. Danthanarayana and colleagues have fabricated a smartphone imaging system for the evaluation of a nanophosphors-based LFA for PSA and hCG detection. An iphone 5S was attached to a 3D printed holder that enabled the alignement of the LFA cartridge with the smartphone camera. An app was used to control the phone's flash, which was

used to excite the luminiscent nanoparticles for 3 seconds. Then, the flash is switched off and the camera captured the image after a 100 milliseconds time-delay. The time-gated imaging served as an strategy to decrease the background signal since it allowed the flash light to decay before image capture. Finally, the images were analysed with Image J software, resulting in the achievance of 0.1 ng/ml and 1 ng/ml LoD for PSA and hCG, respectively.[222] Moreover, Liu *et al.* have developed a smartphone-based quantification reader for dual colorimetric and fluorescent LFAs. They fabricated a 3D printed cartridge (70 x 70 x 70 mm) using black photosensitive materails. The cartridge contained both white and UV LEDs as optical modules for visible light and fluorescence detection (Figure 1.19.). The capture images were analyzed with Android Studio app, in which the pixel value of the red channel was chosen for the fluorescence detection and the pixel value of average reverse green and blue channels were selected for visible light detection. The achieved LoQs proved to have good consistency with the sophisiticated and precise Liquid chromatography–mass spectrometry (LC-MS/MS).[223]
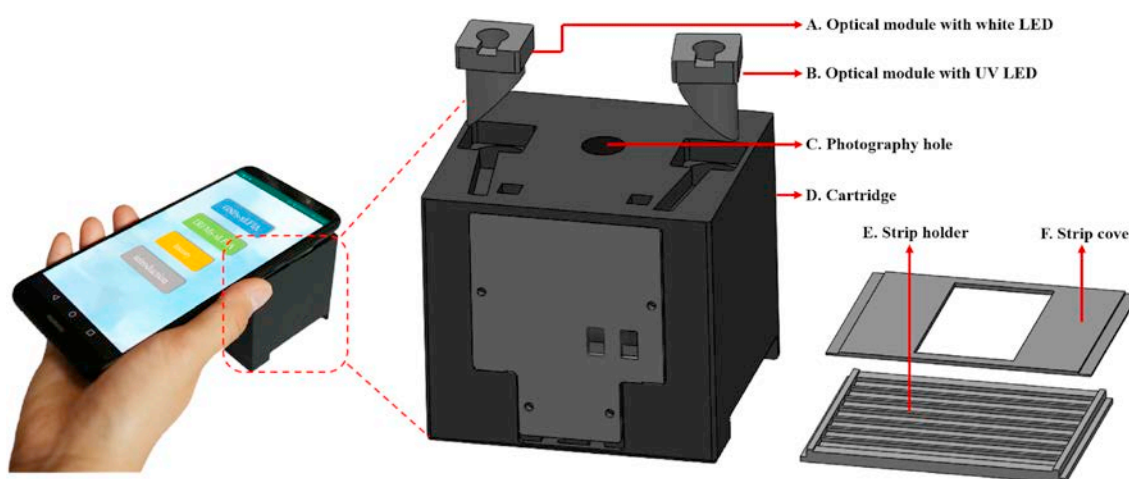
Figure 1.19. Schematic representation of a 3D printed cartridge that contains all the optical apparatus for smartphone-based quantification of colorimetric and fluorescent LFA. Reprinted (adapted) with permission from Liu, Z. *et al.* A smartphone-based dual detection mode device integrated with two lateral flow immunoassays for multiplex mycotoxins in cereals. ***Biosens. Bioelectron.*** **158**, 112178 (2020). Copyright (2020) ELSEVIER.

Currently there are several commercial smartphone-based lateral flow readers, where a smartphone is integrated into the device.[151] This is the case of SkanSmart and SkanEasy, developed by Skannex AS, in which the smartphone takes a picture of the

strip after scanning the barcode on the cassette. The barcode determines the camera parameters required for each assay. Moreover, the results are automatically stored and can be printed, emailed or exported in XML file.[150]

1.4.1.3.1 Portable readers for alternative detection methods

1.4.1.3.1.1 Magnetic detection

Magnetic particle quantification (MPQ) offers several advantages over the traditional colorimetric evaluation, such as deep signal registrations (considering the labels present in the overall nitrocellulose membrane width), extremely wide dynamic linear range (up to 7 orders of magnitude) and insensitive to opaque samples. The use of portable and cost-effective MPQ readers offers robust near-patient quantification. Orlov *et al.* took advantage of an updated MPQ reader with zero drift of baseline and a 100-fold wider dynamic range to quantify the presence of PSA in blood samples (Figure 1.20.).
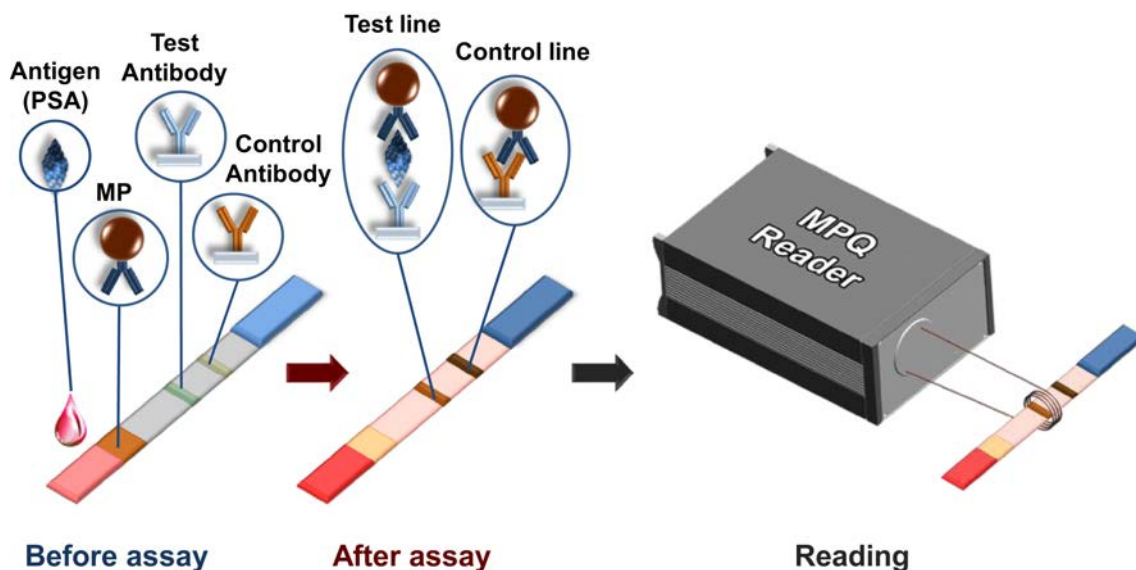
Figure 1.20. Schematic representation of a magnetic particle quantification (MPQ)-based LFA evaluated by a portable reader. Reprinted (adapted) with permission from Orlov, A. V., Bragina, V. A., Nikitin, M. P. & Nikitin, P. I. Rapid dry-reagent immunomagnetic biosensing platform based on volumetric detection of nanoparticles on 3D structures. ***Biosens. Bioelectron.*** **79**, 423–429 (2016). Copyright (2016) ELSEVIER.

The clinical relevant LoD and wide dynamic range achieved was superior to ELISA.[224] Besides, Orlov and colleagues have validated the same MPQ reader for multiplexing purposes. Three strips are introduced in a hollow polyethylene cartridge (95 mm long, 4.5 mm inner diameter), which is inserted in the measuring coils of the MPQ reader. Each strip is fixed in different positions within the cartridge in order to avoid magnetic signal overlapping. The device was validated for the quantification of botulinum neurotoxin types A, B and E in milk, apple and orange juice, achieving interesting LoDs.[215] It would be interesting to obtain more details regarding the price of the MPQ reader so as to evaluate the feasibility of its application in POC scenarios.

1.4.1.3.1.2 Thermal contrast detection

Thermal contrast detection mode has been widely reported in recent years, proving great analytical sensitivity compared to the colorimetric detection in LFA. However, advances in the field where not accompanied by the development of portable and cost-effective detection readers. The development of the first POC thermal contrast device by Qu and colleagues have open new possibilities for the application of this sophisticated detection mode in real scenarios. The device has a dimension of 133 x 108 x 73 mm and has been fabricated with cost-effective surface mounted components. A laser diode provides a NIR light source and gold nanoprisms are used as light-to-heat transducers. The heat generation is detected by a semiconductor sensor (conduction mode) and infrared thermometer (radiation mode), with 16-bit (0.0078 °C) and 17 bit temperature resolution, respectively. A low-power operation motherboard is used to process the data. The analytical capability of the device has been validated for the quantification of hCG, showing a 12-fold improvement of the LoD compared to visual detection. The radiation mode proved to be the most sensitive but also the most affected by ambient temperature upon high concentrations of the target analyte. Thus, either sensing modes can be selected depending of the assay requirements.[225]

1.4.1.3.1.3 Photoacoustic detection

Photoacoustic (PA)-based detection relies on the PA effect, which consists in the generation of acoustic radiation caused by adsorption of light in matter. In LFA, a laser beam is focused on the labelled bioreceptors in test line and a dedicated reader records the generated acoustic waves. The great advantage of photoacoustic detection (PA)

mode over the conventional AuNPs-LFA colorimetric detection is the reduced systems noise, due to the different energy domains of the input and output signals. Thus, PA detection is not affected by the scattered light interferences of complex samples. One of the reasons why PA imaging has grown faster than PA detection is the lack of portable and cost-effective detection readers. In this sense, Zhang *et al.* have developed a miniaturized PA detection device (40 x 20 x 20 mm) consisting in a 520 nm laser as light source, a PA cell for sample introduction, microphone for sound collection and laptop as signal processing unit. The device has been validated for glucose detection in whole blood, in which starch-I_2 is used as generate heat and produce acoustic waves. Despite being applied for glucose sensing, this PA reader has great potential to be used in LFA. However, in order to be totally useful at the POC some issues should be solved. Firstly, the laser takes 15 minutes to pre-heat and secondly, the assay is performed outside of the PA reader. The integration of the assay performance and evaluation in a single step will definitely simplify the procedure, while the reduction of the assay time will allow a fast diagnosis.[226]

1.4.1.3.1.4 SERS detection

The major drawback of current SERS-LFA quantification is the readout time, which range from dozens of minutes to several hours. This is not compatible with POC applications. The reason is that the laser spots in Raman microscopes are micrometer-sized and take seconds before they move to the next scanning position. In order to solve this limitation, Tran and colleagues have developed a portable SERS-LFA reader with a fiber optical probe able to scan 50 positions in 5 seconds. The key aspect is that the strip is scanned orthogonally to the line focus and that the motorized stage just takes 10 ms per step (Figure 1.21). The developed reader has proved several orders of magnitude shorter acquisition times compared to the expensive and bulky Raman microscopes. Moreover the method appeared to be 15 times more sensitive than the conventional AuNPs-based colorimetric detection of hCG.[227]
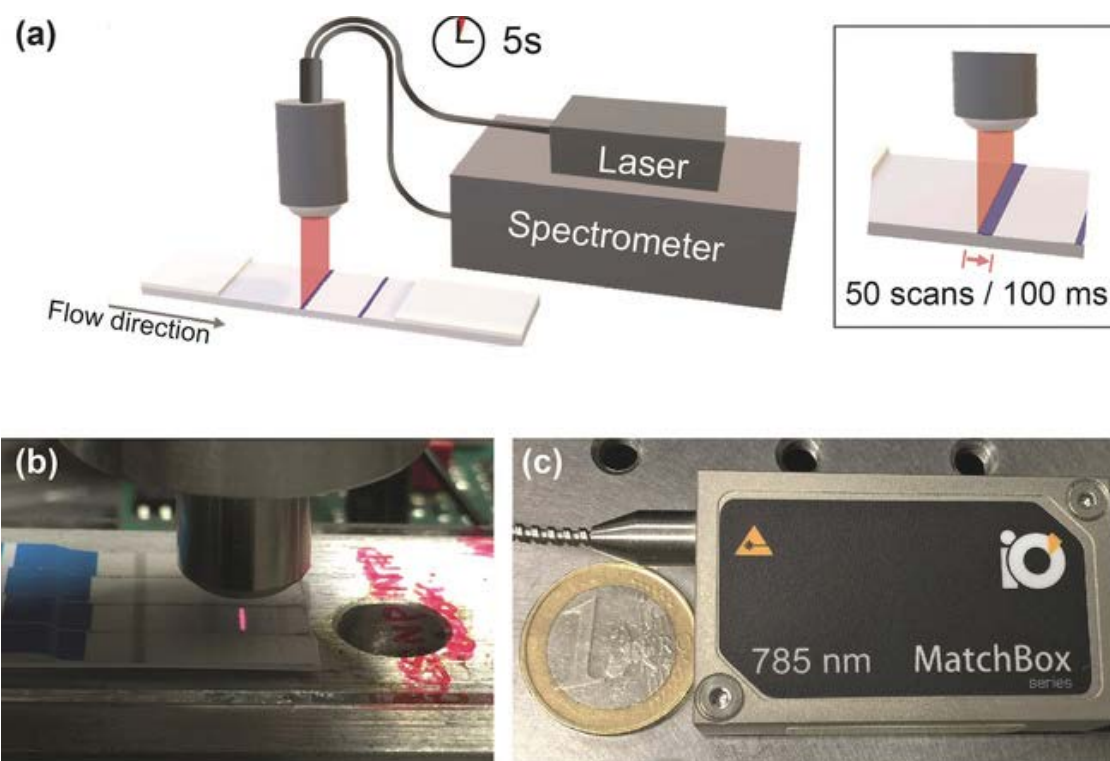
Figure 1.21. (A) Schematic representation of the reader set-up. **(B)** Picture of the optical fiber probe. **(C)** Picture of the laser diode. Reprinted (adapted) with permission from Tran, V., Walkenfort, B., König, M., Salehi, M. & Schlücker, S. Rapid, Quantitative, and Ultrasensitive Point-of-Care Testing: A Portable SERS Reader for Lateral Flow Assays in Clinical Chemistry. *Angew. Chemie - Int. Ed.* **58**, 442–446 (2019).

1.4.1.3.1.4 Up-converting luminescence detection

The current equipment for evaluating UCNPs-based LFA uses either dynamic scanning type or static imaging type. The former are less convenient for POC applications as they requiere computer software to perform the background correction and peak-area determination. The latter are more cost-effective, fast and portable. Thus, they are more convenient for real-time quantification. In order to overcome the issues related to the dynamic scanning, Zhang *et al.* have modified a commercial portable fluorescent reader (Niutaier, China) to function as up-conversion luminescence reader. The reader, which is small ($30 \times 30 \times 15$ cm^3) and light (2 kg), has the software and electronics already integrated in the device. In order to achieve near-infrared excitation, the reader's LEDs have been replaced by a 300 mW laser, which excites the UCNPs at 980 nm. This

system has been validated for the detection of triamcinolone acetonide in cream, masks and essence cosmetics, proving a fast and reliable quantification.[228] Alternatively, Gong and co-workers have developed a smartphone-assisted static imaging quantification device. The reader is also very small (24 x 9.4 x 5.4 cm^3) and ultra-light (0.9 kg). As observed in figure 1.22, the reader is composed of a compact infrared laser (exc. at 980 nm), a dichroic mirror with 98% light transmission at 980 nm and an infrared filter with nearly 0 % transmittance at 980 nm. Moreover, the smartphone includes an analysis app that enables simple operation and easy result's interpretation. The device has been validated for the detection nucleic acids, small proteins, heavy metal ions and bacteria, proving a great versatility. Furthermore the great correlation with the gold-standard methods makes this UCNPs-LFA reader very promising for commercialization.[229] Similarly, Jin and colleagues have developed a portable detection reader based on a 980 nm laser that excites the test zone at a 45° angle. They have evaluated the UCNPs-LFA strips with both a CCD camera (Nikon) and a smartphone (and using Image J software), proving that the smartphone was not as sensitive as the camera but still had a good linear correlation for Ochratoxin A, mercury ions and Salmonella.[230]
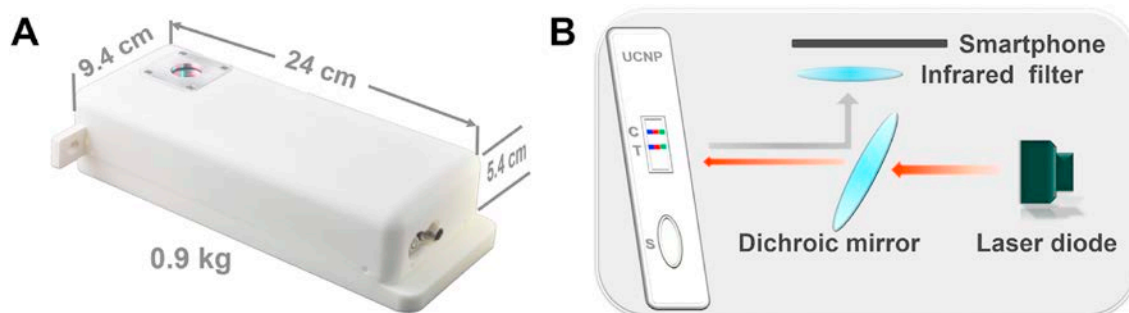
Figure 1.22. (A) Picture of a portable UCNPs-LFA reader with dimensions of 24 x 9.4 x 5.4 cm^3 and 0.9 Kg weight. **(B)** Schematic representation of the strips evaluation, in which the laser light is transmitted by the dichroic mirror at 45° to the detection zone. The smartphone camera captures the luminescence emission of the UCNPs present in test and control line, while the infrared filter blocks the laser's residual light. Reprinted (adapted) with permission from Gong, Y. *et al.* A portable and universal upconversion nanoparticle-based lateral flow assay platform for point-of-care testing. *Talanta* **201**, 126–133 (2019). Copyright (2019) ELSEVIER.

1.4.2. Conclusions and future perspectives

The reported sensitivity enhancement strategies are based on flow rate control, sample pre-concentration, increase of sample volume, use of signal transducers with higher extinction coefficient, signal amplification, increase of signal-to-noise ratio and use of more sensitive detection methods. It is difficult to select the best sensitivity enhancement strategy, as many factors must be considered apart from the sensitivity itself. For instance, the ideal strategy should provide the highest sensitivity enhancement without sacrifying the great advantages of LFA, as ease-of-use, cost-effectiveness, rapidness and portability. We have used these criteria to infer which are the most promising strategies and how they should be further improved to solve their current limitations.

Another important factor that must be considered when comparing the different approaches is the method used to calculate the sensitivity, as this varies between authors. Some of them evaluate the sensitivity improvement by comparing the achieved limit of detection while others consider the calibration curve slope. Despite of both being valid, it is not accurate to compare percentage sensitivity enhancements obtained using different criteria.

It is noteworthy that the strategies related to the decrease in the flow rate are the most simple to implement. However they provide the worse sensitivity enhancements. Besides, sample pre-concentration by magnetic focusing has proved an outstanding sensitivity enhancement, but the requirement of several washing steps reduces the simplicity of LFA. Similarly, the enzyme and metal-catalytic signal amplification strategies are interesting but also requiere washing steps. Conversely, the silver staining approach for signal amplification is probably the finest as the reagents required for signal amplification are integrated in the strip. Thus, the simplicity and ease-of-use of LFA is maintained. Nevertheless, this strategy doesn't allow as high sensitivity enhancement as the approaches related to the increase in the signal-to-noise ratio (1000-fold) and the use of SERS detection mode (2000-fold). However, the former is only relevant for DNA detection and the latter includes a magnetic sample pre-concentration step. Moreover, the strategies that concern the use of alternative detection methods such as PA and TCA are without any doubt the most promising but are still limited by the

requirement of expensive and complex dedicated readers. Though, research is focus on solving this aspect by developing portable and cost-effective readers for these alternative detection modes.

In relation to the reported multiplexing approaches, it is evident that the accommodation of multiple lines is the most direct approach but is limited to the detection of up to 3 analytes. Alternatively, the use of dots/spots increases the number of detected analytes up to 7. Taranova *et al.* has been able to include 32 dots in the nitrocellulose membrane, but the reduced size of the dots difficult the result's interpretation by the end user. In this sense, the use of different coloured labels appears as an interesting approach for multiplexing. The combination of different lines and 2 fluorophores has enabled the detection of 13 different target analytes. Besides, the multiplex detection in a single line is probably the most promising strategy. Although the authors have just reported the detection of 3 analytes, this can be exponentially increased upon the incorporation of more lines and labels. In this sense, the use of SERS nanolabels is of high interest as it enables both multiplexing and outstanding sensitivities. However, as discussed previously, the SERS dedicated reader must be first designed for POC applications. Moreover, it is noteworthy that all the reported approaches lack of cross-reactivity issues after being validated with real samples. Thus, the developed strategies are closer than ever to be implemented in the current health care systems.

Furthermore, quantification at the point-of-care is possible by the use of smartphone-based LFA readers. These have been developed for both colorimetric and fluorescence detection. It is encouraging to see that most of the reported devices have been fabricated with low-cost materials. Moreover, the apps used for data processing and interfacing has been customized with simple and cost-effective tools, such as Android studio. However, the quality of the image acquisition relies on the use sophisticated smartphone cameras, which unfortunately are not within everyone's reach. Nevertheless, the telecommunications field is experiencing an incredible expansion that involves the implementation of more sophisticated cameras in low-cost smartphones. Additionally, the development of portable quantification readers for alternative detection modes is without doubt the breakthrough of this decade. It has been widely reported that SERS, TCA, PA and magnetic detection provide outstanding analytical sensitivities in LFA, reduced signal interferences in complex samples and the possibility to perform

multiplexing analysis. Thus, the development of portable quantification readers devoted to these detection modes has been the last piece of the puzzle to achieve the next generation lateral flow assay.

1.5. References

1.   A. D. McNaught and A. Wilkinson. Blackwell. *IUPAC. Compendium of Chemical Terminology*. (Scientific Publications, Oxford, 1997).

2.   Cammann, K. Bio-sensors based on ion-selective electrodes. *Anal. Chem.* **287**, 1–9 (1977).

3.   Turner, A. P. F., Karube, I., Wilson, G. S. & Worsfold, P. J. *Biosensors: fundamentals and applications. Analytica Chimica Acta* **201**, (1987).

4.   Thevenot, D. *et al.* Electrochemical biosensors: recommended definitions and classification. *Biosens. Bioelectron.* **16**, 121–131 (2001).

5.   Dincer, C. *et al.* Disposable Sensors in Diagnostics , Food , and Environmental Monitoring. *Adv. Mater.* **31**, 1806739 (2019).

6.   Nelson JM, G. E. Adsorption of Invertase. *J. Am. Chem. Soc.* **38**, 1109–1115 (1916).

7.   Yoo, E. & Lee, S. Glucose Biosensors: An Overview of Use in Clinical Practice. *Sensors (Switzerland)* **10**, 4558–4576 (2010).

8.   EvaEngvall, P. Enzyme-linked immunosorbent assay (ELISA) quantitative assay of immunoglobulin G. *Immunochemistry* **8**, 871–874 (1971).

9.   Catt K, T. G. Solid-phase radioimmunoassay in antibody-coated tubes. *Science (80-.).* **158**, 1570–2 (1967).

10. Avrameas, Stratis Uriel, J. Method for labeling antigens and antibodies with enzymes and their application in immunodiffusion. *Comptes Rendus des Seances l'Academie des Sci. Ser. D Sci. Nat.* **262**, 2543–5 (1966).

11. Trans., F. S. R. E. O. Development of the pH concept: A historical survey. *J.*

Chem. Educ. **41**, 105 (1964).

12. Touchstone, J. C. History of Chromatography. *J. Liq. Chromatogr.* **16**, 1647–1665 (1993).

13. Califano, J. A. FDA Consumer. *U.S. Department of health, education and walfare* 2–6 (1979).

14. Martinez, A. W., Phillips, S. T., Butte, M. J. & Whitesides, G. M. Patterned Paper as a Platform for Inexpensive , Low-Volume , Portable. *Angew. Chemie - Int. Ed.* **46**, 1318–1320 (2007).

15. Liana, D. D., Raguse, B., Gooding, J. J. & Chow, E. Recent Advances in Paper-Based Sensors. *Sensors (Switzerland)* **12**, 11505–11526 (2012).

16. Zhang, X., Guo, Q. & Cui, D. Recent Advances in Nanotechnology Applied to Biosensors. *Sensors (Switzerland)* **9**, 1033–1053 (2009).

17. Rica, R. De & Stevens, M. M. Plasmonic ELISA for the ultrasensitive detection of disease biomarkers with the naked eye. *Nat. Nanotechnol.* **7**, 821–824 (2012).

18. Quesada-González, D. & Merkoçi, A. Nanoparticle-based lateral flow biosensors. *Biosens. Bioelectron.* **73**, 47–63 (2015).

19. Li, Y., Schluesener, H. J. & Xu, S. Gold nanoparticle-based biosensors. *New Dev. Gold Nanomater. Res.* **43**, 95–116 (2016).

20. Nikhil Bhalla, Pawan Jolly, N. F. and P. E. Introduction to Biosensors. *Essays Biochem.* **60**, 1–8 (2016).

21. Calvert, J. G. Glossary of atmospheric chemistry terms. *Pure Appl. Chem.* **62**, 2167–2219 (1990).

22. Sensor Terminology. *National Instrumets* (2019). Available at: https://www.ni.com/es-es/innovations/white-papers/13/sensor-terminology.html#section-783620926. (Accessed: 16th March 2020)

23. Currie, L. A. & Svehla, G. Nomenclature for the presentation of results of

chemical analysis (IUPAC Recommendations 1994). *Pure Appl. Chem.* **66**, 595–608 (1994).

24. Mehrotra, P. Biosensors and their applications - A review. *J. Oral Biol. Craniofacial Res.* **6**, 153–159 (2016).

25. Francesca Bettazzi, Giovanna Marrazza, Maria Minunni, I. P. and S. S. Biosensors and Related Bioanalytical Tools. in *Past, Present and Future Challenges of Biosensors and Bioanalytical Tools in Analytical Chemistry: A Tribute to Professor Marco Mascini* 1–26 (Elsevier, 2017).

26. Monošíka, R., Streďanskýb, M. & Šturdíka, E. Biosensors-classification, characterization and new trends. *Acta Chim. Slovaca* **5**, 109–120 (2012).

27. O'Beirne, A. J. & Cooper, H. R. Heterogeneous Enzyme Immunoassay. *J. Histochem. Cytochem.* **27**, 1148–1162 (1979).

28. Darwish, I. A. Immunoassay Methods and their Applications in Pharmaceutical Analysis: Basic Methodology and Recent Advances. *Int. J. Biomed. Sci.* **2**, 217–235 (2006).

29. Ellington, A. D. & Szostak, J. W. In vitro selection of RNA molecules that bind specific ligands. *Nature* **346**, 818–822 (1990).

30. Stoltenburg, R., Reinemann, C. & Strehlitz, B. SELEX-A (r)evolutionary method to generate high-affinity nucleic acid ligands. *Biomol. Eng.* **24**, 381–403 (2007).

31. Bousse, L. Whole cell biosensors. *Sensors actuators B* **34**, 270–275 (1996).

32. Rawson, D. M., Willmer, A. J. & Turner, A. P. P. Whole-cell biosensors for environmental monitoring. *Biosensors* **4**, 299–231 (1989).

33. Svitel, J. & Katrl, J. Optical biosensors. *Essays Biochem.* **60**, 91–100 (2016).

34. Habimana, J. D. D., Ji, J. & Sun, X. Minireview : Trends in Optical-Based Biosensors for Point-Of-Care Bacterial Pathogen Detection for Food Safety and Clinical Diagnostics. *Anal. Lett.* **51**, 2933–2966 (2018).

35. Alhadrami, H. A. Biosensors : Classifications , Medical Applications and Future Prospective. *Biotechnol. Appl. Biochem.* **65**, 497–508 (2018).

36. Mucic, R. C., Storhoff, J. J., Letsinger, R. L. & Mirkin, C. A. A DNA-based method for rationally assembling nanoparticles into macroscopic materials. *Nature* **382**, 607 (1997).

37. Xiao, L. *et al.* Colorimetric Biosensor for Detection of Cancer Biomarker by Au Nanoparticles-Decorated Bi2Se3 Nanosheets. *ACS Appl. Mater. Interfaces* **9**, 6931–6940 (2017).

38. Leunga, A., Shankarb, M. P. & Mutharasan, R. A review of fiber-optic biosensors. *Sensors Actuators B Chem.* **125**, 688–703 (2007).

39. Daniel Thevenot, Klara Toth, Richard Durst, G. W. Electrochemical biosensors: recom- mended de nitions and classi cation. *Pure Appl. Chem. Gruyter* **71**, 2333–2348 (1999).

40. Honeychurch, K. C. Printed thick-film biosensors. in *Printed Films Materials Science and Applications in Sensors, Electronics and Photonics* 366–409 (Woodhead Publishing, 2012).

41. Arlett, J. L., Myers, E. B. & Roukes, M. L. Comparative advantages of mechanical biosensors. *Nat. Publ. Gr.* **6**, 203–215 (2011).

42. Fu, Z., Lu, Y. & Lai, J. J. Recent Advances in Biosensors for Nucleic Acid and Exosome Detection. *Chonnam Med J.* **55**, 86–98 (2019).

43. Zhang, Y. & Tadigadapa, S. Calorimetric biosensors with integrated microfluidic channels. *Biosens. Bioelectron.* **19**, 1733–1743 (2004).

44. Nabaei, V., Chandrawati, R. & Heidari, H. Magnetic biosensors : Modelling and simulation. *Biosens. Bioelectron.* **103**, 69–86 (2017).

45. SCENIHR. *The appropriateness of existing methodologies to assess the potential risks associated with engineered and adventitious products of nanotechnologies.* (2006).

46. Turner, A. P. F. Biosensors: Sense and sensibility. *Chem. Soc. Rev.* **42**, 3184–

3196 (2013).

47.   Vigneshvar, S., Sudhakumari, C. C. & Senthilkumaran, Balasubramanian Prakash, H. Recent Advances in Biosensor Technology for Potential Applications – An Overview. *Front. Bioeng. Biotechnol.* **4**, 1–9 (2016).

48.   Zamora-Gálvez, Alejandro Morales-Narváez, E., Mayorga-Martineza, C. C. & Merkoçi, A. Nanomaterials connected to antibodies and molecularly imprinted polymers as bio/receptors for bio/sensor applications. *Appl. Mater. Today* **9**, 387–401 (2017).

49.   Vashist, S. K. *et al.* Nanotechnology-Based Biosensors and Diagnostics: Technology Push versus Industrial/Healthcare Requirements. *BioNanoSci.* **2**, 115–126 (2012).

50.   Holzinger, M., Goff, A. Le & Cosnier, S. Nanomaterials for biosensing applications : a review. *Front. Chem.* **2**, 1–10 (2014).

51.   Leonard, P. *et al.* Advances in biosensors for detection of pathogens in food and water. *Enzyme Microb. Technol.* **32**, 3–13 (2003).

52.   Poltronieri, P., Mezzolla, V., Primiceri, E. & Maruccio, G. Biosensors for the Detection of Food Pathogens. *Foods* **3**, 511–526 (2014).

53.   Thakur, M. S. & Ragavan, K. V. Biosensors in food processing. *J Food Sci Technol.* **50**, 625–641 (2013).

54.   Brooks, S. L., Ashby, R. E., Turner, A. P. F., Calder, M. R. & Clarke, D. J. Development of an On-line Glucose Sensor for Fermentation Monitoring. *Biosensors* **3**, 45–46 (1988).

55.   Newman, J. D. & Turner, A. P. F. Home Blood Glucose Biosensors : A Commercial Perspective. *Biosens. Bioelectron.* **20**, 2435–2453 (2005).

56.   Sin, M. L. Y., Mach, K. E., Wong, P. K. & Liao, J. C. Advances and challenges in biosensor-based diagnosis of infectious diseases. *Expert Rev. Mol. Diagn.* **14**, 225–244 (2014).

57.   Pashchenko, O., Shelby, T., Banerjee, T. & Santra, S. A Comparison of Optical,

Electrochemical, Magnetic, and Colorimetric Point-of-Care Biosensors for Infectious Disease Diagnosis. *ACS Infect. Dis.* **4**, 1162–1178 (2018).

58. Damborska, Dominika Bertok, T., Dosekova, E., Holazova, Alena Lorencova, L., Kasak, P. & Tkac, J. Nanomaterial-based biosensors for detection of prostate specific antigen. *Mikrochim Acta.* **184**, 3049–3067 (2017).

59. Tothill, I. E. Biosensors for cancer markers diagnosis. *Semin. Cell Dev. Biol. Biosens. cancer markers diagnosis* **20**, 55–62 (2009).

60. Pohanka, M. Current Trends in the Biosensors for Biological Warfare Agents Assay. *Mater.* **12**, 2303 (2019).

61. Verma N, S. M. Biosensors for heavy metals. *Biometals.* **18**, 121–9 (2005).

62. Justino, C. I. L., Duarte, A. C. & Rocha-Santos, T. A. P. Recent Progress in Biosensors for Environmental Monitoring: A Review. *Sensors (Basel).* **17**, 2918 (2017).

63. Caldorera-Moore, M. E., Liechty, W. B. & Peppas, N. A. Responsive theranostic systems: Integration of diagnostic imaging agents and responsive controlled release drug delivery carriers. *Acc. Chem. Res.* **44**, 1061–1070 (2011).

64. Yang, Z. *et al.* Stimuli-responsive nanotheranostics for real-time monitoring drug release by photoacoustic imaging. *Theranostics* **9**, 526–536 (2019).

65. Kim, H., Kwak, G., Kim, K., Yoon, H. Y. & Kwon, I. C. Theranostic designs of biomaterials for precision medicine in cancer therapy. *Biomaterials* **213**, 119207 (2019).

66. Mura, S. & Couvreur, P. Nanotheranostics for personalized medicine. *Adv Drug Deliv Rev* **64**, 1394–1416 (2012).

67. Thakor, A. S. & Gambhir, S. S. Nanooncology: The future of cancer diagnosis and therapy. *CA. Cancer J. Clin.* **63**, 395–418 (2013).

68. Kojima, R., Aubel, D. & Fussenegger, M. Novel theranostic agents for next-generation personalized medicine: small molecules, nanoparticles, and engineered mammalian cells. *Curr. Opin. Chem. Biol.* **28**, 29–38 (2015).

69. Roma-Rodrigues, C. *et al.* Nanotheranostics Targeting the Tumor Microenvironment. *Front. Bioeng. Biotechnol.* **7**, 197 (2019).

70. Chen, X., Song, J., Chen, X. & Yang, H. X-ray-activated nanosystems for theranostic applications. *Chem. Soc. Rev.* **48**, 3073–3101 (2019).

71. Yang, K., Feng, L., Shi, X. & Liu, Z. Nano-graphene in biomedicine: Theranostic applications. *Chem. Soc. Rev.* **42**, 530–547 (2013).

72. Qi, C., Lin, J., Fu, L. H. & Huang, P. Calcium-based biomaterials for diagnosis, treatment, and theranostics. *Chem. Soc. Rev.* **47**, 357–403 (2018).

73. Tao, Y., Li, M., Ren, J. & Qu, X. Metal nanoclusters: novel probes for diagnostic and therapeutic applications. *Chem. Soc. Rev.* **44**, 8636–8663 (2015).

74. Liu, Y., Bhattarai, P., Dai, Z. & Chen, X. Photothermal therapy and photoacoustic imaging: Via nanotheranostics in fighting cancer. *Chem. Soc. Rev.* **48**, 2053–2108 (2019).

75. Lim, E.-K. *et al.* Nanomaterials for Theranostics: Recent Advances and Future Challenges. *Chem. Rev.* **115**, 327–394 (2015).

76. Kost, G. J., Tran, N. K. & Louie, R. F. Point-of-Care Testing: Principles, Practice, and Critical-Emergency-Disaster Medicine. in *Principles & Practices of Point-of-Care Testing.* 3–12 (Philadelphia: Lippincott Williams & Wilkins, 2002). doi:10.1002/9780470027318.a0540.pub2

77. Quesada-Gonzalez, D. & Merkoci, A. Nanomaterial-based devices for point-of-care diagnostic applications. *Chem. Soc. Rev.* (2018). doi:10.1039/C7CS00837F

78. Cullen, D. K. *et al.* Color changing photonic crystals detect blast exposure. *Neuroimage* **54**, S37–S44 (2011).

79. Strangman, G. E. *et al.* Deep-space applications for point-of-care technologies. *Curr. Opin. Biomed. Eng.* **11**, 45–50 (2019).

80. Lode, P. Von. Point-of-care immunotesting : Approaching the analytical performance of central laboratory methods. *Clin. Biochem.* **38**, 591–606

(2005).

81. Dincer, C., Bruch, R., Kling, A., Dittrich, P. S. & Urban, G. A. Multiplexed Point-of-Care Testing – xPOCT. *Trends Biotechnol.* **35**, 728–742 (2017).

82. Schols, A. M. R. *et al.* International definition of a point-of-care test in family practice: A modified e-Delphi procedure. *Fam. Pract.* **35**, 475–480 (2018).

83. El-Osta, A. *et al.* Does use of point-of-care testing improve cost-effectiveness of the NHS Health Check programme in the primary care setting? A cost-minimisation analysis. *BMJ Open* **7**, 1–10 (2017).

84. Pregnancy Tests. *Clearblue* (2020). Available at: https://uk.clearblue.com/pregnancy-tests. (Accessed: 10th March 2020)

85. ACCU-CHEK. *Roche* (2020).

86. Kosack, C. S., Page, A.-L. & Klatser, P. R. *Policy & practice A guide to aid the selection of diagnostic tests. Bull World Health Organ* **95**, (2017).

87. Zaman, G. W. & M. H. Low-cost tools for diagnosing and monitoring HIV infection in low-resource settings. *Bull World Health Organ* (2012). Available at: https://www.who.int/bulletin/volumes/90/12/BLT-12-102780-table-T1.html. (Accessed: 10th March 2020)

88. Inan, H. *et al.* Photonic crystals: emerging biosensors and their promise for point-of-care applications. *Chem. Soc. Rev.* **46**, 366–38 (2017).

89. Biosensors Market. *Markets and Markets* (2019). Available at: https://www.marketsandmarkets.com/Market-Reports/biosensors-market-798.html?gclid=EAIaIQobChMIlu7v0LeP6AIVTcreCh1i3gSOEAAYASAAEgIy7fD_BwE. (Accessed: 10th March 2020)

90. Price, C. P. Clinical review Point of care testing. 1285–1288 (2001).

91. Brangel, P. *et al.* A Serological Point-of-Care Test for the Detection of IgG Antibodies against Ebola Virus in Human Survivors. *ACS Nano* **12**, 63–73 (2018).

92. Wonderly, B. *et al.* Comparative performance of four rapid Ebola antigen-detection lateral flow immunoassays during the 2014-2016 Ebola epidemic in West Africa. *PLoS One* **14**, 1–14 (2019).

93. Drain, P. K. *et al.* Validation of clinic-based cryptococcal antigen lateral flow assay screening in HIV-infected adults in South Africa. *Sci. Rep.* **9**, 4–11 (2019).

94. Chamorro-Garcia, A. *et al.* Detection of parathyroid hormone-like hormone in cancer cell cultures by gold nanoparticle-based lateral flow immunoassays. *Nanomedicine Nanotechnology, Biol. Med.* **12**, 53–61 (2016).

95. Barnett, J. M. *et al.* An inexpensive, fast and sensitive quantitative lateral flow magneto-immunoassay for total prostate specific antigen. *Biosensors* **4**, 204–220 (2014).

96. Schenk, F. *et al.* Development of a paper-based lateral flow immunoassay for simultaneous detection of lipopolysaccharides of Salmonella serovars. *Anal. Bioanal. Chem.* **410**, 863–868 (2018).

97. Wang, Y. *et al.* Rapid and sensitive detection of the food allergen glycinin in powdered milk using a lateral flow colloidal gold immunoassay strip test. *J. Agric. Food Chem.* **63**, 2172–2178 (2015).

98. Land, K. J., Boeras, D. I., Chen, X. S., Ramsay, A. R. & Peeling, R. W. REASSURED diagnostics to inform disease control strategies, strengthen health systems and improve patient outcomes. *Nat. Microbiol.* **4**, 46–54 (2019).

99. Drain, P. K. *et al.* Evaluating Diagnostoic Point-of-Care Test in Resource-Limited Setting. *Lancet Infect Dis.* **14**, 239–249 (2014).

100. Quesada-González, D., Jairo, G. A., Blake, R. C., Blake, D. A. & Merkoçi, A. Uranium (VI) detection in groundwater using a gold nanoparticle/paper-based lateral flow device. *Sci. Rep.* **8**, 8–15 (2018).

101. López-Marzo, A. M., Pons, J., Blake, D. A. & Merkoçi, A. High sensitive gold-nanoparticle based lateral flow Immunodevice for Cd2+ detection in drinking waters. *Biosens. Bioelectron.* **47**, 190–198 (2013).

102. Wong, Raphael, Tse, H. *Lateral Flow Immunoassay*. (Springer, 2009).

103. Parolo, C. & Merkoçi, A. Paper-based nanobiosensors for diagnostics. *Chem. Soc. Rev.* **42**, 450–457 (2013).

104. Berlina, A., Bartosh, A., Zherdev, A., Xu, C. & Dzantiev, B. Development of Immunochromatographic Assay for Determination of Tetracycline in Human Serum. *Antibiotics* **7**, 99 (2018).

105. Morales-Narváez, E., Naghdi, T., Zor, E. & Merkoçi, A. Photoluminescent Lateral-Flow Immunoassay Revealed by Graphene Oxide: Highly Sensitive Paper-Based Pathogen Detection. *Anal. Chem.* **87**, 8573–8577 (2015).

106. Du, D., Wang, J., Wang, L., Lu, D. & Lin, Y. Integrated lateral flow test strip with electrochemical sensor for quantification of phosphorylated cholinesterase: Biomarker of exposure to organophosphorus agents. *Anal. Chem.* **84**, 1380–1385 (2012).

107. Posthuma-Trumpie, G. A., Korf, J. & Van Amerongen, A. Lateral flow (immuno)assay: Its strengths, weaknesses, opportunities and threats. A literature survey. *Anal. Bioanal. Chem.* **393**, 569–582 (2009).

108. Jones, K. D. *Membrane-based tests. The Latex Course Proceedings.* (2006).

109. Driller, H., Vouzellaud, L., Marchio, F. & Dodson, P. E. A. (12) United States Patent Time (min). **2**, 523–532 (2007).

110. Technologies, mdi M. Blood Separation Membranes. (2018). Available at: https://www.mdimembrane.com/blood-separation-membranes.

111. Dirk M. Koenhen, E. J. & J. Scharstuhl, H. PROCESS AND DEVICE FOR THE SEPARATION OF A BODY FLUID FROM PARTICULATE MATERALS. (1993).

112. Hurst, S. J., Lytton-Jean, A. K. R. & Mirkin, C. A. SUPPORTING INFORMATUIN Maximizing DNA loading on a range of gold nanoparticle sizes. *Anal. Chem.* **78**, 8313–8 (2006).

113. Liu, B. & Liu, J. Methods for preparing DNA-functionalized gold nanoparticles, a key reagent of bioanalytical chemistry. *Anal. Methods* **9**,

2633–2643 (2017).

114. Millipore, M. *Rapid Lateral Flow Test Strips Considerations for Product Development*. (2013).

115. NanoComposix. Conjugate Pad Selection, Treatment, and Conjugate Drying for Lateral Flow Assays. (2019). Available at: https://nanocomposix.com/pages/conjugate-pad-selection-treatment-and-conjugate-drying-for-lateral-flow-assays#target.

116. Biotech, S. stedim. *UniSart Membranes LFIA strip*. (2019).

117. Turkevich, J., Stevenson, P. C. & Hillier, J. A study of the nucleation and growth processes in the synthesis of colloidal gold. *Discuss. Faraday Soc.* **11**, 55–75 (1951).

118. Song, C. *et al.* Rapid and sensitive detection of β-agonists using a portable fluorescence biosensor based on fluorescent nanosilica and a lateral flow test strip. *Biosens. Bioelectron.* **50**, 62–65 (2013).

119. Berlina, A. N., Taranova, N. A., Zherdev, A. V., Vengerov, Y. Y. & Dzantiev, B. B. Quantum dot-based lateral flow immunoassay for detection of chloramphenicol in milk. *Anal. Bioanal. Chem.* **405**, 4997–5000 (2013).

120. N.A. Taranova, A.N. Berlina, A.V. Zherdev, B. B. D. 'Traffic light' immunochromatographic test based on multicolor quantum dots for the simultaneous detection of several antibiotics in milk. *Biosens. Bioelectron.* **63**, 255–261 (2015).

121. Beloglazova, N. V., Goryacheva, I. Y., Niessner, R. & Knopp, D. A comparison of horseradish peroxidase, gold nanoparticles and qantum dots as labels in non-instrumental gel-based immunoassay. *Microchim. Acta* **175**, 361–367 (2011).

122. Wang, S. *et al.* Quantum-Dot-Based Lateral Flow Immunoassay for Detection of Neonicotinoid Residues in Tea Leaves. *J. Agric. Food Chem.* **65**, 10107–10114 (2017).

123. Wen, S. *et al.* Advances in highly doped upconversion nanoparticles. *Nat. Commun.* **9**, (2018).

124. Liu, C. *et al.* Upconversion luminescence nanoparticles-based lateral flow immunochromatographic assay for cephalexin detection. *J. Mater. Chem. C* **2**, 9637–9642 (2014).

125. Muhammad Sajid, Abdel-Nasser Kawde & Muhammad Daud. Designs, formats and applications of lateral flow assay: A literature review. *J. Saudi Chem. Soc.* **19**, 689–705 (2015).

126. Nakamura, K., Tanaka, T. & Takeo, K. Characterization of protein binding to a nitrocellulose membrane. *Seibutsu Butsuri Kagaku* **33**, 293–303 (1989).

127. Saisin, L. *et al.* Significant sensitivity improvement for camera-based lateral flow immunoassay readers. *Sensors (Switzerland)* **18**, 1–8 (2018).

128. C.J.Van Oss, R.J.Good, M. K. C. Mechanism of DNA (southern) and protein (western) blotting on cellulose nitrate and other membranes. *J. Chromatogr. A* **391**, 53–65 (1987).

129. Holstein, C. A. *et al.* Immobilizing affinity proteins to nitrocellulose: A toolbox for paper-based assay developers. *Anal. Bioanal. Chem.* **408**, 1335–1346 (2016).

130. Walter, J. G. *et al.* Protein microarrays: Reduced autofluorescence and improved LOD. *Eng. Life Sci.* **10**, 103–108 (2010).

131. Tang, R. *et al.* Improved Analytical Sensitivity of Lateral Flow Assay using Sponge for HBV Nucleic Acid Detection. *Sci. Rep.* **7**, 1–10 (2017).

132. Sartorius. Unisart® Nitrocellulose Membranes for Lateral Flow Assays. (2019). Available at: https://www.sartorius.es/sartoriusES/es/EUR/membranes-for-ivd-microarray-oem/unisart-lateral-flow.

133. mdi membrane technologies. Nitrocellulose Membrane. (2018). Available at: https://www.mdimembrane.com/nitrocellulose-membrane.

134. NanoComposix. Nitrocellulose Membrane Selection and Striping for Lateral Flow Assays. (2018).

135. Quesada-González, D. *et al.* Iridium oxide (IV) nanoparticle-based lateral flow immunoassay. *Biosens. Bioelectron.* **132**, 132–135 (2019).

136. Choi, J. R. *et al.* Sensitive biomolecule detection in lateral flow assay with a portable temperature–humidity control device. *Biosens. Bioelectron.* **79**, 98–107 (2016).

137. Miller, B. S. *et al.* Quantifying Biomolecular Binding Constants using Video Paper Analytical Devices. *Chem. - A Eur. J.* **24**, 9783–9787 (2018).

138. Chen, A. & Yang, S. Replacing antibodies with aptamers in lateral flow immunoassay. *Biosens. Bioelectron.* **71**, 230–242 (2015).

139. Koczula, K. M. & Gallotta, A. Lateral flow assays. *Essays Biochem.* **60**, 111–120 (2016).

140. Wen, H. W., Borejsza-Wysocki, W., Decory, T. R. & Durst, R. A. Development of a competitive liposome-based lateral flow assay for the rapid detection of the allergenic peanut protein Ara h1. *Anal. Bioanal. Chem.* **382**, 1217–1226 (2005).

141. Anfossi, L., Baggiani, C., Giovannoli, C., D'Arco, G. & Giraudi, G. Lateral-flow immunoassays for mycotoxins and phycotoxins: A review. *Anal. Bioanal. Chem.* **405**, 467–480 (2013).

142. Apilux, A., Rengpipat, S., Suwanjang, W. & Chailapakul, O. Development of competitive lateral flow immunoassay coupled with silver enhancement for simple and sensitive salivary cortisol detection. *EXCLI J.* **17**, 1198–1209 (2018).

143. Posthuma-Trumpie, G. A., Korf, J. & Van Amerongen, A. Development of a competitive lateral flow immunoassay for progesterone: Influence of coating conjugates and buffer components. *Anal. Bioanal. Chem.* **392**, 1215–1223 (2008).

144. Elizabeth Rey, Dakota O'Dell, PhD, Saurabh Mehta, MBBS, ScD, and David Erickson, P. Mitigating the hook effect in lateral flow sandwich immunoassays using real-time reaction kinetics. **89**, 5095–5100 (2017).

145. Corstjens, P. L. A. M. *et al.* A user-friendly, highly sensitive assay to detect the IFN-γ secretion by T cells. *Clin. Biochem.* **41**, 440–444 (2008).

146. Rivas, L., Medina-Sánchez, M., de la Escosura-Muñiz, A. & Merkoçi, A. Improving sensitivity of gold nanoparticle-based lateral flow assays by using wax-printed pillars as delay barriers of microfluidics. *Lab Chip* **14**, 4406–4414 (2014).

147. Quesada-González, D. & Merkoçi, A. Mobile phone-based biosensing: An emerging "diagnostic and communication" technology. *Biosens. Bioelectron.* **92**, 549–562 (2017).

148. Ozcan, A. Mobile Phones Democratize and Cultivate Next-Generation Imaging, Diagnostics and Measurement Tools. *Lab Chip* **14**, 3187–3194 (2014).

149. Roda, A. *et al.* Smartphone-based biosensors: A critical review and perspectives. *TrAC - Trends Anal. Chem.* **79**, 317–325 (2016).

150. SKANNEX Bioassay reader systems. SkanEasy. (2018).

151. Ltd, N. D. Novarum mobile reader solutions. (2019).

152. You, D. J., Park, T. S. & Yoon, J. Y. Cell-phone-based measurement of TSH using Mie scatter optimized lateral flow assays. *Biosens. Bioelectron.* **40**, 180–185 (2013).

153. Quesada-González, D. & Merkoçi, A. Nanomaterial-based devices for point-of-care diagnostic applications. *Chem. Soc. Rev.* **47**, 4697–4709 (2018).

154. Gong, M. M. & Sinton, D. Turning the Page: Advancing Paper-Based Microfluidics for Broad Diagnostic Application. *Chem. Rev.* **117**, 8447–8480 (2017).

155. Abcam. Antibody storage guide. (2019). Available at:

https://www.abcam.com/protocols/antibody-storage-guide.

156. Park, J. W. *et al.* Comparison of stabilizing effect of stabilizers for immobilized antibodies on QCM immunosensors. *Sensors Actuators, B Chem.* **91**, 158–162 (2003).

157. Chang, L., Shepherd, D., Sun, J., Tang, X. & Pikal, M. J. Effect of sorbitol and residual moisture on the stability of lyophilized antibodies: Implications for the mechanism of protein stabilization in the solid state. *J. Pharm. Sci.* **94**, 1445–1455 (2005).

158. Bahadır, E. B. & Sezgintürk, M. K. Lateral flow assays: Principles, designs and labels. *TrAC - Trends Anal. Chem.* **82**, 286–306 (2016).

159. Quesada-González, D. *et al.* Signal enhancement on gold nanoparticle-based lateral flow tests using cellulose nanofibers. *Biosens. Bioelectron.* **141**, 111407 (2019).

160. Chin, C. D., Linder, V. & Sia, S. K. Commercialization of microfluidic point-of-care diagnostic devices. *Lab Chip* **12**, 2118–2134 (2012).

161. Clearblue.

162. Dincer, C., Bruch, R., Kling, A., Dittrich, P. S. & Urban, G. A. Multiplexed Point-of-Care Testing – xPOCT. *Trends Biotechnol.* **35**, 728–742 (2017).

163. Couturier, K. E. H. and M. R. Multiplexed Molecular Diagnostics for Respiratory, Gastrointestinal, and Central Nervous System Infections. *Clin. Infect. Dis.* **63**, 1361–1367 (2015).

164. Mohd Hanafiah, K. *et al.* Development of Multiplexed Infectious Disease Lateral Flow Assays: Challenges and Opportunities. *Diagnostics* **7**, 51 (2017).

165. Fenton, E. M., Mascarenas, M. R., López, G. P. & Sibbett, S. S. Multiplex lateral-flow test strips fabricated by two-dimensional shaping. *ACS Appl. Mater. Interfaces* **1**, 124–129 (2009).

166. Li, J. & MacDonald, J. Multiplex lateral flow detection and binary encoding enables a molecular colorimetric 7-segment display. *Lab Chip* **16**, 242–245

(2016).

167. Wang, L., Zhao, W., O'Donoghue, M. B. & Tan, W. Fluorescent nanoparticles for multiplexed bacteria monitoring. *Bioconjug. Chem.* **18**, 297–301 (2007).

168. Yen, C. W. *et al.* Multicolored silver nanoparticles for multiplexed disease diagnostics: Distinguishing dengue, yellow fever, and Ebola viruses. *Lab Chip* **15**, 1638–1641 (2015).

169. Cinti, S., Moscone, D. & Arduini, F. Preparation of paper-based devices for reagentless electrochemical (bio)sensor strips. *Nat. Protoc.* (2019). doi:10.1038/s41596-019-0186-y

170. Tsai, T. T. *et al.* Development a stacking pad design for enhancing the sensitivity of lateral flow immunoassay. *Sci. Rep.* **8**, 1–10 (2018).

171. Fu, E. *et al.* Enhanced sensitivity of lateral flow tests using a two-dimensional paper network format. *Anal. Chem.* **83**, 7941–7946 (2011).

172. Hu, J. *et al.* Oligonucleotide-linked gold nanoparticle aggregates for enhanced sensitivity in lateral flow assays. *Lab Chip* **13**, 4352–4357 (2013).

173. Bruno, J. Application of DNA Aptamers and Quantum Dots to Lateral Flow Test Strips for Detection of Foodborne Pathogens with Improved Sensitivity versus Colloidal Gold. *Pathogens* **3**, 341–355 (2014).

174. Li, X. *et al.* Ultrasensitive lateral-flow assays based on quantum dot encapsulations with signal amplification. *J. Nanoparticle Res.* **20**, (2018).

175. Kaarj, K., Akarapipad, P. & Yoon, J. Y. Simpler, Faster, and Sensitive Zika Virus Assay Using Smartphone Detection of Loop-mediated Isothermal Amplification on Paper Microfluidic Chips. *Sci. Rep.* **8**, 1–11 (2018).

176. Jauset-Rubio, M. *et al.* Ultrasensitive, rapid and inexpensive detection of DNA using paper based lateral flow assay. *Sci. Rep.* **6**, 1–10 (2016).

177. Bishop, J. D., Hsieh, H. V., Gasperino, D. J. & Weigl, B. H. Sensitivity enhancement in lateral flow assays: a systems perspective. *Lab Chip* **19**, 2486–2499 (2019).

178. Asiaei, S., Bidgoli, M. R., ZadehKafi, A., Saderi, N. & Siavashi, M. Sensitivity and colour intensity enhancement in lateral flow immunoassay tests by adjustment of test line position. *Clin. Chim. Acta* **487**, 210–215 (2018).

179. Yew, C. H. T., Azari, P., Choi, J. R., Li, F. & Pingguan-Murphy, B. Electrospin-coating of nitrocellulose membrane enhances sensitivity in nucleic acid-based lateral flow assay. *Anal. Chim. Acta* **1009**, 81–88 (2018).

180. Katis, I. N., He, P. J. W., Eason, R. W. & Sones, C. L. Improved sensitivity and limit-of-detection of lateral flow devices using spatial constrictions of the flow-path. *Biosens. Bioelectron.* **113**, 95–100 (2018).

181. He, X. *et al.* Sensitivity Enhancement of Nucleic Acid Lateral Flow Assays through a Physical-Chemical Coupling Method: Dissoluble Saline Barriers. *ACS Sensors* **4**, 1691–1700 (2019).

182. Shen, M., Chen, Y., Zhu, Y., Zhao, M. & Xu, Y. Enhancing the Sensitivity of Lateral Flow Immunoassay by Centrifugation-Assisted Flow Control. *Anal. Chem.* **91**, 4814–4820 (2019).

183. Kim, C. *et al.* Battery operated preconcentration-assisted lateral flow assay. *Lab Chip* **17**, 2451–2458 (2017).

184. Ren, W., Mohammed, S. I., Wereley, S. & Irudayaraj, J. Magnetic Focus Lateral Flow Sensor for Detection of Cervical Cancer Biomarkers. *Anal. Chem.* **91**, 2876–2884 (2019).

185. Pan, R. *et al.* Gold nanoparticle-based enhanced lateral flow immunoassay for detection of Cronobacter sakazakii in powdered infant formula. *J. Dairy Sci.* **101**, 3835–3843 (2018).

186. Parolo, C., Medina-Sánchez, M., De La Escosura-Muñiz, A. & Merkoçi, A. Simple paper architecture modifications lead to enhanced sensitivity in nanoparticle based lateral flow immunoassays. *Lab Chip* **13**, 386–390 (2013).

187. Sun, W. *et al.* A novel multi-walled carbon nanotube-based antibody conjugate for quantitative and semi- quantitative lateral flow assays. *Biosci.*

Biotechnol. Biochem. **8451**, 1–9 (2017).

188. Rajendran, V. K., Bakthavathsalam, P., Mohammed, B. & Ali, J. Smartphone based bacterial detection using biofunctionalized fluorescent nanoparticles. *Microchim. Acta* **181**, 1815–1821 (2014).

189. Salminen, T. *et al.* Effects of blood sample anticoagulants on lateral fl ow assays using luminescent photon-upconverting and Eu (III) nanoparticle reporters. *Anal. Biochem.* **492**, 13–20 (2016).

190. Li, Z. *et al.* Rapid and Sensitive Detection of Protein Biomarker Using a Portable Fluorescence Biosensor Based on Quantum Dots and a Lateral Flow Test Strip. *Anal. Chem.* **82**, 7008–7014 (2010).

191. Wang, P., Wang, R., Zhang, W., Su, X. & Luo, H. Novel fabrication of immunochromatographic assay based on up conversion phosphors for sensitive detection of clenbuterol. *Biosens. Bioelectron.* **77**, 866–70 (2015).

192. Duan, H. *et al.* Quantum-DoT submicrobead-based immunochromatographic assay for quantitative and sensitive detection of zearalenone. *Talanta* **132**, 126–131 (2015).

193. Ye, H. & Xia, X. Enhancing the sensitivity of colorimetric lateral flow assay (CLFA) through signal amplification techniques. *J. Mater. Chem. B* **6**, 7102–7111 (2018).

194. Kim, W., Lee, S. & Jeon, S. Enhanced sensitivity of lateral flow immunoassays by using water-soluble nanofibers and silver-enhancement reactions. *Sensors Actuators, B Chem.* **273**, 1323–1327 (2018).

195. Parolo, C., de la Escosura-Muñiz, A. & Merkoçi, A. Enhanced lateral flow immunoassay using gold nanoparticles loaded with enzymes. *Biosens. Bioelectron.* **40**, 412–416 (2013).

196. Panferov, V. G., Safenkova, I. V., Varitsev, Y. A., Zherdev, A. V. & Dzantiev, B. B. Enhancement of lateral flow immunoassay by alkaline phosphatase: a simple and highly sensitive test for potato virus X. *Mikrochim Acta.* **185**, 25 (2017).

197. Gao, Z. *et al.* Platinum-Decorated Gold Nanoparticles with Dual Functionalities for Ultrasensitive Colorimetric in Vitro Diagnostics. *Nano Lett.* **17**, 5572–5579 (2017).

198. Shah, K. G. & Yager, P. Wavelengths and Lifetimes of Paper Autofluorescence: A Simple Substrate Screening Process to Enhance the Sensitivity of Fluorescence-Based Assays in Paper. *Anal Chem.* **89**, 12023–12029 (2017).

199. Li, S., Gu, Y., Lyu, Y., Jiang, Y. & Liu, P. Integrated Graphene Oxide Purification-Lateral Flow Test Strips (iGOP-LFTS) for Direct Detection of PCR Products with Enhanced Sensitivity and Specificity. *Anal Chem.* **89**, 12137–12144 (2017).

200. Wang, Y. *et al.* A Thermal Contrast Amplification Reader Yielding 8-fold Analytical Improvement for Disease Detection with Lateral Flow Assays. *Anal. Chem.* **88**, 11774–11782 (2016).

201. Zhao, Y., Huang, Y., Zhao, X., McClelland, J. F. & Lu, M. Nanoparticle-Based Photoacoustic Analysis for Highly Sensitive Lateral Flow Assays. *Nanoscale* **8**, 19204–210 (2016).

202. Wang, C. *et al.* Magnetic SERS Strip for Sensitive and Simultaneous Detection of Respiratory Viruses. *ACS Appl. Mater. Interfaces* **11**, 19495–19505 (2019).

203. Zheng, W. *et al.* Lateral Flow Test for Visual Detection of Multiple MicroRNAs. *Sens Actuators B Chem.* **264**, 320–326 (2018).

204. Crannell, Z. *et al.* Multiplexed Recombinase Polymerase Amplification Assay To Detect Intestinal Protozoa. *Anal Chem.* **88**, 1610–6 (2016).

205. Zhang, D. *et al.* Quantitative and ultrasensitive detection of multiplex cardiac biomarkers in lateral flow assay with core-shell SERS nanotags. *Biosens Bioelectron.* **106**, 204–211 (2018).

206. Lee, J. H. *et al.* Multiplex diagnosis of viral infectious diseases (AIDS, hepatitis C, and hepatitis A) based on point of care lateral flow assay using engineered proteinticles. *Biosens Bioelectron.* **69**, 213–25 (2015).

207. Washburn, E. W. The Dynamics of Capillary Flow. *Phys. Rev.* **17**, 273–283 (1921).

208. Xu, Y. *et al.* Fluorescent probe-based lateral flow assay for multiplex nucleic acid detection. *Anal Chem.* **86**, 5611–4 (2014).

209. Gomez-Martinez, J. *et al.* Multiplex Lateral Flow Assay for Rapid Visual Blood Group Genotyping. *Anal Chem.* **90**, 7502–7509 (2018).

210. Taranova, N. A. *et al.* Integration of lateral flow and micro array technologies for multiplex immunoassay: application to the determination of drugs of abuse. *Microchim. Acta* **180**, 1165–1172 (2013).

211. Lee, S., Mehta, S. & Erickson, D. Two-Color Lateral Flow Assay for Multiplex Detection of Causative Agents Behind Acute Febrile Illnesses. *Anal Chem.* **88**, 8359–63 (2016).

212. Anfossi, L. *et al.* Silver and gold nanoparticles as multi-chromatic lateral flow assay probes for the detection of food allergens. *Anal Bioanal Chem.* **411**, 1905–1913 (2019).

213. Zhang, D. *et al.* Quantitative detection of multiplex cardiac biomarkers with encoded SERS nanotags on a single T line in lateral fl ow assay. *Sensors Actuators B. Chem.* **277**, 502–509 (2018).

214. Zhao, Y. *et al.* Rapid multiplex detection of 10 foodborne pathogens with an up- converting phosphor technology- based 10-channel lateral flow assay. *Sci. Rep.* **6**, 21342 (2016).

215. Orlov, A. V., Znoyko, S. L., Cherkasov, V. R., Nikitin, M. P. & Nikitin, P. I. Multiplex Biosensing Based on Highly Sensitive Magnetic Nanolabel Quantification: Rapid Detection of Botulinum Neurotoxins A, B, and E in Liquids. *Anal Chem.* **88**, 10419–10426 (2016).

216. Cozart Bioscience Limited. *A Drug Screening Instrument Microcontroller Technology Automates Visual Inspection System.* (1999).

217. Qiagen. ESEQuant Lateral Flow System Technical Information. (2011).

218. Zamora-Gálvez, A., Morales-Narváez, E., Romero, J. & Merkoçi, A. Photoluminescent lateral flow based on non-radiative energy transfer for protein detection in human serum. *Biosens. Bioelectron.* **100**, 208–213 (2018).

219. Quesada-González, D. & Merkoçi, A. Mobile phone-based biosensing: An emerging "diagnostic and communication" technology. *Biosens. Bioelectron.* **92**, 549–562 (2017).

220. Bankmycell.com. HOW MANY PHONES ARE IN THE WORLD? (2019).

221. Jung, Y., Heo, Y., Joong, J., Deering, A. & Bae, E. Smartphone-based lateral flow imaging system for detection of food-borne bacteria E . coli O157:H7. *J. Microbiol. Methods* **168**, 105800 (2020).

222. Danthanarayana, A. N. *et al.* A multicolor multiplex lateral flow assay for high-sensitivity analyte detection using persistent luminescent nanophosphors. *Anal. Methods* **12**, 272–280 (2020).

223. Liu, Z. *et al.* A smartphone-based dual detection mode device integrated with two lateral flow immunoassays for multiplex mycotoxins in cereals. *Biosens. Bioelectron.* **158**, 112178 (2020).

224. Orlov, A. V., Bragina, V. A., Nikitin, M. P. & Nikitin, P. I. Rapid dry-reagent immunomagnetic biosensing platform based on volumetric detection of nanoparticles on 3D structures. *Biosens. Bioelectron.* **79**, 423–429 (2016).

225. Qu, Z., Wang, K., Alfranca, G., de la Fuente, J. M. & Cui, D. A plasmonic thermal sensing based portable device for lateral flow assay detection and quantification. *Nanoscale Res. Lett.* **15**, (2020).

226. Zhang, Y. J., Chen, S., Yu, Y. L. & Wang, J. H. A miniaturized photoacoustic device with laptop readout for point-of-care testing of blood glucose. *Talanta* **209**, 120527 (2020).

227. Tran, V., Walkenfort, B., König, M., Salehi, M. & Schlücker, S. Rapid, Quantitative, and Ultrasensitive Point-of-Care Testing: A Portable SERS Reader for Lateral Flow Assays in Clinical Chemistry. *Angew. Chemie - Int. Ed.*

58, 442–446 (2019).

228. Zhang, S. *et al.* Upconversion luminescence nanoparticles-based immunochromatographic assay for quantitative detection of triamcinolone acetonide in cosmetics. *Spectrochim. Acta - Part A Mol. Biomol. Spectrosc.* **214**, 302–308 (2019).

229. Gong, Y. *et al.* A portable and universal upconversion nanoparticle-based lateral flow assay platform for point-of-care testing. *Talanta* **201**, 126–133 (2019).

230. Jin, B. *et al.* Lateral flow aptamer assay integrated smartphone-based portable device for simultaneous detection of multiple targets using upconversion nanoparticles. *Sensors Actuators, B Chem.* **276**, 48–56 (2018).

CHAPTER 2. THESIS OBJECTIVES

The main objective of the present Thesis is to learn in detail about optical biosensors applied at the point-of-care, particularly on nanoparticles-based LFAs. Study the state-of-the-art of this technology, including the development and optimization procedures. This PhD thesis is focused in the development of low-cost and simple strategies that can solve the reported limitations of LFAs, such as low sensitivity and underperformance in complex samples.

More in detail, the objectives of the Thesis can be summarized as following:

- Study the integration of paper-based electrophoresis in LFA as a strategy for the sensitive detection of target analytes in complex samples, such as serum and whole blood.
    - Develop a paper-electrophoretic bioassay (PEB) operated with a smartphone.
    - Evaluate the electrophoretic mobility of QDs and AuNPs in PEB.
    - Validate PEB for detection of H-IgG in whole blood.

- Develop a LFA modified with a time-delay wax barrier as a sensitivity and signal enhancement strategy.
    - Evaluate several barrier widths and Tween-20 concentrations in order to obtain different flow retention times.
    - Evaluate the sensitivity and signal enhancement achieved with the different conditions for the detection of H-IgG (as a proof-of-concept).

- Take advantage of the glass fiber, commonly used as conjugate pad in LFA, to develop a simple and low-cost lab-on-a-tube platform for the detection of *E. coli.*
    - Develop a biosensing mechanism based on Förster Resonance Energy Transfer (FRET), being the AuNPs and AuNCs the energy acceptors and donors, respectively.
    - Validate the lab-on-a-tube platform for the detection of *E.coli* in river and tap water samples.

# CHAPTER 3. PAPER-ELECTROPHORETIC BIOASSAY (PEB): DIAGNOSIS IN WHOLE BLOOD OPERATING VIA SMARTPHONE

3.1. Introduction

The ability to measure a specific biomarker within minutes and in the easiest possible way is crucial for a variety of healthcare-related scenarios, ranging from the daily measurement of glucose level to the monitoring of a pandemic.[1,2] In this context laboratory-based technologies are not useful, considering that they require expensive/bulky equipment, long/multi-step protocols and qualified personnel.[3,4] Instead Point of Care (POC) tests represent a valid solution thank to their ease-of-use, speed, low cost and portability.[5–7] In the realm of PoC technologies, Lateral Flow Assays (LFAs) stand out as the most widely used PoC sensors across many disciplines from environmental analysis to safety and diagnostics. Their success lies on their single step procedure (the user has just to apply the sample and in some cases a washing buffer) and their ability to provide a result within 10-15 minutes.[8,9] The combination of their practicality with a low fabrication cost makes them a particularly attractive sensing platform for both developers and users. Indeed the simple operation of LFAs is one of their major advantages over other sensing technologies, but it also comes with a major drawback: the inability to perform efficient sample treatments. This limitation of LFAs precludes their use for more challenging applications, for example the detection of biomarkers at low concentrations in complex media.

Most commercially available LFAs are either single-step (i.e. pregnancy tests) or double-step (i.e. serological tests) assays. The only sample treatment included in the former type of assays is the modification of the physical-chemical properties of the sample thanks to the use of a pre-stored buffer (i.e. a buffer dried into the sample pad, which is the region of the test where the sample is applied). This allows for the stabilization of the pH, ionic strength and viscosity of the sample, which may be enough for clear samples with low viscosity (i.e. urine) but it is not sufficient for more viscous and complex matrixes (i.e. serum/blood).[10] Regarding the latter type of LFAs, they can include either a dilution step (prior the addition of the sample onto the sample pad) or a washing step (the addition of a washing buffer after the application of the sample).[11,12] In this case, LFAs can also work with blood and serum samples but it compromises their ease of use (i.e. the user has to dilute the sample or add a washing buffer at a fixed time) and possibly their sensitivity (the dilution of the sample implies a dilution of the

target analyte). Finally LFAs can also include reagents or materials that remove specific contaminants (for example antibodies for the removal of albumin or filters to remove blood cells), but this increases the complexity and cost of the fabrication.[13]

Here we propose a novel sensing platform that allows the use of highly-concentrated blood samples, while keeping all the characteristics that make LFAs the most popular POC diagnostic technology. In particular we developed a paper-based electrophoretic bioassay (PEB) that uses the main components of LFAs but, instead of relying on the capillary force to move the sample, it uses electrophoresis. The use of a continuous and tuneable flow to move the sample easily overcomes the main issues observed when using blood samples in LFAs, like non-specific binding or the clogging of the strip. We validated the PEB using as test bed the detection of Human Immunoglobulin G (H-IgG) in untreated blood samples. Finally we demonstrated the applicability of PEB at the point of care using a smartphone-based system that controls the electrophoresis and quantify the optical signal (Figure 3.1.).
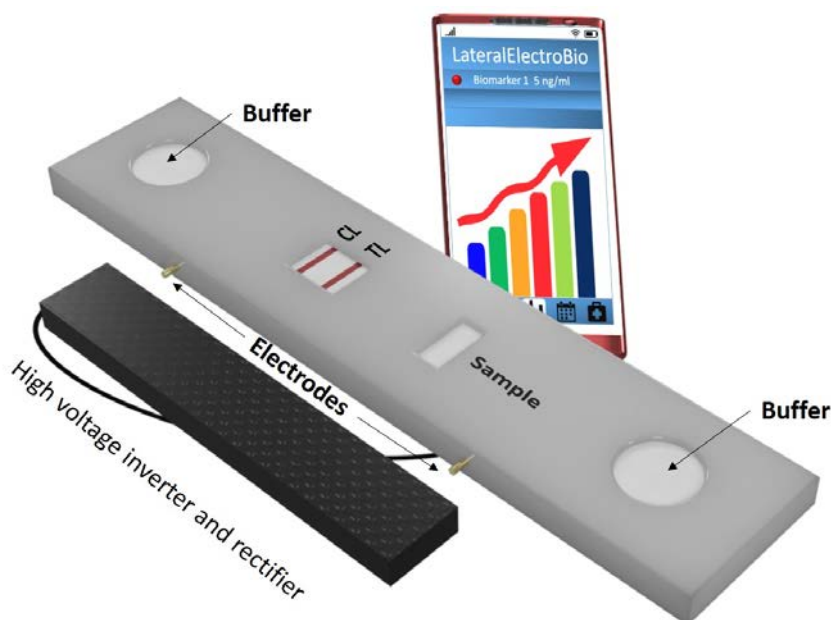
Figure 3.1. Schematic representation of PEB device enclosed in a cassette. The cassette consists of two reservoirs for the insertion of the electrophoresis buffer, a reservoir for the addition of the sample and a window for the assay evaluation. The cassette is connected to the smartphone that serves together with the high voltage inverter and rectifier as a portable read-out system. Figure courtesy of PhD. Ruslan Álvarez-Diduk.

3.2. Materials and methods

3.2.1. Materials and reagents

Polyclonal goat to H-IgG antibodies (I1886), IgG from human serum (I2511), Bovine serum albumin (A3294), Sucrose (84097), Phosphate buffered saline tablets (P4417), Tween-20 (P1379), Sodium tetraborate decahydrate (B9876), boric acid (B-7901-500G), Citric acid (251275-500G), Hydrochloric acid, 37% (320331), L-Cysteine (168149-100G), tetrachloroauric (III) acid (520918-1G) and sodium citrate (1613859) were purchased from Sigma-Aldrich. Polyclonal chicken to goat IgG (ab86245) was purchased from Abcam. Sodium hydroxide (131687) was purchased from PanReac. MilliQ water was produced using Milli-Q system (>18.2MΩ*cm). Streptavidin-functionalized CdSe@ZnS QDs (Q10121MP) were purchased from Thermofisher. CdTe QDs (Hydrophilic CdTe Quantum Dots Kit) were purchased from Plasma Chem. Nitrocellulose membranes (UniSart CN95, CN110 and CN150) were purchased from Sartorius Stedim. Cellulose membrane (CFSP001700) was purchased from Merck Millipore. Sample pad for whole blood (CytoSep) was purchased from Ahlstrom-Munksjö. Glass fiber (Standard 14) was purchased from GE Healthcare. Laminated cards were purchased from (Kenosha). Adhesive copper tape (B018RDZ3HG) was purchased from Kraftex. Polylactic acid (PLA) filaments were purchased from BCN3D. Chicken Blood (In Sodium Citrate) (ABIN1044904) was purchased from antibodies-online GmBH.

3.2.2. Instruments

3D-printer (Sigma R19) was purchased from BCN3D. Thermoshaker for microtubes (TS-100) was purchased from Biosan. Centrifuge (Allegra 64R) was purchased from Beckman Coulter. Reagent dispenser (IsoFlow reagent dispenser) was purchased from Imagene Technology. Programmable strip cutter (ZQ2002) was purchased from Kinbio. Oven (2001246) was purchased from P. Selecta. Laboratory pump (N938.50KN.18) was purchased from KNF lab, Laboport. Vacuum Desiccator (550) was purchased from Karnell. pH meter (pH meter Basic 20+) was purchased from Crison. Teflon-equipped stainless-steel autoclave (TOPT-HT150) was purchased from Toption instrument co. Analytical balance (Readability: 0.001 g) was purchased from Ohaus Discovery. Milli-

Q system (>18.2MΩcm-1) was purchased from Millipore. Samsung Galaxy S7 Edge was purchased from Samsung.

3.2.3. PEB device design and fabrication

A nitrocellulose membrane with size of 10 cm x 0,49 cm was used as platform for running the electrophoresis. Two adhesive copper electrodes were stacked at 0.5 cm from both ends of the strip. Moreover, reservoir pads (6 cm x 4 cm) of cellulose membrane were used instead of wells for the storage and gradual dispensing of the electrophoresis buffer. They were stacked over the adhesive copper electrodes towards the extremes of the strip. For the performance of the electrophoresis, the copper electrodes where connected to the battery system that contained all the electronics inside a 3D-printed PLA cartridge. For the evaluation of the QDs mobility, a cover was fabricated. The cover was made of polylactic acid and fabricated using a 3D printer. Two LEDs (365 nm excitation wavelength) and two white LEDs were introduced inside the device cover and connected by an OTG wire to a Smartphone (Figure 3.2.).

Figure 3.2. Pictures of the cover of the device containing the LEDs.

3.2.4. Nitrocellulose membrane strip fabrication

The nitrocellulose membranes used for the evaluation of the electrophoresis performance were CN95, CN110 and CN150. For the detection of H-IgG, CN95 nitrocellulose membrane was used. Polyclonal goat to H-IgG antibodies were deposited in TL and polyclonal chicken to goat IgG antibodies in CL, using a bioreagent dispenser. The antibodies were dried for 2 hours at 37 °C.

3.2.5. Evaluation of the electrophoresis performance

Commercial streptavidin functionalized CdSe@ZnS QDs and CdTe QDs were used. The G-QDs were synthesized homemade following the procedure of Dong, et.al.[14] The N-S-doped G-QDs were synthesized following the procedure reported by Dong, et.al.[15] The evaluation of the effect of the buffer pH on the electrophoretic mobility of the QDs was carried out drop-casting 1 mL of sodium borate buffer (10mM, pH 8) to the cellulose pads. The pH of the buffer was adjusted with boric acid and sodium hydroxide. The AuNPs were synthesized by the Turkevich method[16] using a 25 mM solution of $HAuCl_4$ and sodium citrate. The AuNPs were characterized by TEM and UV-Vis spectrum (see figure S9 and S10). They were conjugated with anti-HIgG following the experimental procedure already reported by the group.[17]

3.2.6. Detection of H-IgG in SB buffer and whole blood

1 mL of sodium borate buffer (10mM, pH 8) was drop-casted to the cellulose pads. Once the entire strip was embedded with the electrophoresis buffer, the electrodes corresponding to the positive and negative charged poles where connected to the battery. Next, 3 μL of the conjugated AuNPs were incubated with 3 μL of chicken whole blood samples for 30 seconds and drop-casted on 1 cm from the TL. The battery was connected and the electrophoresis was performed for 15 minutes.

3.2.7. Evaluation of the PEB

A picture of the strips was taken adjusting the camera parameters of the smartphone (ISO 160, A 1/10, Manual focus). The picture was evaluated using Image J software following the procedure reported by our group.[18] The signal intensity was normalized following the equation: (TL - BG)/(CL - BG), were TL, CL and BG were the signal

intensities of test line, control line and background. The LoD was calculated as Optical density (LoD) = blank + 3 σ blank (i.e. the corresponding value of blank sample plus 3 times its standard deviation). The LoQ was calculated as Optical density (LoQ) = blank + 10 σ blank.[19]

3.2.8. Detection of H-IgG in whole blood using LFA

The LFA strips were fabricated following the procedure already reported by our group.[9] CytoSep membrane was used as sample pad. The anti-HIgG functionalized AuNPs solution used in the conjugate pad was the same as the one used for the PEB experiments. The calibration curve for H-IgG was performed by spiking H-IgG (0 to 10000 ng/mL) in PBS buffer (10 mM, pH 7.4). 100 μL of each solution were drop-casted onto the sample pad. For the calibration curve of H-IgG in whole blood, a solution of chicken whole blood spiked with H-IgG (1 μg/ml) was prepared. The solution was diluted 2.4-fold and 5-fold using PBS buffer (10 mM, pH 7.4). 100 μL of the un-diluted and diluted whole blood samples were drop-casted onto the sample pad. Pictures of the strips were taken after 15 minutes using the smartphone and adjusting the same camera parameters as for the PEB evaluation.

3.3. Results

3.3.1. Concept

Electrophoresis is a term that describes the migration of charged particles under the influence of an electric field. The system is based on two electrodes of opposite charge (cathode and anode) connected by a conductive medium (electrolyte). The charged particles are able to separate due to differences in their velocity (*v*), which depends on the particle's mobility (*μ*) and the applied field strength (*E*) in such a way:

$$v = \mu E$$

Moreover, the particle's mobility (*μ*) is determined by their size, shape, and charge and by the temperature during the separation. The mobility is constant under defined electrophoretic conditions, which are characterized both by electrical parameters (current, voltage, power) and factors related to the electrophoresis medium (ionic

strength, pH value, viscosity and pore size). In this sense, the electrophoretic mobility (μ) can be expressed as:

$$\mu = \frac{q}{6\pi r \eta}$$

Where q is the charge on the particle, η is the viscosity of the media and r is the hydrodynamic radius related to the size of the particle. This means that under defined electrophoretic conditions, small and highly charged molecules will move towards the electrode with the opposite charge faster than bulky and neutral ones. From the perspective of sample treatment, this allows for an active and precise separation of contaminants from the target molecule, dramatically reducing non-specific interactions.[20–22]

Electrophoresis can be carried out either in free solution (capillary electrophoresis) or in a support medium (paper or gel). The former offers fast and high-resolution separation but requires great electric fields, which limits their application at the PoC. The latter are simpler, cheaper and enable facile visualization of the separation zone by direct staining. Within the types of support media, gel provides better resolution than paper but is more affected by heat generation, which causes variations in the particle's migration rate and band's distortion.[2123] Contrary to free electrophoresis, the particle's movement in support-medium-electrophoresis is a sum of electrophoretic and electroendosmotic mobility. Electroendosmosis is the movement of liquid towards anode or cathode depending on the type of support medium, potential gradient, electrolyte ionic strength and pH. Counterintuitively, this means that depending on the specific conditions we could even observe charged molecules moving towards the electrode with the same charge.[24–26]

Importantly, unexpected particle's mobility or band's distortion is commonly observed upon heat generation during gel electrophoresis.[27] This phenomenon is explained by Joule's law and the generalized power equation:

$$P = \frac{V^2}{R}$$

Where (P) is the power converted from electrical energy to thermal energy, (V) is the voltage applied and (R) is the resistance to current.[28] Considering this equation,

electrical systems that exert higher resistance to current produce less heat. In this sense, paper electrophoresis is less prone to heat generation than agarose gel electrophoresis because nitrocellulose membrane has 10^9 –fold higher resistivity than agarose gel, and therefore it provides higher resistance to current.[29,30]

The foundation of PEB is the field of paper electrophoresis, which, since 1950s, has been developing strategies for the examination of a variety of different samples, ranging from water to human serum. Most of those works aimed at the separation of target analytes (including inorganic salts, amino acids, enzymes and proteins) along a filter paper and their subsequent analysis, such as the measurement of their concentration and/or specific activity.[27] Nonetheless those worked relied on complex and tedious techniques for the identification of the separated components, which are based on staining or immunoblotting. The former serves for an estimation of the molecular size of the components upon comparison with a ladder/marker. The latter provides a more specific determination of the separated components but it still requires several complex steps (membrane transferring, incubation with primary antibody, washing, incubation with secondary antibody, washing, signal revealing) and high volumes of antibodies.

For the development of PEB, we took advantage of the sample treatment capabilities of paper-electrophoresis and merged them with the convenience of LFAs. The result is a diagnostic platform the can receive an undiluted drop of blood and produce an easy-to-read optical signal in less than 15 minutes.

3.3.2. Design and operation

We designed the PEB device to assure its deployment at the point of care, so keeping the portability, usability and low cost of a LFA. For this reason, we employed the standard LFA materials: cellulose and nitrocellulose membranes. We used the former as buffer reservoirs to maintain the nitrocellulose constantly wet; while we used the latter as main platform for both carrying out the electrophoretic separation and the signal generation. We also used two sticky copper electrodes instead of applying the voltage directly on the nitrocellulose strip. Compared to crocodile clips or similar electrical connectors, the copper sticky tape provides a higher contact surface on the nitrocellulose strip. In addition, it is disposable and cheaper to be replaced once oxidized (electrical connectors tend to oxidize during electrophoresis). Regarding the

reagents, we used antibodies as bioreceptors (printed on the nitrocellulose membrane as for normal LFA) and analyte, while we employed gold nanoparticles (AuNPs) and quantum dots (QDs) as labels. In order to perform the electrophoresis separation, we designed a miniaturized and portable power source as an alternative to the bulky and expensive power source used in conventional electrophoresis systems. We connected the smartphone battery to a Joule thief inverter and a rectifier (Figure 3.3.) to obtain a stable 200v DC. It is worth to mention that, although the low intensity of the output current may suggest its inadequacy to perform an electrophoresis, the high resistance of the system (several mega ohms) allows keeping a constant voltage in the device.
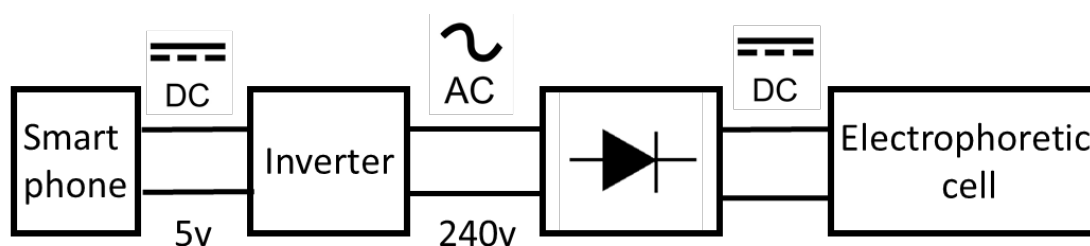

Figure 3.3. Diagram of the components and connections in the electrophoretic device.

The test is 22 x 4 cm (Figure 3.4.), weighs less than 200 grams and costs around 1 euro (excluding the power source, which costs approximately 10 euros). A detailed description of the fabrication of the PEB device is in the Materials and Methods section.
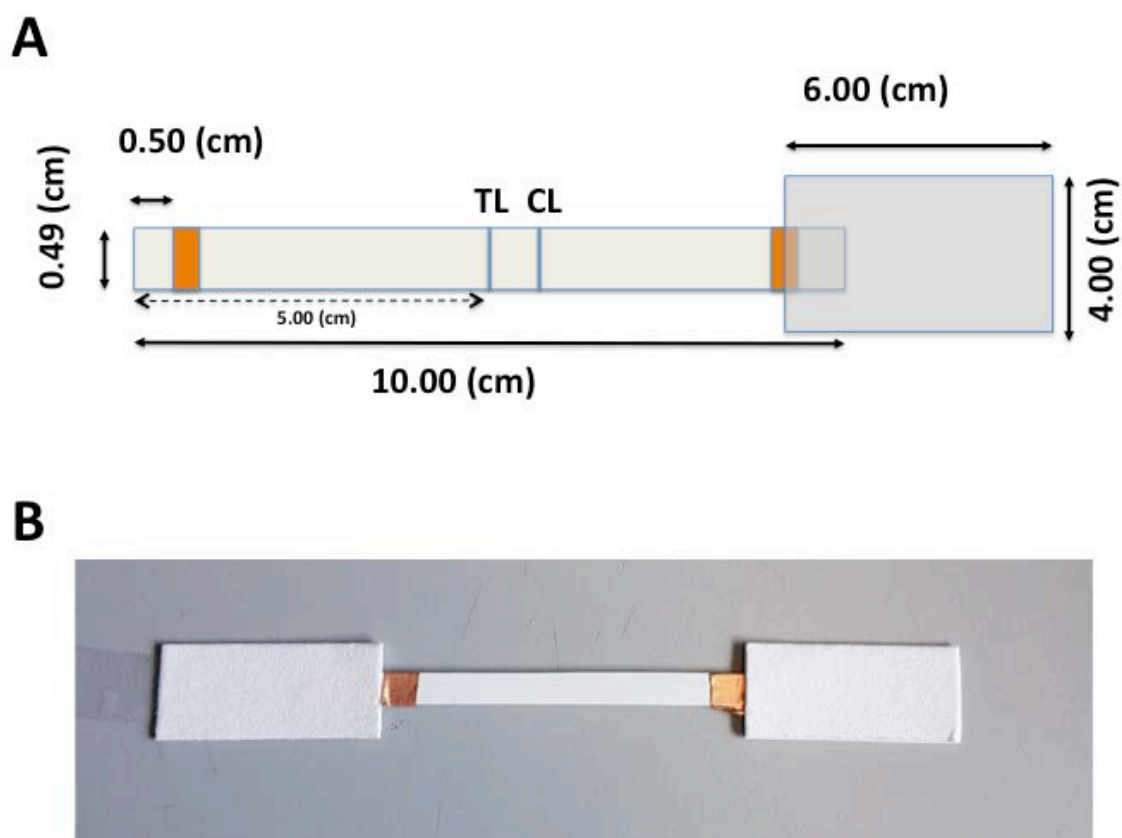
Figure 3.4. (A) Scheme of the device components and dimensions. The components are nitrocellulose membrane (white), adhesive cupper electrodes (orange), cellulose membrane (grey) and capture antibodies in TL and CL (blue). **(B)** Picture of the PEB strip.

The operation of the sensor consists in few simple steps: 1) the two cellulose pads at the two extremities of the sensor are wet with the electrophoresis buffer, which contains the electrolytes enabling the electric bridge between the cathode and the anode. The high void volume of the two cellulose pads ensures the complete and homogenous wetting of the nitrocellulose membrane for the whole duration of the assay (15 min). 2) Once the nitrocellulose membrane is fully wet (approximately in 2 min from the addition of the electrophoresis buffer), the labelled sample (6 µL) is drop-casted onto the membrane. 3) The electrophoretic potential is applied moving the sample along the membrane and generating the optical read out. The full operation is schematized in Figure 3.5. It is important to note that the whole operation could be condensed into a single-step procedure for a commercial application by keeping the sensor wet in a sealed container and employing a conjugate pad on top of the nitrocellulose membrane.
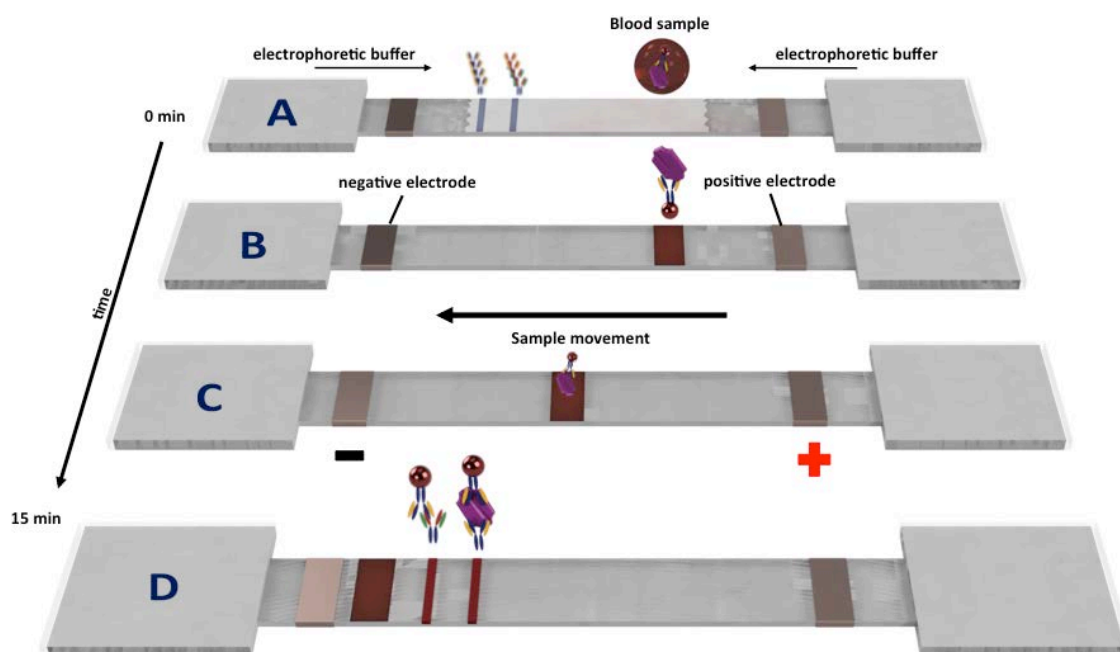
Figure 3.5. Schematic representation of PEB strip and assay operation. PEB strip is composed of a nitrocellulose (NC) membrane strip functionalized with capture antibodies in TL and CL. **(A)** Two pieces of adhesive copper tape are stacked on both sides of the strip and serve as cathode and anode electrodes. Two pieces of cellulose membrane are stacked on both ends of the strip and serve as electrophoresis buffer reservoirs. The electrophoresis buffer is drop-casted on both cellulose pads and is gradually dispensed to the NC membrane. **(B)** The conjugate solution is mixed with the whole blood sample and it is drop-casted on the strip. **(C)** The sample moves by electrophoresis towards the detection zone. **(D)** The target analyte and the labeled antibodies are captured by the antibodies in TL and CL. The non-specific interfering components of the whole blood sample flow out of the detection zone enabling a clear visualization of the signal in TL and CL. Figure courtesy of PhD. Ruslan Álvarez-Diduk.

3.3.4. Characterization of PEB as electrophoretic platform

Given the complexity of paper-based electrophoresis, we first characterized how using different materials and reagents during the fabrication of the PEB would affect its electrophoretic behavior. We studied four main components: the moving particles, the pore-size of the nitrocellulose membrane, the applied voltage and the pH of the electrophoresis buffer.

The first elements we validated were how the size, shape and charge of nanoparticles affect their migration speed. Following the principles of electrophoresis, we expect that bigger and less charged particles would move slower than smaller and more charged ones, given a fixed pore size, electrophoretic buffer and applied potential. In order to validate this hypothesis, we used three different QDs: CdSe@ZnS QDs functionalized with streptavidin (Ø 20 nm, considering the streptavidin), CdTe QDs (Ø 5 nm) and G-QDs (Ø 2.5 nm). We chose these three QDs, because they cover the size range of most proteins and their charge has been previously studied. G-QDs have a high negative charge due to the oxygen functional groups (C-OH, C=O and COOH)[31]; CdTe QDs also have a negative charge due to their functionalization with carboxyl groups.[32] The streptavidin (pI ≈ 5) functionalization of the CdSe@ZnS QDs also confers them a negative surface charge at pH 8. . Their detailed characterization can be found in Figure 3.6 A, B & C.

For this experiment, we fixed the field strength using sodium borate buffer 10 mM at pH 8 and an operating voltage of 200 V and the CN150 nitrocellulose membrane. Since the buffer solution has a pH value lower than the pKa of the boric acid (pKa=9.24) the predominant concentration of positive charged ions makes the buffer move towards the cathode (negative electrode), and by electroendosmosis it drags also all the QDs. As expected we found a correlation between the size/charge and the migration speed. In particular the CdSe@ZnS QDs moved at an average speed of 0.32 cm/min towards the negative electrode due to their bigger size and the negative surface charge provided by the streptavidin (pI ≈ 5-6). Instead the G-QDs and CdTe QDs moved at an average speed of 0.37 and 0.72 cm/min, respectively, due to their smaller size and negative surface charge provided by the functional groups.
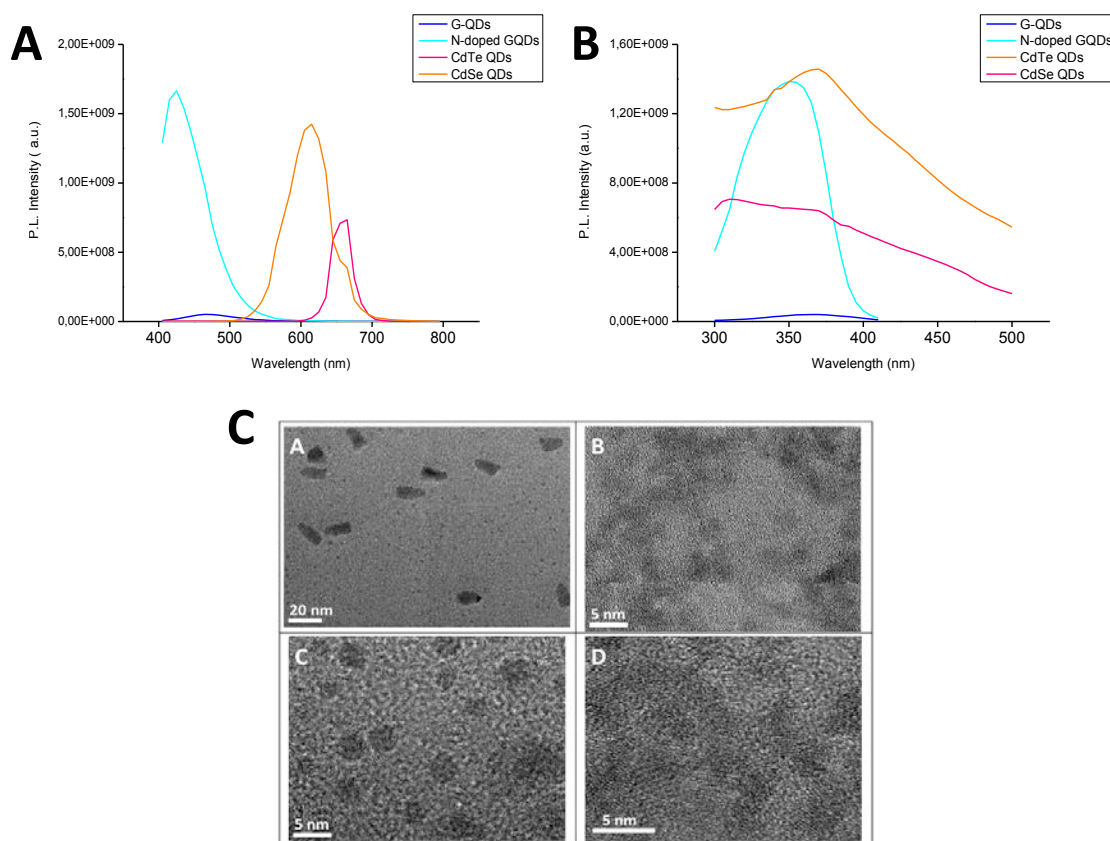
Figure 3.6. (A) Wavelength emission spectrum of the N-S-doped G-QDs (light blue), G-QDs (dark blue), CdTe QDs (orange) and CdSe@ZnS QDs (pink). **(B)** Wavelength excitation spectrum of the N-S-doped G-QDs (light blue), G-QDs (dark blue), CdTe QDs (orange) and CdSe@ZnS QDs (pink). **(C)** TEM images of (A) CdSe@ZnS QDs (B) CdTe QDs (C) G-QDs (D) N-S-doped G-QDs.

The second parameter that we studied was the effect of different nitrocellulose membrane over the migration speed. For this study we used three different nitrocellulose membranes (CN95, CN110 and CN150) commonly used for the development of LFAs. In particular they provide three different capillary flow rates of 95s/4cm, 110s/4cm and 150s/4cm, respectively for CN95, CN110 and CN150. The capillary flow rate represents that time required for the sample to cover 4 cm of the nitrocellulose membrane, and it is thus inversely related to the membrane pore size. For example CN150 with a capillary flow rate of 150s/4cm has the smallest pore size of the three membranes tested in this work. Producers of nitrocellulose membrane tend not to give information on the pore size of the membranes as the polymeric structure dues not actually create pores but rather a sponge-like pathway.[33] We refer the reader to the

Figure 3.7. for the SEM images of the three different membranes and to the estimation of their relative pore size.
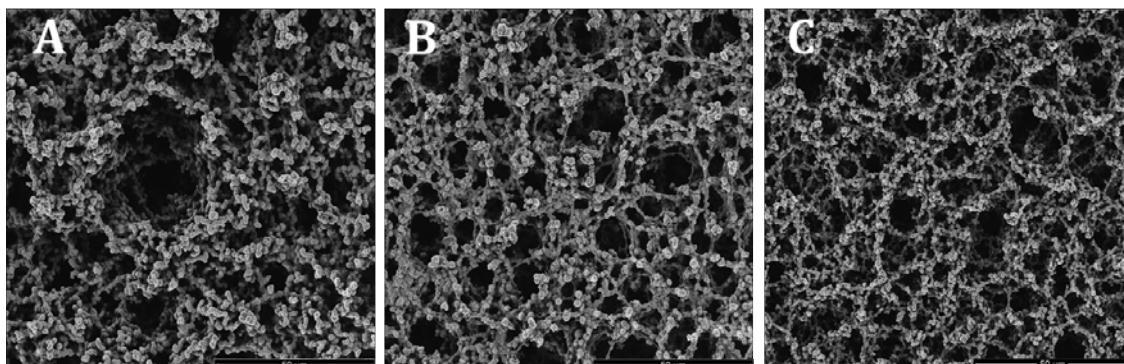
Figure 3.7. SEM images of (A) CN95 (B) CN110 (C) CN150 nitrocellulose membranes.

Again the PEB device responded accordingly to the principles of electrophoresis. For this experiment, we used sodium borate buffer 10 mM at pH 8, an operating voltage of 200 V and the same QDs. As expected the CN95 membrane produced 2.67-, 1.37- and 2.30-fold faster migration speed of G-QDs, CdTe and CdSe@ZnS QDs, respectively, compared to CN150 membrane (Figure 3.8. A).

The third parameter we tested was the applied voltage. The principles of electrophoresis states that under a uniform electric field, the field strength is directly proportional to the voltage applied and hence to the particle's velocity. Therefore higher voltage produces a faster migration speed if the other parameters are fixed. From the engineering point of view of the sensor fabrication and design, this is a crucial parameter, since we need to be able to achieve a quick migration applying a low voltage in order to have a sensor deployable at the point of care. In Figure 3.8. B we show the behaviour of the voltage on the electrophoretic mobility at 100, 200 and 300V. For this experiment we used CN95 NC membrane. As expected, a higher voltage caused a faster movement of the QDs to the negative electrode. G-QDs, CdTe and CdSe QDs moved 2.86, 1.50 and 1.54-times faster when applying 300V rather than 200V. However, higher voltages resulted in less reproducible velocities. The standard deviation of the velocity of G-QDs, CdTe and CdSe QDs was 2.56, 3.55 and 6.60-times higher when applying 300V rather than 100V. The CdTe QDs moved the fastest, particularly they moved 1.3-times

faster than the GQDs when applying 300V. Instead the CdSe QDs followed the same trend as in figure 3A and moved the slowest to the negative electrode.

Finally, to evaluate the effect of the pH on the particle mobility direction and speed, we tested SB buffer (10 mM) at three different pH values (8, 9 and 10). Given the principles of electrophoresis, the particle's rate and direction of movement is influenced by the electrophoretic and electroendosmotic mobility. Variations in the pH have a drastic effect on both forces. In the former the pH determines the magnitude and sign of particle's surface charge, while in the latter the pH determines the rate and direction of movement of the electrolyte solution. Being able to tune not only the speed but also the direction of the flow is paramount to achieve a complete sample treatment. In fact just by changing the pH of the electrophoresis buffer we could separate the target analyte form other compounds. For this experiment we challenged the PEB device with G-QDs since their surface functional groups are deprotonated when the pH value is higher than 7.[34] This means that the G-QDs have higher negative surface charge upon pH values higher than 7. However, we observed that at pH 8, the G-QDs moved towards the negative electrode, at pH 9 they slightly moved and at pH 10 they moved towards the positive electrode (Figure 3.8. C, D). This means that the mobility of the G-QDs was mostly influenced by the electroendosmotic mobility: at pH 8 the pH value of the buffer was lower than the pKa of the boric acid (pKa = 9.24) and therefore the predominant ions in the electrolyte solution were positively charged. The buffer dragged the G-QDs to the negative electrode. At pH 9 the pH value of the buffer was nearly equal to the pKa of the boric acid (pKa = 9.24), therefore there were no predominant charged ions in the electrolyte solution and the G-QDs had enough negative surface charge to slightly move towards the positive electrode. Conversely, at pH 10 the predominant ions in the electrolyte were negatively charged, thus the buffer dragged the G-QDs towards the positive electrode. Once again the PEB device showed the ability to properly perform electrophoresis.
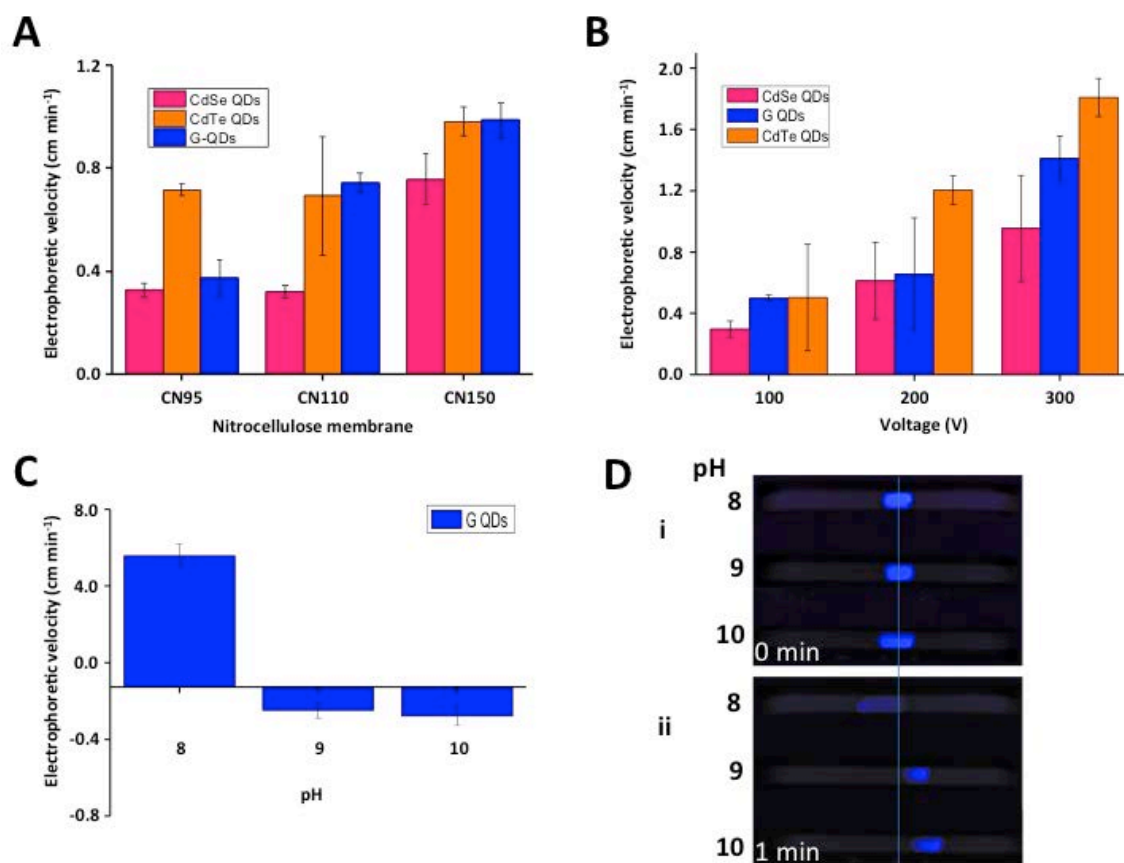
Figure 3.8. Electrophoresis performance evaluation. **A)** The effect of the nitrocellulose membrane pore size on the electrophoretic mobility of different QDs. Nitrocellulose membranes CN95, CN110 and CN150 were selected due to their big, medium and small pore size, respectively. **B)** Evaluation of the voltage effect applied on the electrophoresis mobility using the same QDs. **C)** Effect of the pH value on the electrophoretic mobility. **D)** GQDs image at different pH values before applying the voltage 0 min **(i)** and after 1 min of voltage **(ii)**.

3.3.5. Separation of quantum dots with the PEB device

After demonstrating that the PEB device was following the principles of electrophoresis using simple homogenous buffer solutions, we verified that it could actually separate different particles from a heterogeneous sample. In order to this, we used two different solutions: one containing N-S-doped G-QDs and CdSe@ZnS QDs (at 25 nM), while the other containing CdTe QDs and CdSe@ZnS QDs (both at 25 nM). The choice of these two couples of QDs gives relevant information on the influence of the surface charge and size on the particle's mobility. For instance, in the previous section we observed

that the G-QDs moved faster to the cathode than the CdSe@ZnS QDs, mainly due to their big difference in size (2.5 nm and 20 nm, respectively). However, we wanted to check if this phenomenon could be conversed by manipulating the surface charge of the G-QDs. In this sense we doped the G-QDs with nitrogen and sulphur functional groups to increase their negative surface charge, which provides repulsion to the cathode. It is reported that the N-S-doped G-QDs have a more negative ζ-potential value than the G-QDs (-31.6 mV and -20 mV, respectively).[3733] The system set up included the use of the SB buffer at pH 8, a potential of 200V and the CN150 nitrocellulose membrane. Again, the system responded as expected. The N-S-doped G-QDs moved slower than the CdSe@ZnS QDs to the negative electrode despite of their smaller size, indicating that the CdSe@ZnS QDs have less negative surface charges than the N-S-doped G-QDs (Fig. 3.9. A). Instead for the second mixture, the smaller CdTe QDs (diameter 5 nm) moved faster than the bigger CdSe@ZnS QDs (Fig. 3.9. B), which is similar to what we observed in Fig. 3.8. A. Crucially, in both cases we achieved the complete separation of the different QDs in the respective solutions in 10 min. This result supports the ability of the PEB device to carry out sample treatment for the separation of both particles with different sizes and different charges.
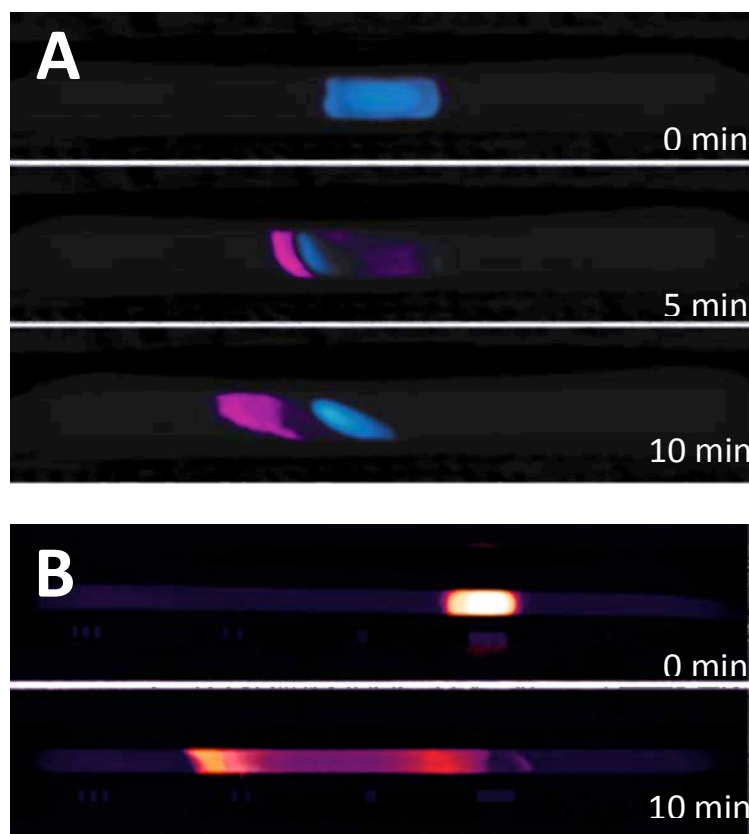
Figure 3.9. Separation of QDs by electrophoresis. **A)** N-S-doped G-QDs are mixed with CdSe@ZnS QDs and drop-casted in the centre of the nitrocellulose membrane strip that is immersed in electrophoresis buffer pH 8. After running the electrophoresis for 10 minutes, the CdSe@ZnS QDs (pink) moves to the left side of the strip (negative electrode) separating from the N-S-doped G-QDs (blue), which have slightly moved to the left side. **B)** CdTe QDs are mixed with CdSe@ZnS QDs and drop-casted in the centre of the nitrocellulose membrane strip that is immersed in electrophoresis buffer pH 8. After running the electrophoresis for 10 minutes, CdSe@ZnS QDs (orange) have moved faster to the left side (negative electrode) separating from the CdSe@ZnS QDs (red), which have slightly moved to the left side.

3.3.6. PEB optimization for gold nanoparticles

Supported by the ability of the PEB device to separate different types of QDs, we decided to test its ability to move also AuNPs. Aiming at the development of a POC platform, the use of AuNPs (the most used label in LFA) is fundamental to translate the device from the benchtop to the market, since they provide a cost effective synthesis, a straightforward functionalization and the naked-eye visualization.[38–40] The AuNPs we

used had a spherical shape and a diameter of around 15 ± 2 nm and a ζ-potential value of around -38.3 mV[41] (the reader can find a complete characterization of the AuNPs in Figure 3.10. A & B.
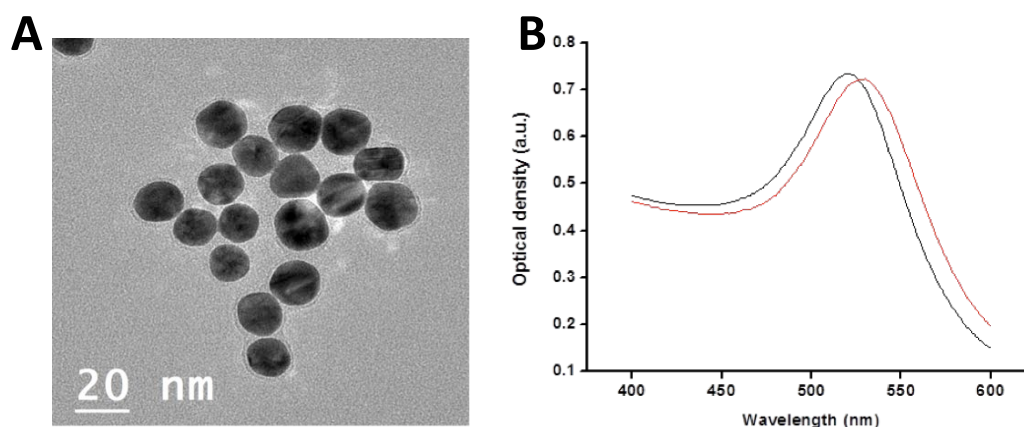
Figure 3.10. A) TEM image of the synthesized AuNPs. The AuNPs are homogeneously distributed, spherically shaped and with a diameter of around 15 nm. **B)** Optical spectra of the AuNPs (black) and the antibody-functionalized AuNPs (red). The AuNPs have the maximum absorbance peak at 520 nm that shifts to the right upon the surface functionalization with antibodies and BSA.

In particular, we evaluated the mobility of both citrate-capped AuNPs and AuNPs functionalized with BSA and goat IgG (which are the detection reagents used in the final application). The system set up consisted in the use of a CN150 NC membrane, 10 mM SB buffer pH 8 and a potential of 200 V. As expected the citrate-capped AuNPs had a higher mobility compared to the bio-functionalized AuNPs. The electrophoretic velocity decreased 1.25, 1.38 and 1.51-fold upon the functionalization with BSA, BSA + anti-HIgG and BSA + anti-HIgG + H-IgG (target molecule), respectively. This behaviour is due to two main factors: the increase of the hydrodynamic diameter of the AuNPs (BSA has an approx. diameter of 3 nm, while IgG of 10 nm)[42] and the increase in negative surface charge (BSA and IgG have pIs of 4.8 and 7.5-8.3 respectively). As expected, we observed that the AuNPs moved to the negative electrode due to the movement of the buffer towards the cathode, related to electroendosmosis (Figure 3.11.).[24–26]
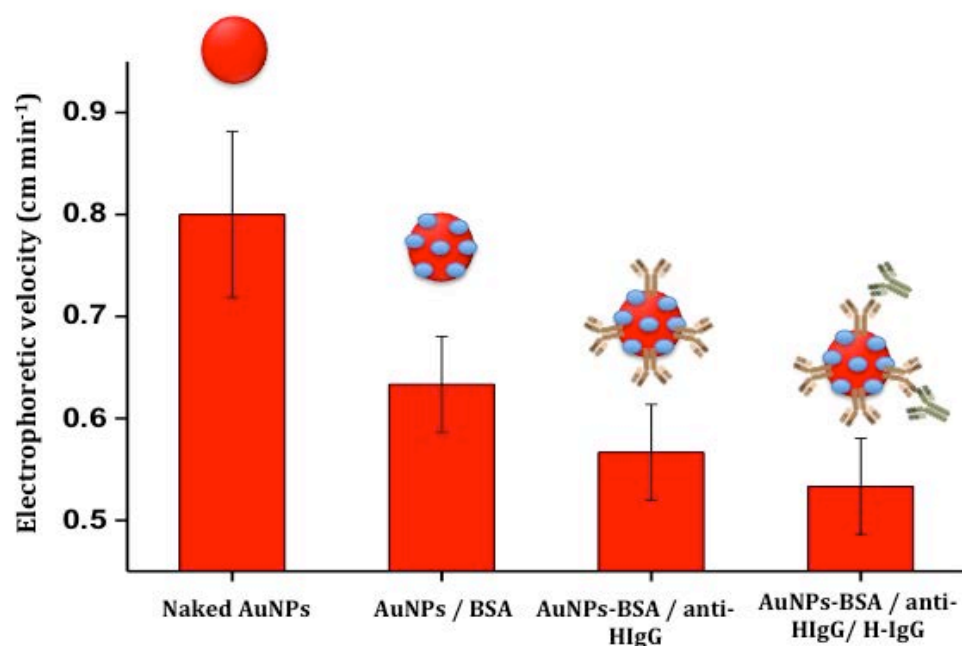
Figure 3.11. Electrophoretic velocity (cm min^{-1}) of naked AuNPs and AuNPs functionalized with BSA, BSA and antibody against H-IgG and BSA, anti-HIgG and H-IgG (see inset).

3.3.7. PEB optimization for blood samples

As we previously described the type of nitrocellulose membrane used can dramatically affect the performance of the PEB device. For this reason, we tested the ability of CN95, CN110 and CN150 membranes to move whole blood while applying a potential of 200 V in the SB buffer at pH 8. Similarly to what it is reported in other works, we observed that the flow rate was greater at the anode and decreased towards the cathode.[31] This effect is related to the equilibrium reached between the electro-endosmotic force and the osmotic pressure, two opposite forces leading to the accumulation of liquid nearby the cathode. This means that while the applied potential induces the movement of the electrolyte solution towards the cathode, the accumulation of the electrolyte solution at the cathode creates an osmotic pressure towards the anode, until reaching equilibrium of forces. The result is that the sample stops moving after 15 minutes. We observed that CN95 was the only NC membrane capable of washing out the blood from the detection zone in 15 minutes (see figure 3.12.). This observation is

according with the electrokinetic theory, stating that bigger pores produces a faster mobility.[43] Therefore this NC membrane was used in the next experiments.
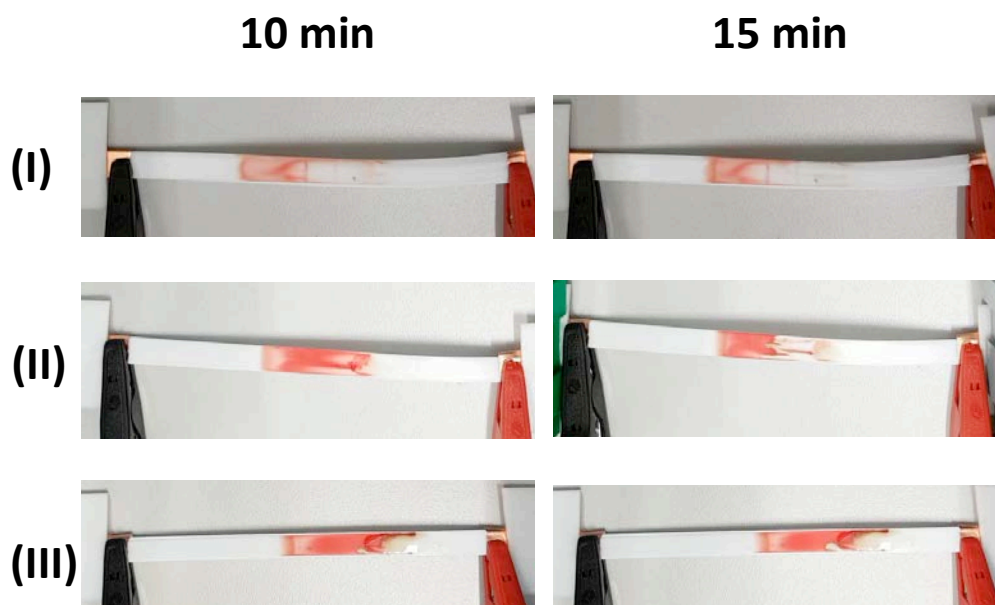
Figure 3.12. Pictures of the PEB assay for H-IgG detection in whole blood using (I) CN95, (II) CN110 and (III) CN150 NC membranes after 10 and 15 minutes. CN95 proved to be the only NC membrane capable of washing out the blood from the detection zone in 15 minutes.

Another important parameter that we optimized before performing the calibration curve for H-IgG detection in whole blood was the incubation time between the conjugated AuNPs and the whole blood samples. In this end, we performed the assay for the detection of H-IgG using the previously spiked whole blood samples and the same electrophoresis conditions, but evaluating different incubation times (15, 30, 60 and 180 s). We quantified the signal in TL following the procedure explained in the experimental section and we used this information to select the best incubation time. The incubation for 30 seconds enabled the appearance of the highest signal in TL, while higher incubation times proved to reduce the singal intensity in TL (see Figure 3.13.). However, there where not much differences in singal between 30 and 60 seconds, so these should not challenge the ease-of-use of the PEB device upon non-specialized end-users.
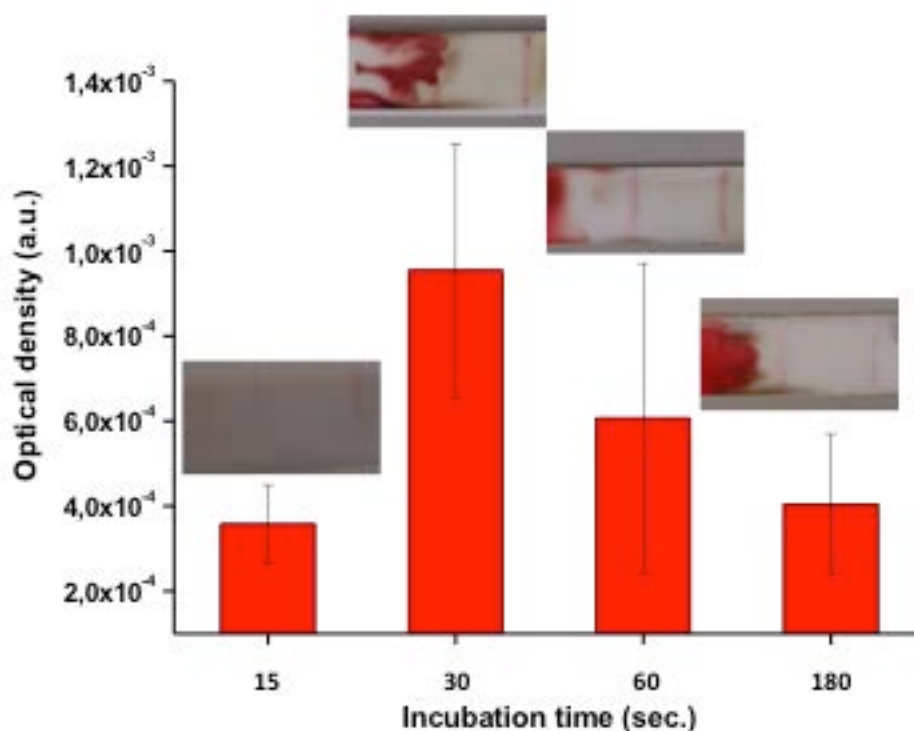
Figure 3.13. Comparison of the singal intensity in TL when incubation the conjugate solution and the whole blood sample for 15, 30, 60 and 180 s. Inset of the PEB pictures after performing the assay, showing the TL and CL.

3.3.8. Detection of H-IgG in whole blood

As final step toward demonstrating the applicability of PEB device as point of care diagnostic platform, we employed it for the detection of a biomarker in whole blood samples. As test bed, we used a model system previously optimized in our lab, the detection of human IgG. The choice of this analyte has two main reasons: 1) it provides a convenient comparison to LFAs developed in our lab and 2) the detection of H-IgG in blood represents a real clinical scenario, as showed by the recent pandemic.[1,44] In order to facilitate the interpretation of the results and limiting the sample-to-sample variation, we spiked chicken whole blood with H-IgG, in this way we removed the variability lead by endogenous concentration of human IgG in human blood. Detailed experimental procedure can be found in the Material and Methods section.

Before moving to whole blood samples, we characterized the analytical performance of the PEB device and compared it with the one of LFAs using buffered solutions spiked

with H-IgG. For this, we first performed a calibration curve in LFA covering the range from 0 to 1000 ng/mL for H-IgG concentration (values above 1000 ng/mL are usually not of clinical relevance) (Figure 3.14.).
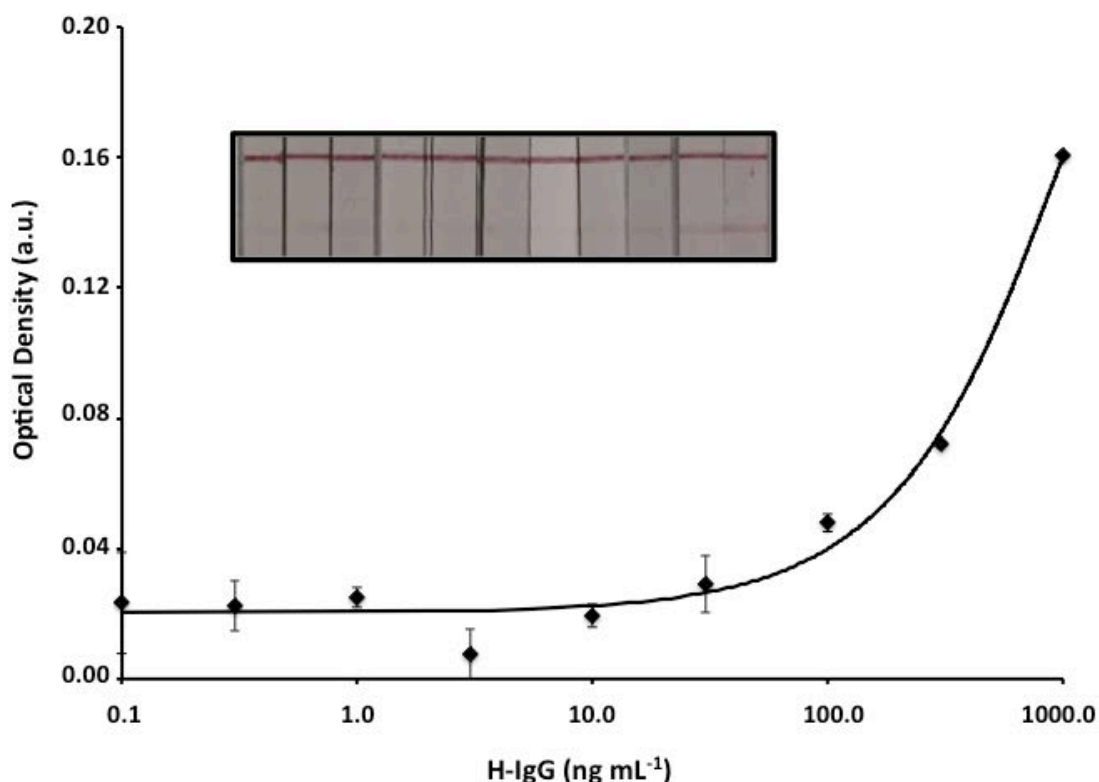
Figure 3.14. Calibration curve in LFA covering the range from 0.1 to 1000 ng/mL of H-IgG in buffer media. The curve equation was (Optical density = 0.0065 [H-IgG (ng mL^{-1})]$^{0.4459}$ r^2 = 0.98). Inset of LFA pictures taken after performing the assay.

We then performed a calibration curve in PEB covering the same range of H-IgG (Figure 3.15. A). The LoD and LoQ achieved in LFA were 265.56 and 1876.94 ng/mL; while the ones for PEB were 489.78 and 856.09 ng/mL, respectively. Besides showing a higher LoD, PEB proved a 2.2-fold lower LoQ and a 4.5-fold higher sensitivity than LFA when comparing the curve slopes. Finally, supported by the positive results obtained with buffer solutions we used the same range of concentrations but using whole blood (Figure 3.15 A). PEB device produced a specific and sensitive response (LoD = 284.52 ng/mL and LoQ = 441.07 ng/mL). It is noteworthy that PEB showed lower LoD and LoQ when detecting H-IgG in whole blood than in buffer medium. The

reason behind this is that the materials and electrophoretic conditions used in PEB have been specifically optimized to achieve the highest sensitivity when analyzing whole blood samples. Conversely, buffer medium samples flow 1.83-fold faster than whole blood samples when using the optimized conditions for whole blood (see figure 3.12. and 3.13.). This has an impact on the assay's sensitivity, which is highly affected by the flow rate.[45]
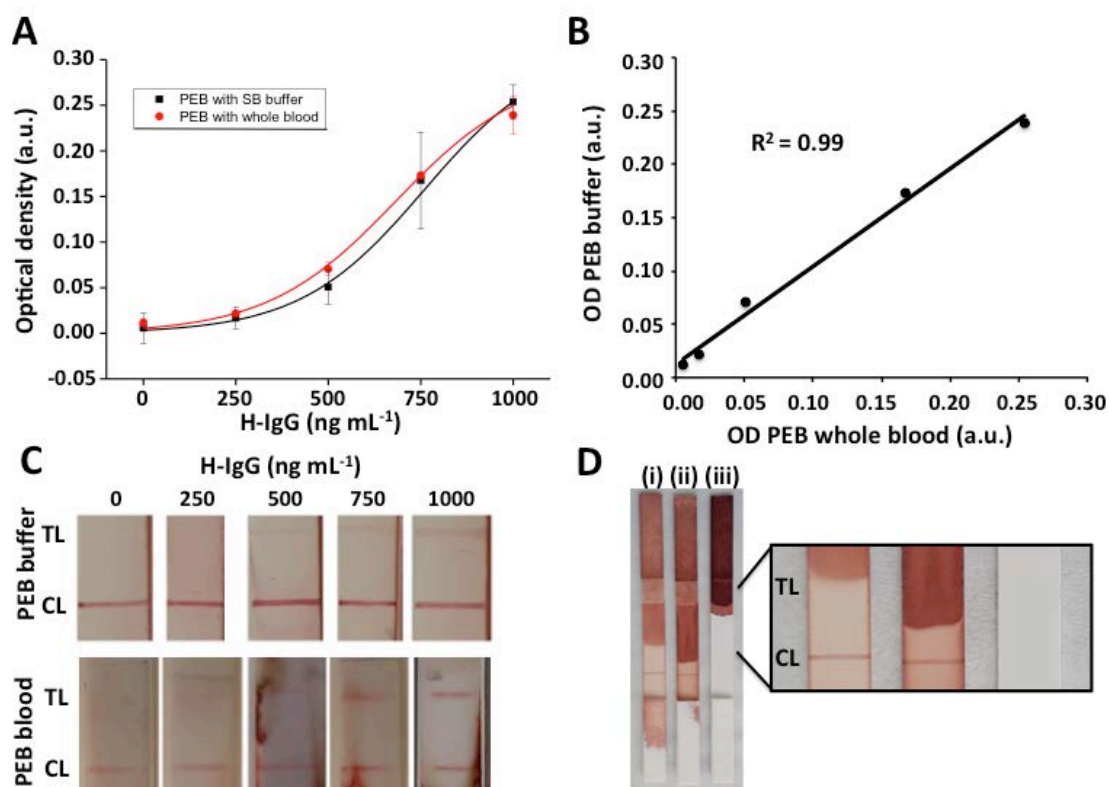
Figure 3.15. Calibration curve for H-IgG detection. **A)** Calibration curve with PEB in buffer media (black) and whole blood (red), covering the range from 0 to 1000 ng/mL. The curve equations PEB in buffer and whole blood were (Optical density = 2E-07 [H-IgG (ng mL^{-1})]$^{2.0248}$ r^2 = 0.98) and (Optical density = 1E-06 [H-IgG (ng mL^{-1})]$^{1.7807}$ r^2 = 0.98), respectively. **B)** Correlation between the signals obtained in PEB when performing the calibration curve (0 to 1000 ng/mL) in buffer and whole blood (r^2 = 0.99). **C)** Pictures of PEB strips after performing the calibration curve (0 to 1000 ng/mL) in buffer and whole blood. **D)** Pictures of LFA strips after the detection of H-IgG (1000 ng/mL) in **(i)** undiluted whole blood **(ii)** 2.4-fold diluted and **(iii)** 5-fold diluted whole blood. Inset picture showing a zoom in on the detection area.

Therefore, the use of a smaller pore size NC membrane or the application of a lower voltage should be sufficient to increase the LOD and LOQ of the assay in buffer media. However, this is not the objective of the present work, which is intended to develop an analytical device for whole blood samples. Moreover, on one side the use of whole blood without H-IgG did not generate a signal on the test line, showing the absence of non-specific interactions even in the presence of such complex media. On the other side the PEB responded accordingly to the increase in H-IgG concentration (Figure 3.15 C). It is remarkable that LFA failed in producing a reading signal due to the lack of movement by the blood sample (Figure 3.15 D).

3.4. Discussion and conclusion

Looking at the principles governing the PEB function, we observed three main forces affecting the movement of particles within the paper-based electrophoretic platform: electroendosmosis, electrophoresis and osmosis. First, we observed that the mobility of QDs was influenced by electroendosmosis, since all QDs moved towards the cathode (in electrolytic cells the cathode is negatively charged), despite of their negative surface charge. We verified this hypothesis by changing the pH of the electrophoresis buffer: when the pH was lower than the pKa of the boric acid (pKa = 9.24) the movement of the electrolytes towards the cathode represented the major force of the system, dragging also the negative particles towards the cathode. Instead, for pH close to the boric acid pKa, the absence of the electrolytes movement made the electrophoresis the main force, directing the negatively charged nanoparticles towards the anode. Obviously for pH higher than the pKa both the electrophoretic and electroendosmosis forces were moving the particles towards the anode. Then, we observed the influence of electrophoresis in the PEB function, since factors such as particle size, particle surface charge, membrane pore size and applied voltage were enhancing or hindering the particle mobility, following the general principle of electrophoresis. Finally we observed the effect of the osmosis limiting the amount of volume that could be displaced.

The PEB demonstrated to perform efficient sample treatment keeping the main characteristics of point-of-care devices. In fact employing either a portable battery or a smartphone, we managed to perform two key activities: the separation of different types of nanoparticles in less than 10 min and the flow of blood samples along nitrocellulose

membranes. Regarding the former, the results we obtained indicate that using nitrocellulose membranes, whose porosity is orders of magnitude higher than the diameter of the nanoparticles generally employed in LFA, the main factor governing the particle movement is their surface charge, rather than their size, whose effect is less determinant. We believe that the ability of PEB to purify particles opens a myriad of opportunities for the treatment and detection of different types of biomarkers. Instead, the latter shows how PEB can handle complex and highly viscous samples without the need for extensive dilutions (which would also decrease the amount of target) or extra washing steps (forcing the user to actuate at different times on the same test). In our opinion, this is a game changer within the field of point of care sensors, allowing the use of media such as blood, serum and other viscous solutions in a simpler and more effective way.

Finally, we validated PEB for the detection of H-IgG in buffered medium and whole blood samples and compared its analytical performance with LFA. PEB proved 2.2-fold lower LoQ and a 4.5-fold higher sensitivity than LFA for H-IgG detection in buffer media. Moreover, while LFAs were incapable to directly handling undiluted blood samples, the signals obtained with PEB when detecting H-IgG in whole blood samples showed a correlation of 0.99 with the ones for the detection in buffer samples. Therefore PEB proved to be capable of maintaining its outstanding analytical sensitivity still when evaluating non-diluted and non pre-treated whole blood samples.

3.5. References

1. Udugama, B. *et al.* Diagnosing COVID-19: The Disease and Tools for Detection. *ACS Nano* **14**, 3822–3835 (2020).

2. Waggoner, J. J. & Pinsky, A. Zika Virus: Diagnostics for an Emerging Pandemic Threat VIRUS. *J. Clin. Microbiol.* **54**, 860–867 (2016).

3. Yager, P., Domingo, G. J. & Gerdes, J. Point-of-Care Diagnostics for Global Health. *Annu. Rev. Biomed. Eng.* **10**, 107–144 (2008).

4. Price, C. P. Regular review: Point of care testing. *Br. Med. J.* **322**, 1285–1288 (2001).

5. Chin, C. D., Linder, V. & Sia, S. K. Commercialization of microfluidic point-of-care diagnostic devices. *Lab Chip* **12**, 2118–2134 (2012).

6. Yetisen, A. K., Akram, M. S. & Lowe, C. R. Paper-based microfluidic point-of-care diagnostic devices. *Lab Chip* **13**, 2210–2251 (2013).

7. Quesada-González, D. & Merkoçi, A. Nanoparticle-based lateral flow biosensors. *Biosens. Bioelectron.* **73**, 47–63 (2015).

8. Posthuma-Trumpie, G. A., Korf, J. & Van Amerongen, A. Lateral flow (immuno)assay: Its strengths, weaknesses, opportunities and threats. A literature survey. *Anal. Bioanal. Chem.* **393**, 569–582 (2009).

9. Quesada-González, D. *et al.* Iridium oxide (IV) nanoparticle-based lateral flow immunoassay. *Biosens. Bioelectron.* **132**, 132–135 (2019).

10. MERCK. IVD Lateral Flow – Sample, Conjugate and Absorbent Pad Basics. (2020). Available at: https://www.sigmaaldrich.com/technical-documents/articles/ivd-immunoassay/lateral-flow/pads-chemistries-selections-specifications-and-conjugates.html. (Accessed: 27th February 2020)

11. Brangel, P. *et al.* A Serological Point-of-Care Test for the Detection of IgG Antibodies against Ebola Virus in Human Survivors. *ACS Nano* **12**, 63–73 (2018).

12. Li, H., Han, D., Hegener, M. A., Pauletti, G. M. & Steckl, A. J. Flow reproducibility of whole blood and other bodily fluids in simplified no reaction lateral flow assay devices. *Biomicrofluidics* **11**, 1–15 (2017).

13. Tate, J. & Ward, G. Interferences in Immunoassay. *Clin Biochem Rev.* **25**, 105–120 (2004).

14. Dong, Y. *et al.* Blue luminescent graphene quantum dots and graphene oxide prepared by tuning the carbonization degree of citric acid. *Carbon N. Y.* **50**, 4738–4743 (2012).

15. Dong, Y. *et al.* Carbon-based dots co-doped with nitrogen and sulfur for high quantum yield and excitation-independent emission. *Angew. Chemie Int. Ed.* **52**, 7800–7804 (2013).

16. Turkevich, J., Stevenson, P. C. & Hillier, J. A study of the nucleation and growth processes in the synthesis of colloidal gold. *Discuss. Faraday Soc.* **11**, 55–75 (1951).

17. Ambrosi, A. *et al.* Double-codified gold nanolabels for enhanced immunoanalysis. *Anal. Chem.* **79**, 5232–5240 (2007).

18. Álvarez-Diduk, R., Orozco, J. & Merkoçi, A. Paper strip-embedded graphene

quantum dots: a screening device with a smartphone readout. *Sci. Rep.* **7**, 976 (2017).

19. Armbruster, D. A. & Pry, T. Limit of blank, limit of detection and limit of quantitation. *Clin. Biochem. Rev.* **29 Suppl 1**, S49-52 (2008).

20. Adamson, N. J. & Reynolds, E. C. Rules relating electrophoretic mobility, charge and molecular size of peptides and proteins. *J. Chromatogr. B Biomed. Sci. Appl.* **699**, 133–147 (1997).

21. R.J. Fritsch, I. K. Electrophoresis. in *Encyclopedia of Food Sciences and Nutrition* 2055–2062 (Academic Press, 2003).

22. Stalcup, A. M. Chiral separations by capillary electrophoresis. in *Chiral analysis* 241–275 (Elsevier Science, 2006).

23. Perrett, D. Electrophoresis. in *Encyclopedia of Separation Science* 103–118 (Academic Press, 2000).

24. Ferencik, M. Preparation of pure immunoglobulins. in *Handbook of immunohistochemistry* 191–196 (Springer, 2012).

25. Bikerman, J. J. Electric surface phenomena. in *Surface Chemistry: Theory and Applications* 405–408 (Academic Press, 1958).

26. Guo, Y., Li, X. & Fang, Y. The effects of electroendosmosis in agarose on electrophoresis. *Prog. Biochem. Biophys.* **24**, 268–272 (1997).

27. Zarei, M., Goharshadi, E. K., Ahmadzadeh, H. & Samiee, S. Improvement of heat dissipation in agarose gel electrophoresis by metal oxide nanoparticles. *RSC Adv.* **5**, 88655–88665 (2015).

28. Experts, D. Electricity, magnetism and light. in *The General Science Compendium* 39–50 (Disha publications, 2018).

29. Takahashi, M. & Takenaka, H. Dc electrical conductivity of cellulose. *Polym. J.* **15**, 625–629 (1983).

30. Kandadai, M. A., Raymond, J. L. & Shaw, G. J. Comparison of electrical conductivities of various brain phantom gels: Developing a 'brain gel model'. *Mater. Sci. Eng. C* **32**, 2664–2667 (2012).

31. WOODS, E. F. & GILLESPIE, J. M. A critical study of the use of paper electrophoresis for separating proteins and measuring their isoelectric points. *Aust. J. Biol. Sci.* **6**, 130–141 (1953).

32. Lin, R. *et al.* A lateral electrophoretic flow diagnostic assay. *Lab Chip.* **15**, 1488–

96 (2015).

33.   Lee, K. H. *et al.* Graphene quantum dots/graphene fiber nanochannels for osmotic power generation. *J. Mater. Chem. A* **7**, 23727–23732 (2019).

34.   Quevedo, I. R. & Tufenkji, N. Mobility of functionalized quantum dots and a model polystyrene nanoparticle in saturated quartz sand and loamy sand. *Environ. Sci. Technol.* **46**, 4449–4457 (2012).

35.   Wong, Raphael, Tse, H. *Lateral Flow Immunoassay*. (Springer, 2009).

36.   Kumawat, M. K., Thakur, M., Gurung, R. B. & Srivastava, R. Graphene quantum dots for cell proliferation, nucleus imaging, and photoluminescent sensing applications. *Sci. Rep.* **7**, 15858 (2017).

37.   Zou, S. *et al.* An efficient fluorescent probe for fluazinam using N, S co-doped carbon dots from L-cysteine. *Sensors Actuators, B Chem.* **239**, 1033–1041 (2017).

38.   Aldewachi, H. *et al.* Gold nanoparticle-based colorimetric biosensors. *Nanoscale* **10**, 18–33 (2018).

39.   Cordeiro, M., Carlos, F. F., Pedrosa, P., Lopez, A. & Baptista, P. V. Gold nanoparticles for diagnostics: Advances towards points of care. *Diagnostics* **6**, 43 (2016).

40.   Quesada-Gonzalez, D. & Merkoci, A. Nanomaterial-based devices for point-of-care diagnostic applications. *Chem. Soc. Rev.* (2018). doi:10.1039/C7CS00837F

41.   Maiorano, G. *et al.* Effects of cell culture media on the dynamic formation of protein-nanoparticle complexes and influence on the cellular response. *ACS Nano* **4**, 7481–7491 (2010).

42.   Flecha, F. L. G. & Levi, V. Determination of the molecular size of BSA by fluorescence anisotropy. *Biochem. Mol. Biol. Educ.* **31**, 319–322 (2003).

43.   Ennis, J. *et al.* Mobility of protein through a porous membrane. *J. Memb. Sci.* **119**, 47–58 (1996).

44.   Bedford, J. *et al.* COVID-19: towards controlling of a pandemic. *Lancet* **395**, 1015–1018 (2020).

45.   Bishop, J. D., Hsieh, H. V., Gasperino, D. J. & Weigl, B. H. Sensitivity enhancement in lateral flow assays: A systems perspective. *Lab Chip* **19**, 2486–2499 (2019).

CHAPTER 4. LATERAL FLOW ASSAY MODIFIED WITH TIME-DELAY WAX BARRIERS AS A SENSITIVITY AND SIGNAL ENHANCEMENT STRATEGY.

CHAPTER 4: LATERAL FLOW ASSAY MODIFIED WITH TIME-DELAY WAX BARRIERS AS A SENSITIVITY AND SIGNAL ENHANCEMENT STRATEGY.
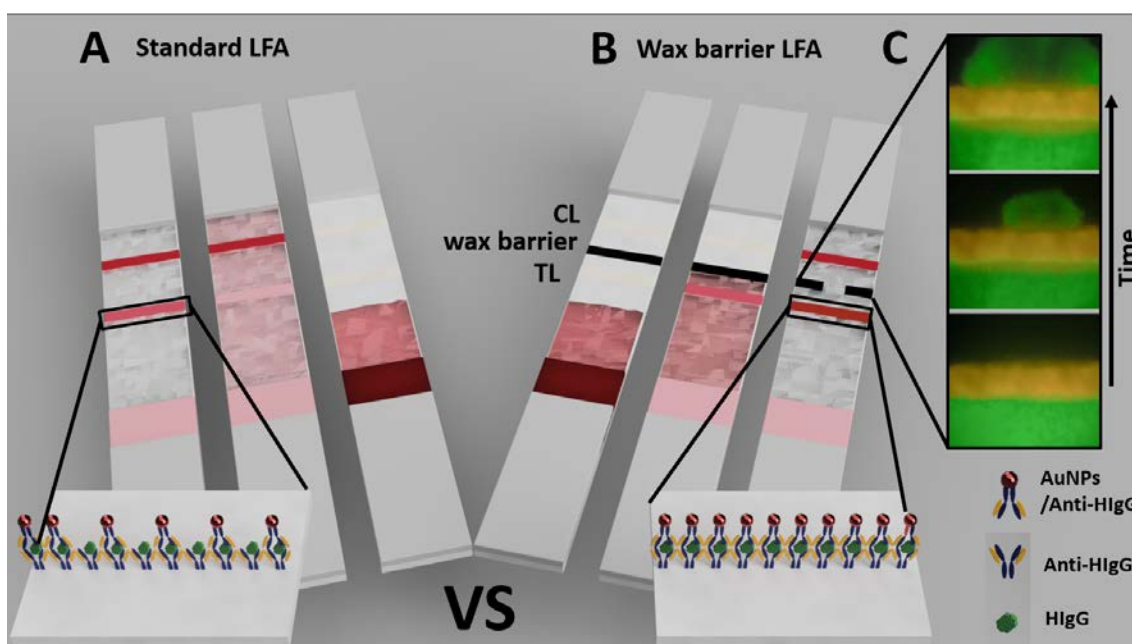
154

4.1. Introduction

During the last decade we have been observing an ever-growing need for fast and reliable sensing devices for healthcare, environmental and safety applications.[1,2] Both developed and developing countries are increasingly relying on the use of point of care tests (POCT) to keep up with the saturation of their health-care systems, to monitor the quality of their environmental resources and to prevent possible threats. The POCTs represent not only convenient analytical tools for rural regions (they are cheap, portable and easy to use), but they are also establishing themselves as key monitoring devices in the busy centralized areas.[3,4,5] For example a faster diagnosis means faster therapy initiation and higher chances to control the spread of a disease; and it also means a quicker response time for starting a remediation campaign in a contaminated river. In this context LFAs are probably the most used POCT covering the widest variety of applications.[6,7] They serve as an excellent tool for healthcare,[8,9] safety[10,11] and environmental applications.[12,13,14]

Being fast and easy to use are key features for the POCTs, but they also come with the drawback that the sensitivity of the POCTs has no match with laboratory-based, slower, multi-steps sensing techniques. For example in the LFA the binding event between bio-receptors (antibodies, aptamers) and their targets happens in the order of seconds (the time required for the flow to pass the TL),[15,16] while in Enzyme-Linked Immunosorbent Assays (ELISA)[17] incubation for several hours is common. Although for many applications the sensitivity of LFAs is sufficient, finding a way to improve it without affecting their being the POC would open a plethora of new applications. Here we are describing just that, a method to increase the time of the bio-recognition event, without affecting the ease of use and the overall sensing time of the LFAs.

The concept at the base of LFAs, is the use of capillary movement to guide the sample through different functional membranes.[6,18] Taking as example an immune-sandwich (non-competitive) assay, first the sample encounters the sample pad, where pre-stored biochemical reagents stabilizes its pH and ionic strength at their optimal values to maximize the signal to noise ratio.[19] Then it flows to the conjugate pad, where the detection antibodies (generally labelled with coloured nanoparticles) recognize the

CHAPTER 4: LATERAL FLOW ASSAY MODIFIED WITH TIME-DELAY WAX BARRIERS AS A SENSITIVITY AND SIGNAL ENHANCEMENT STRATEGY.

155

target in the first bio-recognition event.[20] Then the solution flows along the detection pad, where the complex target/labelled-antibody binds to the capture antibodies of the TL, during the second bio-recognition event. Finally the sample after passing through the control line (CL), reaches the absorbent pad at the end of the LFA. Surprisingly most of the reported works trying to improve the sensitivity of LFA have focused on increasing the time for the first bio-recognition event, but depending on the flow-rate of the pads it can already take minutes.[21,22] Instead of the second bio-recognition event is always in the order of seconds, representing the real bottle neck for the sensitivity of the test.

The possibility to slow down or even temporarily stop the flow above the test line would increase the time for both bio-recognition events, boosting the sensitivity of the LFAs. Here we present how we achieved it by placing a soluble wax barrier 1 mm after the TL. Looking at previous works we find that wax structures were previously employed in LFAs just to control the flow,[23,24,25,26] but never to temporarily stop it. While some paper-based microfluidic devices did incorporate real barrier to achieve incubation steps, but they were introduced before the test line and were based on salt [27] or sugar[28], which once dissolved can affect the ionic strength of the working buffer and thus the binding reaction. Instead, here, the wax barrier is printed on the surface of the nitrocellulose membrane and melted in order to assure its penetration through the membrane pores creating a hydrophobic barrier just after the TL, which is the place where the second bio-recognition event is taking place. The conjugate solution together with the sample solution flows along the nitrocellulose membrane towards the test line, giving time for the first binding event to occur. Once arrived to wax barrier, the solution stops temporarily on top of the test line until the barrier breaks due to the surfactant present on the strip (Figure 4.1). In this sense, the thickness of the wax barrier and the concentration of surfactant can be carefully selected in order to modulate the incubation time and determine the ones that provide the highest sensitivity.

CHAPTER 4: LATERAL FLOW ASSAY MODIFIED WITH TIME-DELAY WAX BARRIERS AS A SENSITIVITY AND SIGNAL ENHANCEMENT STRATEGY.

156

Figure 4.1. Schematic representation of the proposed strategy for the detection of H-IgG. **(A)** In the standard LFA the flow is constantly moving towards the absorbent pad and the bio-recognition event occurs within seconds. Few labelled antibodies are captured in TL, thus the signal intensity is weak. **(B)** In the LFA modified with a wax barrier, the flow is temporarily stopped on the TL. This increases the time for the bio-recognition event and boosts the assay's sensitivity. **(C)** Fluorescent microscope pictures (40X) of the wax barrier on the LFA strip. The wax barrier temporarily retains the solution. Once broken by the Tween-20, the solution goes through the barrier. Figure courtesy of PhD. Ruslan Álvarez-Diduk.

4.2. Experimental details

4.2.1. Materials and reagents

Goat anti-human IgG antibody, human IgG, bovine serum albumin (BSA), Tetrachloroauric acid (HAuCl4), trisodium citrate, phosphate buffer saline (PBS) tablets, sodium phosphate basic and dibasic, sodium tetraborate, boric acid sucrose and Tween 20 were purchased from Sigma Aldrich. Chicken anti-goat antibody was purchased from Abcam. Nitrocellulose membranes (CN95 and CN150) were purchased
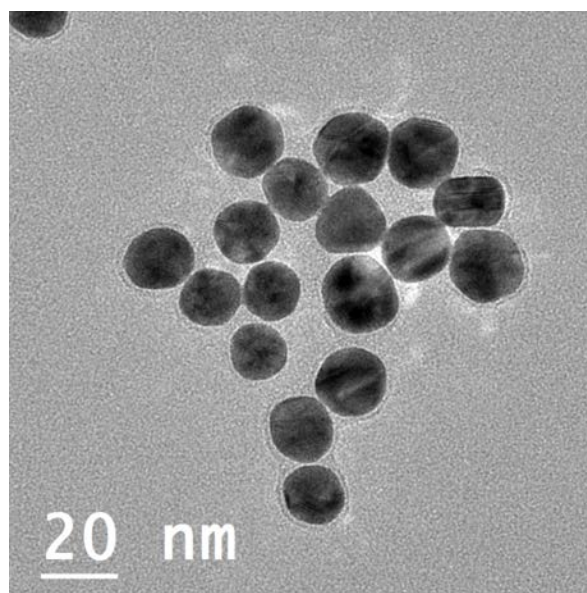
CHAPTER 4: LATERAL FLOW ASSAY MODIFIED WITH TIME-DELAY WAX BARRIERS AS A SENSITIVITY AND SIGNAL ENHANCEMENT STRATEGY.

157

from Sartorius Stediem and CNPF200 from mdi. Cellulose membrane (CFSP001700) was purchased in Merck Millipore, glass fiber (Standard14) from GE Healthcare and supporting adhesive cards were purchased from Kenosha. Decol food colorant red powder was purchased in Torten Deko and wax ink (Xerox 108R00935 black) was purchased in Xerox.

4.2.2. Instruments

Wax printer Xerox ColorQube 8580, Bioreagent dispenser (Imagene Technology), Microscope Olympus cellSense, Centrifuge Allegra 64R, Lateral flow strips cutter (Shanghai Kinbio Tech), Spectrophotometer SpectraMax ID3, SkanMulti (Skannex), TEM Technai F20.

4.2.3. Synthesis and characterization of AuNPs

The gold nanoparticles (AuNPs) were synthesized following the Turkevich method[29] and were characterized with TEM (~ 15 nm) and spectrophotometer (absorbance peak at 515 nm) (Figure 4.2 and 4.3), respectively. The AuNPs were adjusted to pH 9.2 using borate buffer (10 mM pH 9.2) and centrifuged at 14000 rpm for 30 minutes. Finally, they were re-suspended in 250 µL of PBS (10 mM, pH 7.4, 5% sucrose, 1% BSA and 0.5% tween-20) and dried in the glass fiber overnight. Moreover, the sample pad was blocked with PBS (10 mM, pH 7.4, 0.5% BSA and 0.05% to 0.1% tween-20) and dried overnight.

CHAPTER 4: LATERAL FLOW ASSAY MODIFIED WITH TIME-DELAY WAX BARRIERS AS A SENSITIVITY AND SIGNAL ENHANCEMENT STRATEGY.

158

Figure 4.2. TEM image of the synthesized gold nanoparticles (AuNPs). The AuNPs have a spherical shape and a diameter of around 15 nm.

4.2.4. Conjugation of AuNPs with anti-HIgG

The AuNPs were conjugated to antibodies against H-IgG following the procedure previously reported by our group.[30] In order to check if the AuNPs were successfully conjugated with the antibodies, the absorbance spectrum was evaluated. As observed in Figure 4.3, the maximum absorbance peak of the conjugated the AuNPs has a little red shift (about 5 nm), indicating the presence of the antibodies on the surface of the AuNPs.

CHAPTER 4: LATERAL FLOW ASSAY MODIFIED WITH TIME-DELAY WAX BARRIERS AS A SENSITIVITY AND SIGNAL ENHANCEMENT STRATEGY.

159
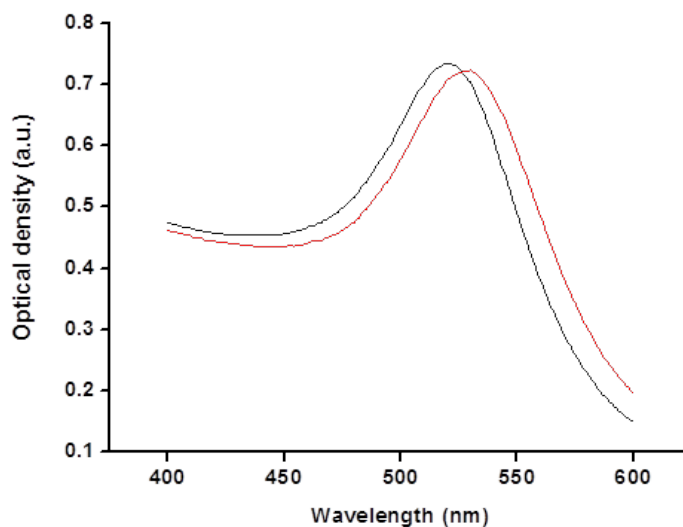
Figure 4.3. Absorbance spectrum of the AuNPs (black) and the AuNPs conjugated with anti H-IgG (red). The maximum absorbance peak shifts to the right after the conjugation of AuNPs with anti H-IgG.

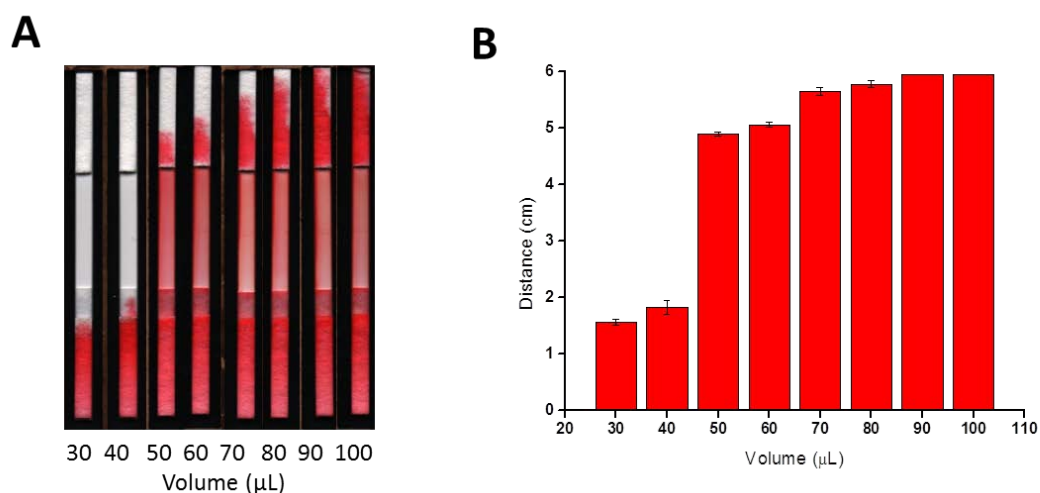## 4.3. Results and Discussion

4.3.1 Evaluation of the retention times with different wax barriers

When developing the POCT, reproducibility is one of the most important parameters to optimize. For this reason, we fixed the lateral flow strip dimensions to 6 x 0.3 cm and verified that the bed volume corresponds to 70 µL (Figure 4.4). We then proceeded to optimize the barrier fabrication by printing black lines with different widths (0.01, 0.03, 0.05 y 0.1 mm) onto CN95 nitrocellulose membrane, and melting homogeneously the wax at 95 ° C for 5 minutes in the oven (Figure 4.5). Next, we evaluated the time required for breaking the barriers at different concentrations of Tween-20, following the former optimized parameters. In particular, we fabricated lateral flow strips containing different concentrations of Tween-20 (0.05%, 0.1%, 0.5% and 0.1%) in the sample pad and the AuNPs in the conjugate pad. The retention time was measured from the moment at which the AuNPs reached the wax barrier until they crossed the barrier.

CHAPTER 4: LATERAL FLOW ASSAY MODIFIED WITH TIME-DELAY WAX BARRIERS AS A SENSITIVITY AND SIGNAL ENHANCEMENT STRATEGY.

160

Figure 4.4. Volume optimization in lateral flow assay. (A) Pictures of lateral flow strips after drop-casting 30 to 100 µL of food colorant. (B) Distance travelled of the food colorant from the furthest point of the sample pad when drop-casting 30 to 100 µL of solution.
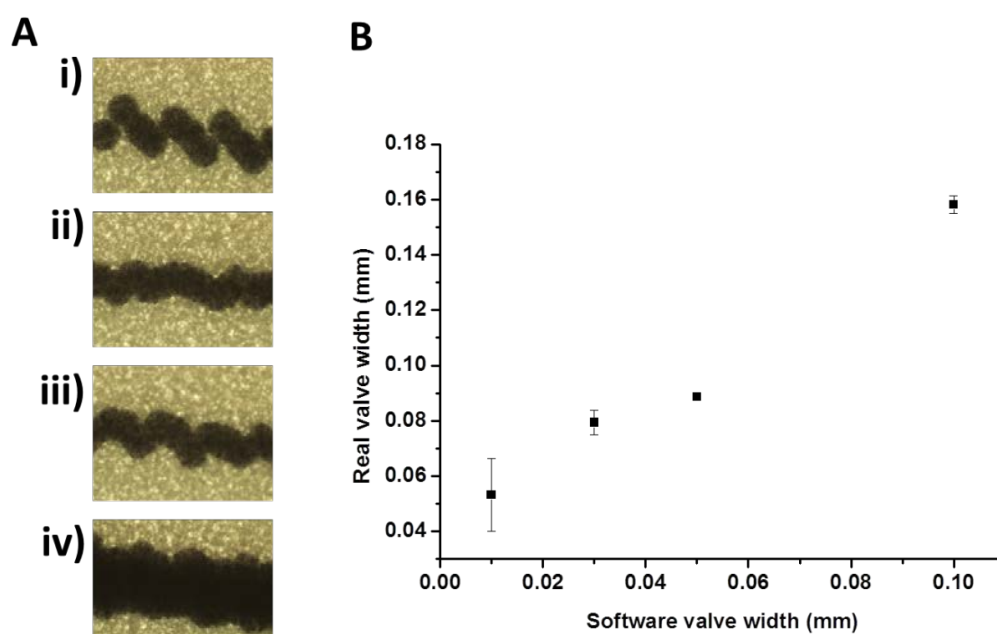
Figure 4.5. (A) Optical microscope pictures (40x) of the wax barriers printed on the nitrocellulose membrane. **(i)** 0.01 mm **(ii)** 0.03 mm **(iii)** 0.05 mm **(iv)** 0.1 mm width. **(B)** Graph representing the linear relationship between the barriers width fixed by the software and the real barriers width measured with the microscope.

CHAPTER 4: LATERAL FLOW ASSAY MODIFIED WITH TIME-DELAY WAX BARRIERS AS A SENSITIVITY AND SIGNAL ENHANCEMENT STRATEGY.
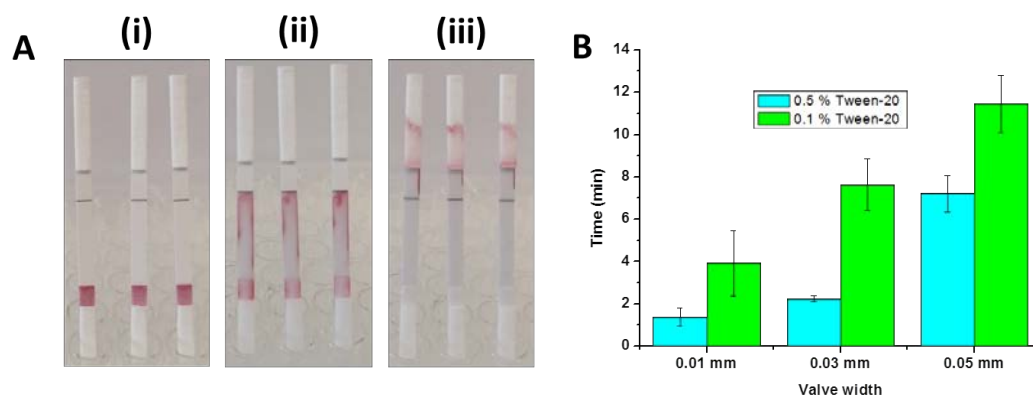
161

As a result, we generated a matrix providing the wax barrier width and Tween-20 concentration that provide different retention times (Table 1 and Figure 4.6). As expected, the retention time increases increasing barrier width and decreasing Tween-20 concentration. In particular, we achieved the longest retention time (12 minutes) by employing barriers of 0.05 mm and a concentration of Tween-20 of 0.1%; while the shortest retention time (1 minute) required a barrier width of 0.01 mm and 0.5% Tween-20. Width of 0.1 mm and Tween-20 concentration of 0.05%, showed to be not suitable for the assay as the barriers broke once the AuNPs solution was already dried out.

Moreover, we printed the barriers in a slower flow rate nitrocellulose membrane (CNPF200 mdi), in order to evaluate how the use of smaller pore sizes can affect the retention time. In this case, the pressure applied by the wax printing process compacted the pore of the nitrocellulose, thereby the flow could not even reach the TL.

Table 1. Retention times on CN95 with different wax barrier width and %Tween-20

Wax width (mm)	0.5% Tween-20	0.1% Tween-20	0.05% Tween-20
0.01	1.40 ± 0.42 min	3.93 ± 1.55 min	NB
0.03	2.25 ± 0.13 min	7.64 ± 1.19 min	NB
0.05	7.23 ± 0.86 min	11.45 ± 1.33 min	NB
0.10	NB	NB	NB

* NB: No Breaking, which means that the solution dried out before breaking the wax barrier.

CHAPTER 4: LATERAL FLOW ASSAY MODIFIED WITH TIME-DELAY WAX BARRIERS AS A SENSITIVITY AND SIGNAL ENHANCEMENT STRATEGY.

162

Figure 4.6. (A) Picture of the lateral flow strips (i) before the assay (ii) during the AuNPs retention (iii) after the barriers breaking. (B) Comparison of the retention time when using a CN95 modified with 0.01, 0.03 and 0.05 mm width barriers and 0.1 and 0.5% Tween-20.

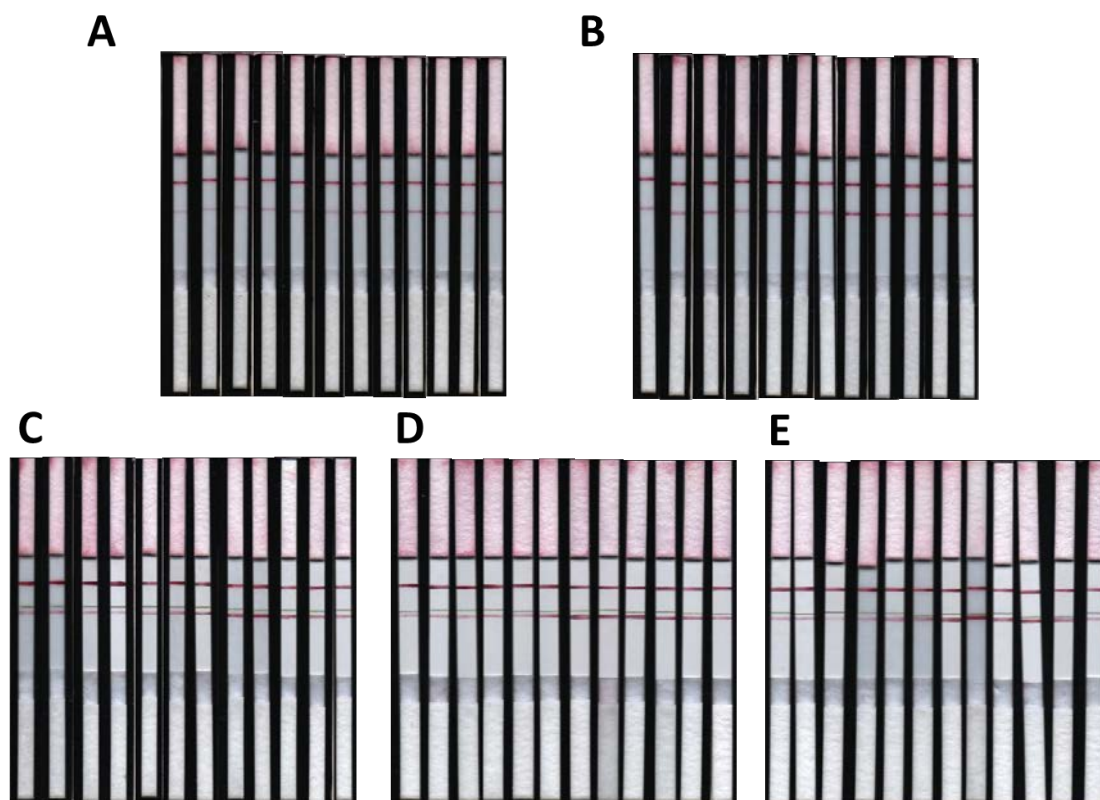### 4.3.2. Evaluation of the signal and sensitivity enhancement with different barriers

Finally, after determining the optimum conditions to achieve the longest flow retention, we performed the lateral flow immunoassay for H-IgG detection. In order to check if there is a correlation between the retention time on the TL and the sensitivity enhancement, we fabricated the strips without barriers and with barriers width of 0.01, 0.03 and 0.05 mm. In this regard, we used CN95 and 0.1% Tween-20 as surfactant to break the barriers. We were expecting to see a progressive sensitivity enhancement when using higher width barriers, obtaining the highest sensitivity by using 0.05 mm width barrier, since this is the one that provides the longest retention time. Next, we prepared the strips by fixing anti H-IgG antibodies (1 mg mL^{-1}) in the TL and anti-goat antibodies (1 mg mL^{-1}) in the CL, both in 10 mM PB buffer pH 7.4. Moreover, we conjugated the AuNPs with anti H-IgG by following the procedure previously reported by our group,[30] explained in the experimental section. Furthermore, we performed calibration curves using serial dilutions of H-IgG (0 ng mL^{-1} to 10^3 ng mL^{-1}). Finally, we evaluated the signal intensity in both the TL and CL the by taking a picture of the strips using a LFA scanner and analyzing them with Image J software.[31] We took the pictures of the strips once the AuNPs solution had completely reached the absorbent

CHAPTER 4: LATERAL FLOW ASSAY MODIFIED WITH TIME-DELAY WAX BARRIERS AS A SENSITIVITY AND SIGNAL ENHANCEMENT STRATEGY.

163

pad. Eventually, we used the signal values of the TL and the CL after background signal subtraction, and normalized the signal value by dividing TL over CL.

Figure 4.7 shows the calibration curves obtained when using CN95 and CN150 without the barriers and CN95 with 0.01, 0.03 and 0.05 mm width barriers. As observed the normalized optical density increases upon the detection of higher concentrations of H-IgG. Figure 4.8 shows the pictures of the lateral flow strips after performing the assays.
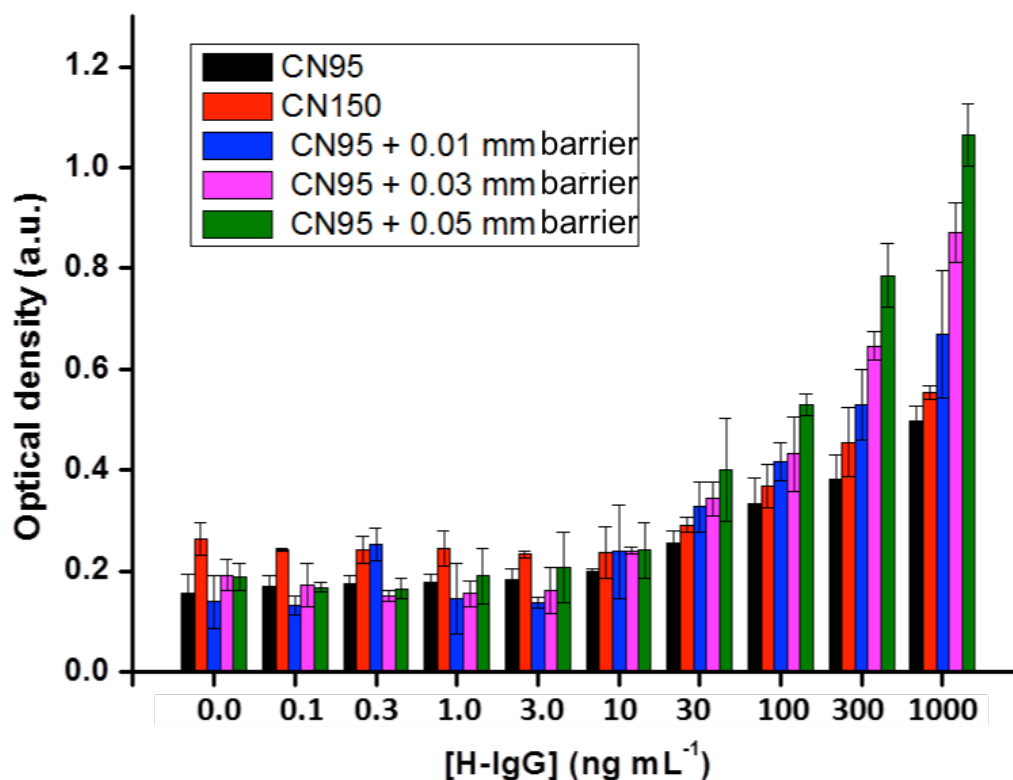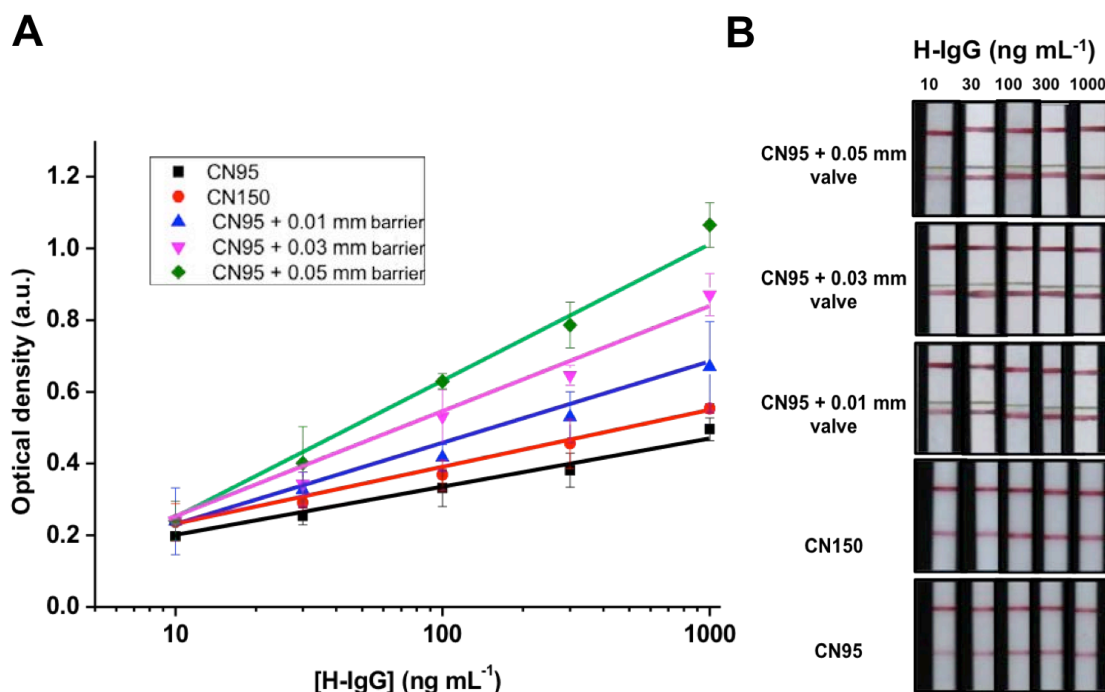

Figure 4.7. Calibration curves from 0 to 1000 ng mL^{-1} using CN95 and CN150 non-modified with wax barriers and CN95 modified with 0.01, 0.03 and 0.05 mm width barriers.

CHAPTER 4: LATERAL FLOW ASSAY MODIFIED WITH TIME-DELAY WAX BARRIERS AS A SENSITIVITY AND SIGNAL ENHANCEMENT STRATEGY.

164

Figure 4.8. Pictures of the lateral flow strips after calibration curves for H-IgG detection (from left to right: 0, 0.1, 0.3, 1, 3, 10, 30, 100, 300 and 1000 ng mL^{-1} from left to right) using (A) CN95 without barriers (B) CN150 without barriers (C) CN95 with 0.01 mm barriers (D) CN95 with 0.03 mm barriers and (E) CN95 with 0.05 mm barriers.

In order to evaluate the sensitivities obtained with each condition we performed a linear fitting from 10 to 1000 ng mL^{-1} and we considered the slope values (Figure 4.9A). As we were expecting, a higher sensitivity is achieved when using wider barriers, as this assures a longer interaction time between the antibodies in TL, AuNPs and the analyte. The highest sensitivity is achieved when using a 0.05 mm width barrier, which provides a 2.8-fold enhancement compared to the same nitrocellulose without barriers. It is noteworthy that, conversely to the reported, there isn't an outstanding sensitivity improvement when reducing the flow rate by using a smaller pore nitrocellulose membrane, as in the case of CN150.[32,33] Besides, we have proved that the outstanding sensitivity enhancement is obtained only when temporarily stopping the flow above the TL.

CHAPTER 4: LATERAL FLOW ASSAY MODIFIED WITH TIME-DELAY WAX
BARRIERS AS A SENSITIVITY AND SIGNAL ENHANCEMENT STRATEGY.

165

Figure 4.9. The LFA for H-IgG detection using time-delay barriers. **(A)** Calibration curve from 10 to 1000 ng mL^{-1} showing the optical density linear range when using CN95 (Optical density = 0.0631 ln [H-IgG (ng mL^{-1})] + 0.0433 r^2=0.98) and CN150 non-modified with the wax barriers (Optical density = 0.0695 ln [H-IgG (ng mL^{-1})] + 0.0627 r^2=0.99) and CN95 modified with 0.01 (Optical density = 0.0925 ln [H-IgG (ng mL^{-1})] + 0.0124 r^2=0.99), 0.03 (Optical density = 0.1359 ln [H-IgG (ng mL^{-1})] - 0.1165 r^2=0.96) and 0.05 mm width barriers (Optical density = 0.1767 ln [H-IgG (ng mL^{-1})] - 0.2056 r^2=0.98). **(B)** Pictures of the LFA strips after performing the calibration curve assay from 10 to 1000 ng mL^{-1} using CN95, CN150 non-modified with the wax barriers and CN95 modified with 0.01, 0.03 and 0.05 mm width barriers.

Moreover, we calculated the limit of detection (LoD) and quantification (LoQ) achieved for every tested condition. The LoD was calculated as $Optical\ density_{LOD} = blank + 3\,\sigma_{blank}$ (i.e. the corresponding value of blank sample plus 3 times its standard deviation).[34] The LoD for CN95, CN150 and CN95 with 0.01, 0.03 and 0.05 mm width barriers were 35.01, 73.23, 21.67, 18.71, 14.47 ng·mL^{-1}, respectively. Furthermore, the LoQ, calculated as $Optical\ density_{LOD} = blank + 10\,\sigma_{blank}$, were 2129.09, 1909.76, 1164.38, 87.49, 41.19 ng·mL^{-1}, respectively. We obtained the lowest LoD and LoQ

CHAPTER 4: LATERAL FLOW ASSAY MODIFIED WITH TIME-DELAY WAX BARRIERS AS A SENSITIVITY AND SIGNAL ENHANCEMENT STRATEGY.

166

values by setting the barriers at the condition that permitted the highest retention time of the conjugate solution on the TL.
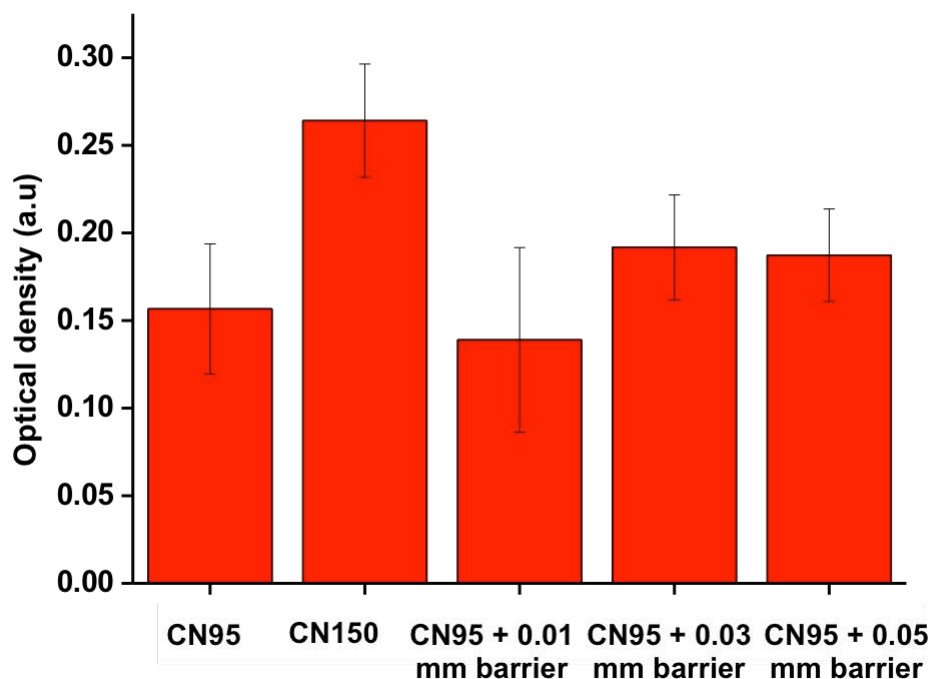
In Figure 4.9. B, we show pictures of the LFA strips after performing the calibration curve assay from 10 to 1000 ng mL^{-1} using CN95, CN150 non-modified with the wax barriers and CN95 modified with 0.01, 0.03 and 0.05 mm width barriers. As observed, there is a signal enhancement in TL when introducing the wax barriers in to the system. The percentage signal enhancement was calculated taking as reference the normalized optical density of the strips with CN95 and without the wax barriers (Table 2). As observed, the percentage signal increase is higher for increasing concentrations of H-IgG. The highest percentage signal increase is 96%, and was achieved for 1000 ng mL^{-1} when using CN95 with a 0.05 mm width barrier.

Table 2. The percentage signal enhancement in TL when using CN150 and CN95 modified with 0.01, 0.03 and 0.05 mm wax barriers.

[H-IgG] (ng mL^{-1})	CN150 %	CN95 + 0.01(mm) %	CN95 + 0.03(mm) %	CN95 + 0.05(mm) %
10	-6.7	7.1	2.6	3.2
30	-12.0	14.5	15.7	38.9
100	-15.4	11.8	10.9	40.8
300	-7.0	24.9	50.1	87.2
1000	-14.8	21.1	56.4	96.0

Note: The calculations where done by taking CN95 with no wax barriers as reference.

Finally, we proved that a longer incubation time of the conjugate solution over the TL didn't favour the generation of non-specific signal in TL. As shown in Figure 4.10, the signal in TL for blank samples (0 ng mL^{-1} of H-IgG) is not higher when using wider wax barriers, as we obtained the highest TL signal for the blank sample when using the CN150 nitrocellulose membrane.

CHAPTER 4: LATERAL FLOW ASSAY MODIFIED WITH TIME-DELAY WAX BARRIERS AS A SENSITIVITY AND SIGNAL ENHANCEMENT STRATEGY.

167

Figure 4.10. Optical density in TL for strips evaluated with no H-IgG (blank sample). The signal in TL corresponds to the non-specific attachment of the antibody-functionalized AuNPs to the capture antibody in TL. As shown, there is no correlation between the higher incubation time of the conjugate solution on TL and the generation of non-specific signal in TL.

4.4. Conclusions

In conclusion, we have developed a LFA modified with time-delay barriers as a strategy for sensitivity and signal enhancement. We have achieved an inner incubation time of 12 minutes, which produced a 2.8-fold enhancement in sensitivity and up to 96% signal enhancement. We believe the proposed method represents an outstanding solution to improve the analytical performance of LFAs, without sacrificing their ease-of-use and low cost.

CHAPTER 4: LATERAL FLOW ASSAY MODIFIED WITH TIME-DELAY WAX BARRIERS AS A SENSITIVITY AND SIGNAL ENHANCEMENT STRATEGY.

168

4.5. References

1. Turner, A. P. F. Biosensors: Sense and sensibility. *Chem. Soc. Rev.* **42,** 3184–3196 (2013).

2. Malhotra, B. D., Singhal, R., Chaubey, A., Sharma, S. K. & Kumar, A. Recent trends in biosensors. *Curr. Appl. Phys.* **5,** 92–97 (2005).

3. Price, C. P. Regular review: Point of care testing. *Br. Med. J.* **322,** 1285–1288 (2001).

4. Land, K. J., Boeras, D. I., Chen, X. S., Ramsay, A. R. & Peeling, R. W. REASSURED diagnostics to inform disease control strategies, strengthen health systems and improve patient outcomes. *Nat. Microbiol.* **4,** 46–54 (2019).

5. Chin, C. D., Linder, V. & Sia, S. K. Commercialization of microfluidic point-of-care diagnostic devices. *Lab Chip* **12,** 2118–2134 (2012).

6. Quesada-González, D. & Merkoçi, A. Nanoparticle-based lateral flow biosensors. *Biosens. Bioelectron.* **73,** 47–63 (2015).

7. Posthuma-Trumpie, G. A., Korf, J. & Van Amerongen, A. Lateral flow (immuno)assay: Its strengths, weaknesses, opportunities and threats. A literature survey. *Anal. Bioanal. Chem.* **393,** 569–582 (2009).

8. Chen, Y. *et al.* A dual-readout chemiluminescent-gold lateral flow test for multiplex and ultrasensitive detection of disease biomarkers in real samples. *Nanoscale* **8,** 15205–15212 (2016).

9. Brangel, P. *et al.* A Serological Point-of-Care Test for the Detection of IgG Antibodies against Ebola Virus in Human Survivors. *ACS Nano* **12,** 63–73 (2018).

10. Quesada-González, D., Jairo, G. A., Blake, R. C., Blake, D. A. & Merkoçi, A. Uranium (VI) detection in groundwater using a gold nanoparticle/paper-based

CHAPTER 4: LATERAL FLOW ASSAY MODIFIED WITH TIME-DELAY WAX BARRIERS AS A SENSITIVITY AND SIGNAL ENHANCEMENT STRATEGY.

169

lateral flow device. *Sci. Rep.* **8,** 8–15 (2018).

11.   Mirasoli, M. *et al.* Development of a chemiluminescence-based quantitative lateral flow immunoassay for on-field detection of 2,4,6-trinitrotoluene. *Anal. Chim. Acta* **721,** 167–172 (2012).

12.   Hassan, A. H. A., Bergua, J. F., Morales-Narváez, E. & Mekoçi, A. Validity of a single antibody-based lateral flow immunoassay depending on graphene oxide for highly sensitive determination of E. coli O157:H7 in minced beef and river water. *Food Chem.* **297,** 124965 (2019).

13.   Schubert-Ullrich, P. *et al.* Commercialized rapid immunoanalytical tests for determination of allergenic food proteins: An overview. *Anal. Bioanal. Chem.* **395,** 69–81 (2009).

14.   Raeisossadati, M. J. *et al.* Lateral flow based immunobiosensors for detection of food contaminants. *Biosens. Bioelectron.* **86,** 235–246 (2016).

15.   Gasperino, D., Baughman, T., Hsieh, H. V., Bell, D. & Weigl, B. H. Improving Lateral Flow Assay Performance Using Computational Modeling. *Annu. Rev. Anal. Chem.* **11,** 219–244 (2018).

16.   Miller, B. S. *et al.* Quantifying Biomolecular Binding Constants using Video Paper Analytical Devices. *Chem. - A Eur. J.* **24,** 9783–9787 (2018).

17.   Van Weemen, B. K. & Schuurs, A. H. W. M. Immunoassay using antigen-enzyme conjugates. *FEBS Lett.* **15,** 232–236 (1971).

18.   Muhammad Sajid, Abdel-Nasser Kawde & Muhammad Daud. Designs, formats and applications of lateral flow assay: A literature review. *J. Saudi Chem. Soc.* **19,** 689–705 (2015).

19.   Millipore, M. *Rapid Lateral Flow Test Strips Considerations for Product Development*. (2013). at <www.merckmillipore.com/offices>

CHAPTER 4: LATERAL FLOW ASSAY MODIFIED WITH TIME-DELAY WAX BARRIERS AS A SENSITIVITY AND SIGNAL ENHANCEMENT STRATEGY.

170

20. Quesada-González, D. *et al.* Iridium oxide (IV) nanoparticle-based lateral flow immunoassay. *Biosens. Bioelectron.* **132,** 132–135 (2019).

21. Zhang, S. F. *et al.* Sensitivity enhancement of lateral flow assay by embedding cotton threads in paper. *Cellulose* **26,** 8087–8099 (2019).

22. Tsai, T. T. *et al.* Development a stacking pad design for enhancing the sensitivity of lateral flow immunoassay. *Sci. Rep.* **8,** 1–10 (2018).

23. Giokas, D. L., Tsogas, G. Z. & Vlessidis, A. G. Programming fluid transport in paper-based microfluidic devices using razor-crafted open channels. *Anal. Chem.* **86,** 6202–6207 (2014).

24. Lai, Y., Tsai, C., Hsu, J. & Lu, Y. Microfluidic Time-Delay Valve Mechanism on Paper-Based Devices for Automated Competitive ELISA. *Micromachines* **10,** (2019).

25. Phillips, E. A., Shen, R., Zhao, S. & Linnes, J. C. Thermally actuated wax valves for paper-fluidic diagnostics. *Lab Chip* **16,** 4230–4236 (2016).

26. Rivas, L., Medina-Sánchez, M., de la Escosura-Muñiz, A. & Merkoçi, A. Improving sensitivity of gold nanoparticle-based lateral flow assays by using wax-printed pillars as delay barriers of microfluidics. *Lab Chip* **14,** 4406–4414 (2014).

27. He, X. *et al.* Sensitivity Enhancement of Nucleic Acid Lateral Flow Assays through a Physical-Chemical Coupling Method: Dissoluble Saline Barriers. *ACS Sensors* **4,** 1691–1700 (2019).

28. Lutz B, Liang T, Fu E, Ramachandran S, Kauffman P, Y. P. Dissolvable fluidic time delays for programming multi-step assays in instrument-free paper diagnostics. *Lab Chip* **13,** 2840–7 (2013).

29. Turkevich, J., Stevenson, P. C. & Hillier, J. A study of the nucleation and growth processes in the synthesis of colloidal gold. *Discuss. Faraday Soc.* **11,** 55–75

CHAPTER 4: LATERAL FLOW ASSAY MODIFIED WITH TIME-DELAY WAX BARRIERS AS A SENSITIVITY AND SIGNAL ENHANCEMENT STRATEGY.

171

(1951).

30.   Ambrosi, A. *et al.* Double-codified gold nanolabels for enhanced immunoanalysis. *Anal. Chem.* **79,** 5232–5240 (2007).

31.   Schneider, C. A., Rasband, W. S. & Eliceiri, K. W. NIH Image to ImageJ: 25 years of image analysis. *Nat. Methods* **9,** 671–675 (2012).

32.   Millipore, M. *Rapid Lateral Flow Test Strips Considerations for Product Development.* (2013).

33.   NanoComposix. Lateral flow assay development guide. *nanoComposix Lateral Flow Handbook v.1.4* 37 (2016). at <http://www.gopixpic.com/940/lateral-flow-assay/http:||www*dxdiscovery*com|wp-content|uploads|2014|02|Screen-Shot-2014-02-22-at-11*55*48-AM*png/>

34.   Armbruster, D. A. & Pry, T. Limit of blank, limit of detection and limit of quantitation. *Clin. Biochem. Rev.* **29 Suppl 1,** S49–52 (2008).

4.6. Contributions

This work has been performed in collaboration with MSc. Duy Ba Ngo and Prof. Werasak Surareungchai, from the School of Bioresources and Technology of King Mongkut's University of Technology Thonburi (KMUTT) (Bangkok, Thailand). MSc. Duy Ba Ngo worked on the development of the biosensor during his internship in the nanobioelectronics and biosensors group (Barcelona, Spain).

CHAPTER 4: LATERAL FLOW ASSAY MODIFIED WITH TIME-DELAY WAX BARRIERS AS A SENSITIVITY AND SIGNAL ENHANCEMENT STRATEGY.

172

CHAPTER 5. LAB IN A TUBE: POINT-OF-CARE DETECTION OF *ESCHERICHIA COLI*.

5.1. Introduction

Nowadays, *Escherichia coli* O157:H7 (*E. coli* O157:H7) is one of the major threats to public healthcare causing serious infectious diseases mainly through contaminated water and food.[1,2] Since the causative pathogen agent can spread rapidly, it is imperative to achieve fast diagnosis. In addition, providing a quick decision in the field to test the safety of water and food will have a great effect on controlling and minimizing mortality rate and financial affliction.

Traditional methods for the identification and detection of pathogenic bacteria are mainly based on plate cultivation,[3] enzyme-linked immunosorbent assay (ELISA) and polymerase chain reaction (PCR).[4–6] Culturing methods requires long analysis time (~ days) and special labour operation. PCR and ELISA need significant instruments, manpower, expense and time that already are not suitable for emergency cases especially in developing countries where medical facilities are unobtainable.[7]

To overcome the aforementioned problems, point-of-care (PoC) diagnostic can be a potential solution for improving the global health managements.[8] Toward this important goal, different PoC devices for detection of *E. coli* have been implemented including colorimetric-based lateral flow immunoassay (LFIA)[9–11] and other non-paper-based microfluidic devices based on electrochemical detection,[12] colorimetry,[13,14] fluorimetry[15] and magneto-fluorimetry.[16] LFIA are limited by their poor sensitivity that usually requires signal amplification, while the other microfluidic systems are relatively expensive and require trained personnel.[17,18] Therefore, there is a lack of a suitable PoC device to detect of *E. coli* for in field assays.

Our research group have been involved in developing photoluminescence paper-based platforms for detecting *E. coli*.[19,20] The reported strategies are related to nanoswitch "Off-On" methodology using photoluminescent quantum dots conjugated with antibodies. In these platforms, despite of being sensitive and specific, there are some drawbacks such as multistep procedures, exclusive readers platforms and particularly the easy to use for end-user that reduce the applicability of these biosensors for in-field measurements.

Previous studies have reported the quenching of gold nanoclusters (AuNCs) fluorescence in the presence of gold nanoparticles (AuNPs).[21] This phenomenon occurs due to the complementary overlapping between the surface plasmon resonance absorption wavelength of AuNPs and the fluorescence emission wavelength of AuNCs. Some biosensors have been developed by exploiting this phenomenon such as the detection of cholesterol[22] and uric acid.[23] In these cases, the detection is carried out through the production of H_2O_2 in an enzymatic reaction, AuNPs seeds start growing, in-creasing the absorbance of AuNPs with the consequently decrease in the fluorescence emission of AuNCs. Although this strategy has been exploited for biosensing applications, so far, to the best of our knowledge none of these nanomaterials have being used together as an immunosensor. Specifically, if we are starting from the OFF state, fluorescence could be recovered if the distance between the donor/acceptor pair becomes big enough

Certainly *E. coli* bacteria are big enough to promote this effect. For this purpose, we developed a simple, fast and cost-effective "lab on a tube" platform for *E. coli* detection. The proposed approach relies on Förster Resonance Energy Transfer (FRET) mechanism based on gold nanoclusters (AuNCs) as energy donor and antibody-functionalized AuNPs as energy acceptor. This enables an ON/OFF fluorescent signal depending on the presence or absence of *E. coli* in the sample. The assay is carried out inside a microtube that contains the reagents embedded in glass fiber membrane. In this regard, the biosensor can be easily transported and stored up to use. The assay starts by just introducing the sample into the micro-tube. After 20 minutes of incubation, the result can be evaluated by naked eye, in which the presence or absence of fluorescence indicates a yes/no response to the bacteria. Conveniently, it can be evaluated quantitatively by using a 3D printed device with an UV-LED, a smartphone camera and an image-analysis app.

5.2. Materials and methods

5.2.1. Materials and Instruments.

All commercial reagents are analytical grade and handled according to the material safety data sheets suggested by the suppliers. Hydrogen tetrachloroaurate (III) dehydrate (HAuCl4 3H2O, 99.9%), Trisodium Citrate, Sodium hydroxide, Phosphate buffered saline tablet (P4417), bovine serum albumin (BSA), were purchased from Sigma-Aldrich (Madrid, Spain). Anti-*E. coli* antibody (Ab, ab68451) was obtained from Abcam (Cambridge, UK). *Escherichia coli* O157:H7 (CECT 4783, *E. coli*) and *Salmonella Typhimurium* (CECT 722T, *S. typhimurium*) strains were obtained from Sigma-Aldrich (Madrid, Spain). Analytical grade nitric acid and hydrochloric acid were purchased from Fisher Scientific. Glass fiber membrane (GFCP00080000) was purchased from Millipore. All glassware was washed with *aqua regia*, and rinsed three times with Milli-Q water. Transmission electron microscopy (TEM) images were performed with a FEI Tecnai G2 20 TWIN electron microscope. Fluorescence emission and Absorbance spectra were collected on a Microplate reader (Molecular device). TS-100 Thermo-Shaker (Biosan, Riga, Latvia) was used as the stirrer for functionalization of AuNPs with anti-bodies.

5.2.2. Synthesis of BSA-AuNCs.

BSA-AuNCs were synthesized ac-cording to a previous protocol.[24] Briefly, aqueous solutions of HAuCl4 (10 mM, 5 mL) and BSA (50 mg/mL, 5 mL) were mixed and subjected to vigorous stirring at 37°C. After 2 min, NaOH solution (1.0 M, 0.5 mL) was added into the reaction mixture. The reaction container was sealed and allowed to proceed in the dark for 12 h. The solution became deep brown and showed strong red emission under a 365-nm UV lamp, pointing out the formation of the AuNCs. The prepared AuNCs were purified through dialysis membrane (MWCO: 1 kDa) against Milli-Q water for one day to remove unreacted HAuCl4 and sodium hydroxide. Purified AuNCs were kept at 4°C for further use. The concentration of BSA-AuNCs was estimated at around 20 mg/mL.

5.2.3. Synthesis and conjugation of AuNPs.

The synthesis of AuNPs was performed following the protocol reported by Bastús and co-workers.[25] In short, the initial AuNPs seeds were prepared by boiling 150 mL of sodium citrate (2.2 mM) in a sealed condenser, followed by the injection of 1 mL of $HAuCl_4$ (25 mM). After 10 minutes, the colour of the solution turned from light yellow to pink and it was cooled up to 90 °C. Next, 1 mL of sodium citrate (60mM) was added and after 2 min, 1 mL of HAuCl4 (25mM) was sequentially added. The solution was kept under stirring at 90 °C for 30 min and the colour of solution finally became wine-red. The final concentration of the AuNPs solution was 3.1×10^{11} NPs/mL.

The AuNPs were bioconjugated with antibodies against *E. coli* following the procedure previously reported by our group.[26] First the pH of the AuNPs was adjusted to 8.9 using Borate buffer (10 mM). Next, 100 μL of anti-*E. coli* (200 μg/mL) were incubated with 1.5 mL AuNPs for 24 h at 350 rpm and 4 °C. Then 100 μL BSA solution in Milli-Q water (final concentration 1%(w/w)) was added to the conjugated AuNPs followed by an incubation for 1 h under the previous conditions. The excess of antibodies and BSA were removed by centrifuging the solution at 14 000 rpm and 4 °C for 30 min, followed by re-suspension with 200 μL of Milli-Q water. Finally, the conjugated AuNPs where stored in 4°C for further use.

5.2.4. Platform fabrication.

Platform fabrication. The glass fiber membranes were cut into a 15 cm × 8 mm strips. 800 μL of the conjugated AuNPs and AuNCs where drop-casted on separate glass fiber strips and dried in a vacuum chamber for 2.5 hours. Finally, they were cut in circles (diameter ≈ 0.6 cm) using a hole puncher and introduced in the microtubes.

5.2.5. Bacteria preparation.

Stock solution (10^{10} *E. coli*/mL) of bacteria was prepared by dissolving 10 mg *E. coli* in 1 mL filtered Milli Q water followed by shaking with vortex. In order to determine the concentration of the prepared stock solution, the optical density at 600 nm (OD600) was measured using a spectrophotometer and corroborated with Agilent geometry software (https://www.chem.agilent.com/store/biocalculators/calcODBacterial.jsp).   Standard

serial solutions of *E. coli* (0 - 10^8 CFU/mL) were prepared by diluting the suspension stock solution (10^{10} CFU/mL $\approx 10^{10}$ *E. coli*/mL) in PBS.

5.2.6. Assay performance.

Serial dilutions of *E. coli* (0 - 10^8 CFU/mL) where prepared in PBS, 200 μL where drop-casted in the microtube and incubated for 20 min in room temperature. The assay was evaluated with a spectrophotometer by transferring the solution into a microplate. The fluorescence intensity was measured at 665 nm (Ext. 365 nm) for each dilution *of E. coli* and normalized with the black (F-F0), where F and F0 corresponded to sample with and without *E. coli*, respectively. For a point-of-care application, the assay was evaluated by taking a picture using a mobile phone camera and analyzing it with Image J software (National Institutes of Health, Maryland, USA) following the protocol already reported by our group.[27] All the experiments were replicated three times.

### 5.3. Results and discussion

5.3.1. Assay principle.

The assay was performed in a polypropylene microtube, which was used as a reservoir and detection platform. Firstly, the fluorescent AuNCs were synthesized, purified and drop-casted on a fiberglass membrane. The glass fiber was then dried using a vacuum desiccator and cut into circular pieces (Ø 0.6 cm) using a hole puncher. The pieces were introduced into the microtube and stored until running the assay. The same procedure was done for the AuNPs, which were previously conjugated with antibodies against *E. coli* O157:H7 following the procedure reported in the experimental section (Figure 5.1. A). In this way, the micro-tube stocked both conjugate pads, one containing the sensing PL probe (AuNCs) and the other containing the quencher label (AuNPs). The fiber glass was used as a porous material with high absorption and release capacity of solutions, appropriate long-term storage of samples, high stability and good flexibility.[28,29] In order to evaluate the presence of *E. coli* in a real environment, the assay starts by introducing the sample solution into the microtube followed by a 20 minutes incubation step (Figure 5.1B). The sample solution enables the rehydration of the conjugate pad and the eventual release of the stored nanomaterials to the solution. The biosensing mechanism is based on Förster Resonance Energy Transfer (FRET), being the AuNPs

and AuNCs the energy acceptors and donors, respectively. In this regard, the AuNPs were able to quench the fluorescence emission of the AuNCs when they were close together. This is known as the "turn-off" mode, which is linked to the absence of *E. coli* in the sample. Conversely, in the presence of *E. coli*, the antibody-functionalized AuNPs is attached to the surface of the bacteria avoiding the approach of the AuNCs. In this way, due to the fact that FRET mechanism is possible up to 30 nm and E. coli where 1µm sized,[30] the fluorescence signal was re-stored, switching to a "turn-on" mode (Figure 5.1C).
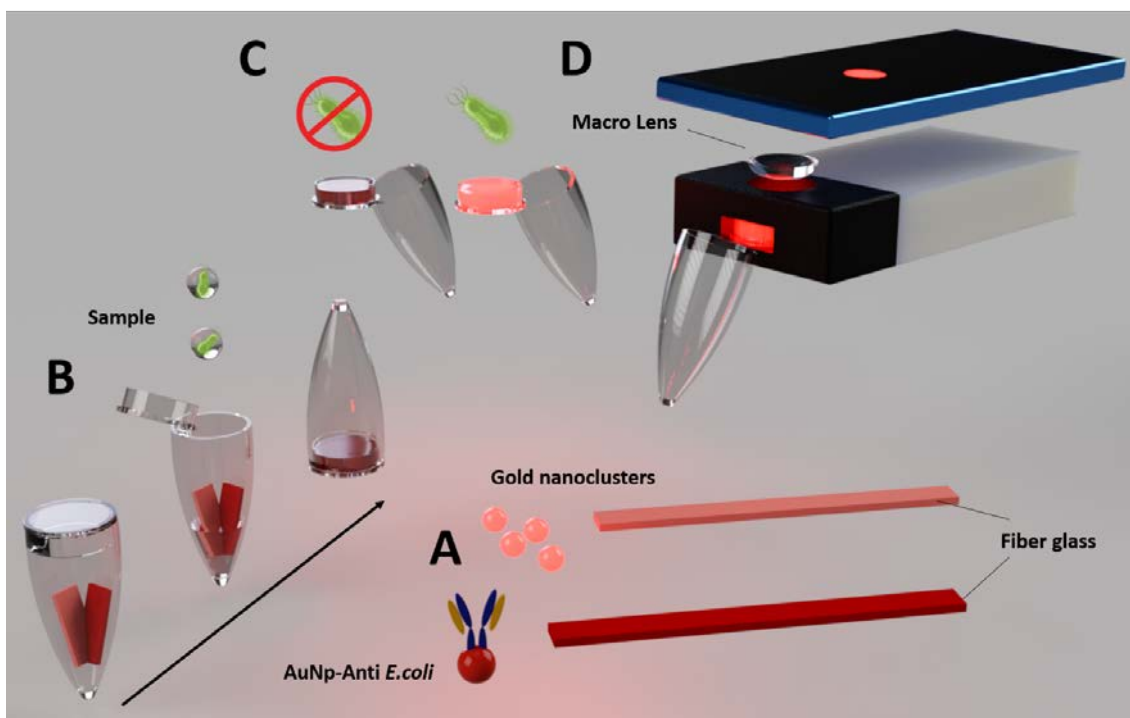
Figure 5.1. Schematic representation of the biosensing platform. **(A)** Two glass fibers strips embedded with AuNCs and AuNPs conjugated with anti-*E. coli* antibody respectively. **(B)** Operation principle; Sample is added directly to the micro-tube containing the two strips. **(C)** Naked eye evaluation of the ON/OFF switch mechanism. **(D)** Smartphone based device for quantitative evaluation of the *E. coli* concentration.

It should be noticed the specificity of the assay. In this regard, AuNCs were mixed with AuNPs with and without bacteria. It can be observed in Figure 5.2. that there is no recovery in the fluorescence of AuNCs when AuNPs are not conjugated with antibodies.
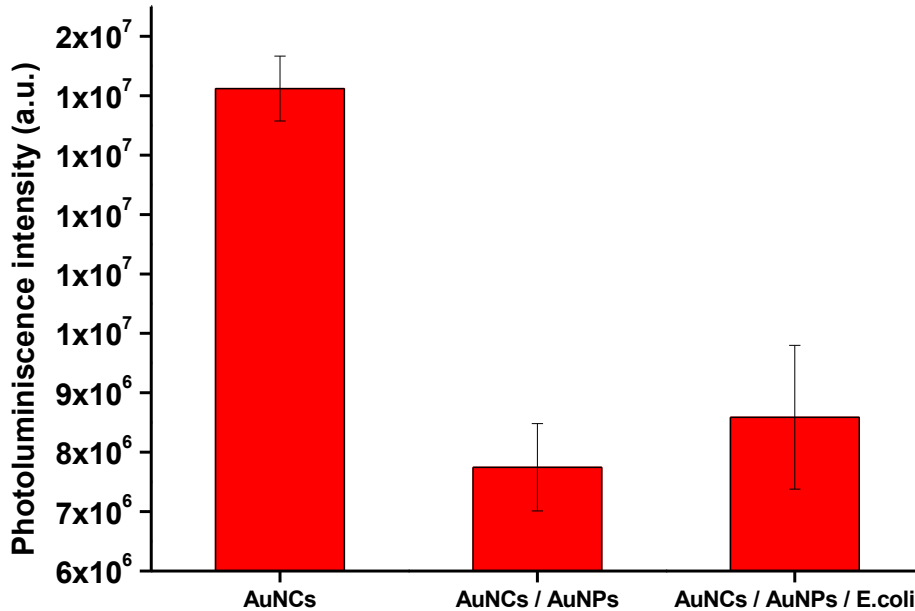

Figure 5.2. AuNCs quenching with AuNPs with and without bacteria in absence of specific receptors

Finally, a quantitative outcome was obtained using a smartphone camera. Nowadays, almost any smartphone has a good quality CMOS sensor and the possibility to fix the picture parameters such as shutter speed, ISO and focus, obtaining reproducible and accurate images. In this regard, a 3D printed device was developed to introduce the micro-tube using the cap as the sample holder. The device contains a 365 nm UV-LED to excite the AuNCs and a micro lens to adjust the focal length of the camera to the minimum possible (Figure 5.1D). The pictures were analyzed using Image J app (smartphone version) to transform the brightness levels into a numerical value, which allows quantification. Since most of the people across the world have a smartphone as common equipment in our day-to-day life, this proof of concept makes a highly promising device for point-of-care assay and field applications without the need to a conventional bulky analyzer such as fluorometer.

5.3.2. Characterization of AuNCs and conjugated-AuNPs.

The synthesized AuNCs were characterized by transmission electron microscopy (TEM). As observed in Figure 5.3A, they have a uniform morphology and a narrow size distribution with an average diameter of about 1.0 nm. Furthermore, a fluorescence emission peak at 665 nm when excited at 365 nm and a strong red emission under UV light (Figure 5.3B). The synthesized AuNPs were also characterized with TEM, as shown in Figure 5.3C and Figure 5.3D.
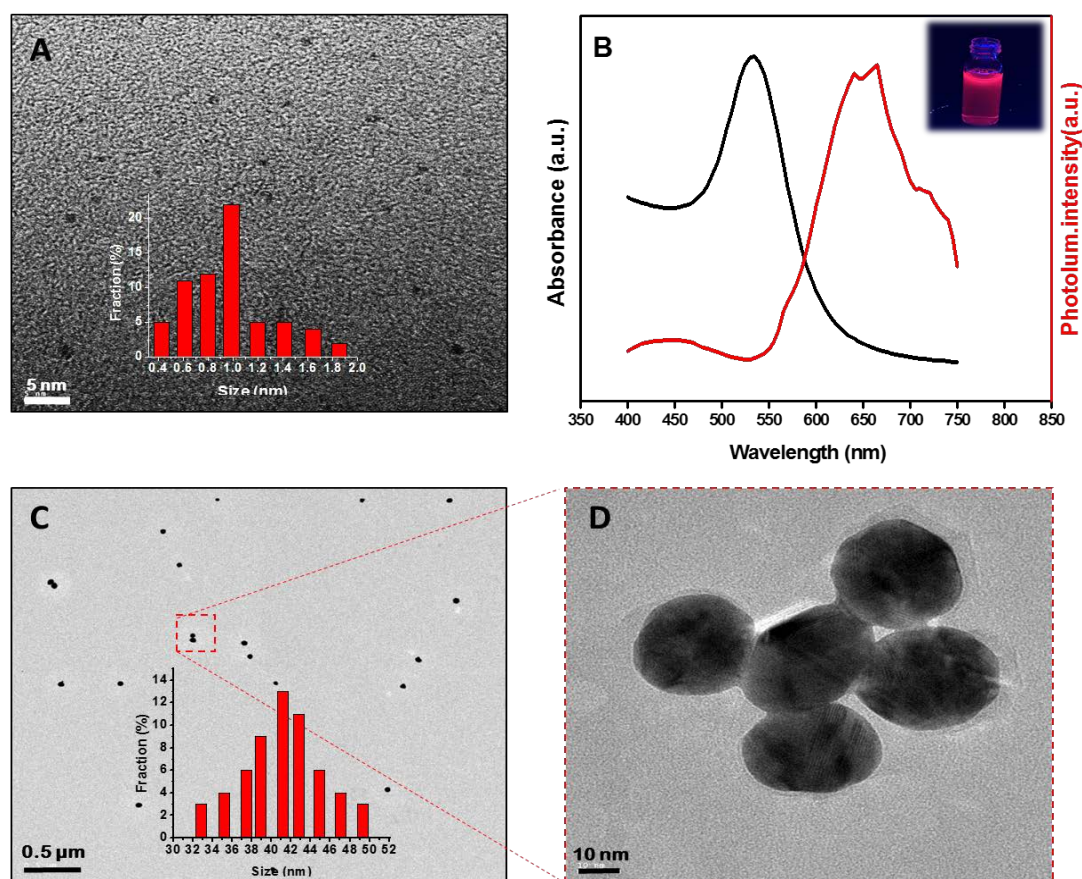
Figure 5.3. (A) TEM image of BSA-AuNCs. Inset: the size distribution histogram of the as prepared AuNCs. **(B)** Fluorescence spectra of BSA-AuNCs (red line) and absorption spectrum of conjugated AuNPs with Anti-*E. coli* (black line). Inset: Digital photo of AuNCs under UV light. **(C)** TEM image of Citrate stabilized- AuNPs. Inset: graph corresponds to size distribution diagram. **(D)** High magnified of as-prepared AuNPs.

AuNPs has a spherical and uniform size of around 40 nm. Besides, its conjugation to antibodies against *E. coli* was corroborated by the presence of red shift from 525 to 535 nm in the UV-vis spectrum, indicating a modification on the AuNPs surface (Figure 5.4).[31] Finally, in order to achieve FRET, the absorbance spectrum of energy acceptor must be overlapped with the emission spectrum of the donor probe. This phenomenon can be observed in Figure 5.3B, where the emission spectrum of the AuNCs was clearly overlapped with the absorbance spectrum of the conjugated-AuNPs.
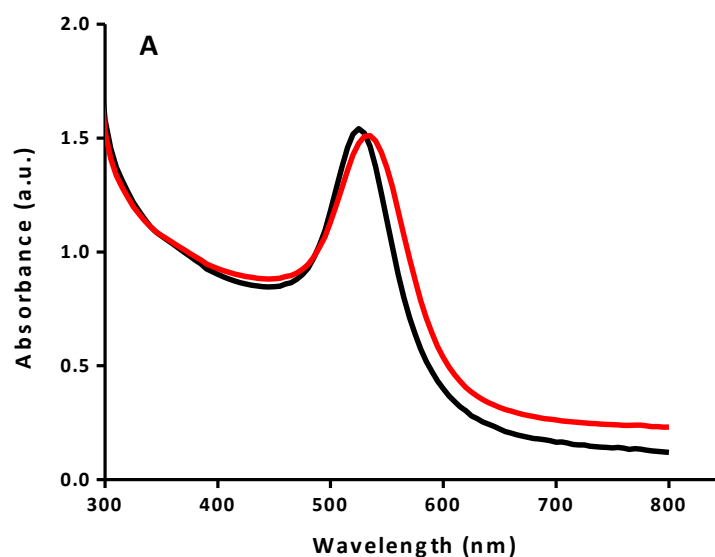

Figure 5.4. UV-vis absorption spectra of bare AuNPs (black line) and AuNPs conjugated with Anti- *E. coli* (Ab-AuNPs) (red line) at the same concentration: [AuNPs &Ab-AuNPs]=1.16×10^{12} NPs.

5.3.3. Assay optimization.

The highest concentration with the higher fluorescence emission of AuNCs was tested to evaluate the size dependence on the quenching efficiency of AuNPs. It is known that, the bigger the size of nanoparticles, the highest the red shift in the wavelength, causing more overlap with the emission of AuNCs.[21] Among the tested sizes, 40 nm was selected as the most suitable for the assay (Figure 5.5). Besides bigger nanoparticles (>40nm) produce more quenching, the antibodies conjugation protocols are fully optimized for 40 nm. Moreover, if bigger nanoparticles are used the required amount of antibodies to cover the surface will be higher, causing a more expensive device. To

evaluate how the AuNPs concentration affects the quenching of AuNCs, the stock solution (3.1×10^{11} NPs/mL) of AuNPs was concentrated (by centrifugation) and diluted. It can be observed in Figure 5.6A that indeed higher concentrations of AuNPs produces more quenching on the light emission of AuNCs. Nevertheless, we have selected 1.16×10^{12} NP/mL as a compromise between efficiency and affordability since there is no noteworthy quenching at higher concentrations.
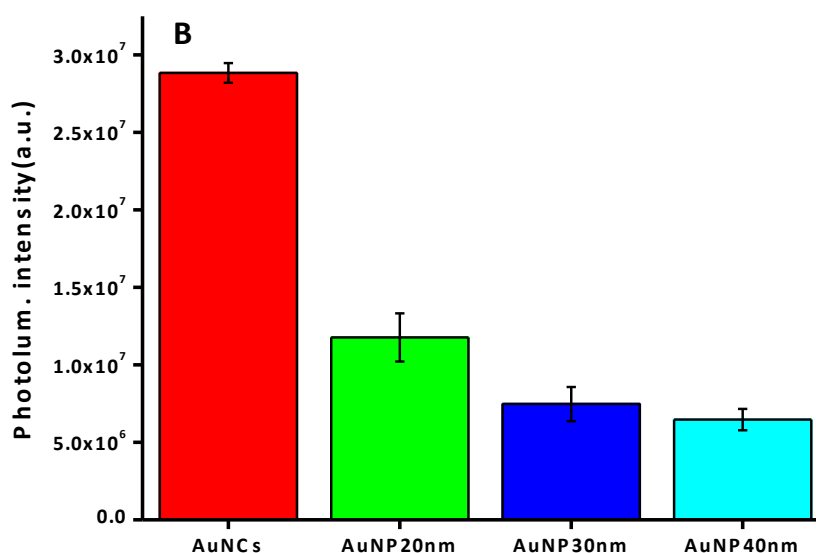

Figure 5.5. Influence of AuNPs different diameters on quenching efficiency of the AuNCs

Furthermore, the antibody concentration on the AuNPs was also optimized as it dramatically affects the sensitivity and the cost-effectiveness of the platform (using less antibody can considerably reduce the development cost of the biosensor). This was done by performing the well-established gold aggregation test (GAT),[26] which determines the maximum concentration of antibody required to cover the AuNPs surface. Based on the results shown in Figure 5.6B, we concluded that 175 µg/mL of anti-*E. coli* were enough to cover the surface of the AuNPs, however we round it up to 200 µg/mL in the subsequent assays.

The required concentration of AuNCs to achieve an effective FRET and recovery was another parameter to be optimized. In this context, (AuNPs at fixed concentration of

1.16×10^{12} NP/mL) the fluorescence recovery in presence of *E. coli* was evaluated using different AuNCs concentrations (from 0.5 to 8.0 mg/mL). As expected, an excess of AuNCs brought to signal saturation while a low concentration of AuNCs let to negligible fluorescence intensity (Figure 5.6C).
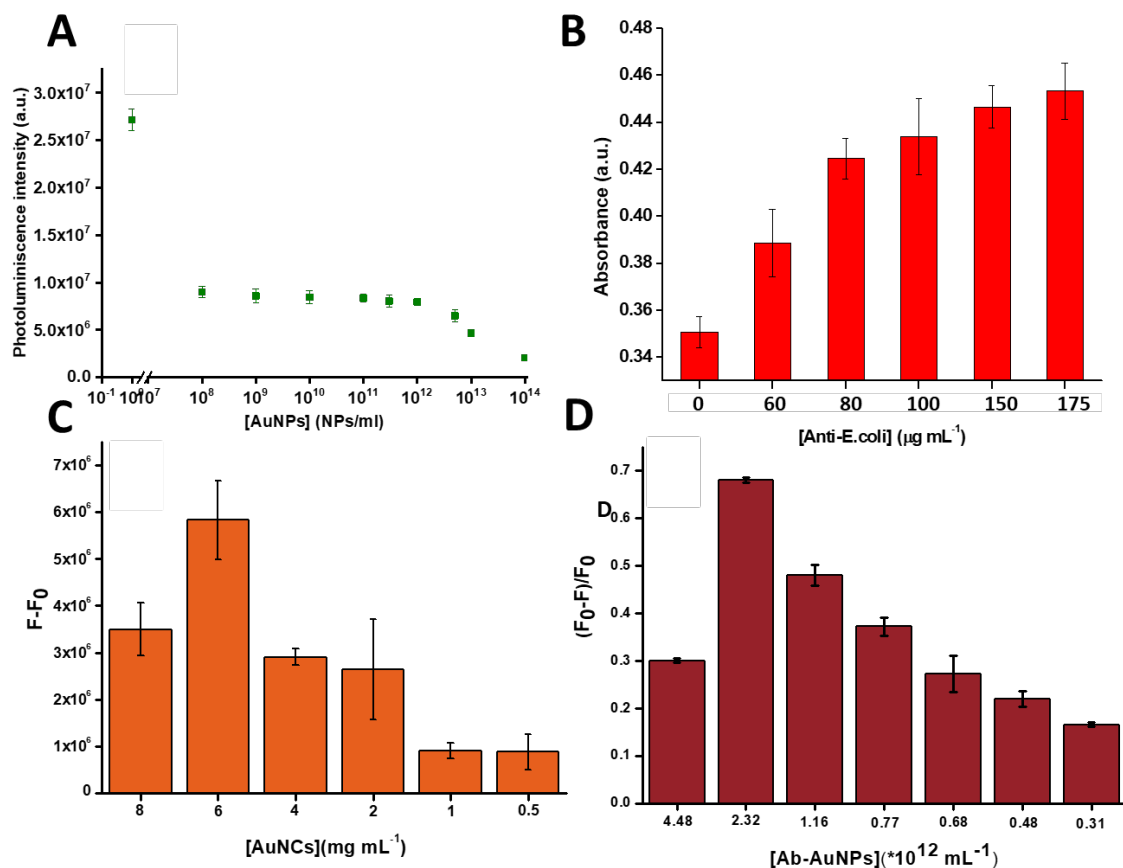
Figure 5.6. Optimization of experimental conditions. **(A)** Pre-optimization of the quenching efficiency due to AuNPs concentration. **(B)** The effect of the concentration of the immobilized antibody on the surface of AuNPs (GAT) at NaCl 1 % and 0.58×10^{12}/mL AuNPs in various concentration of antibody. **(C)** Effect of the concentration of AuNCs as a fluorophore agent on fluorescence recovery efficiency (F-F0) where F and F0 correspond to the fluorescence intensities of AuNCs/AuNPs system in the presence and absence of *E. coli*, respectively at 10^5 CFU/mL *E. coli*. **(D)** The effect of the concentration of anti-*E. coli*- labelled AuNPs on quenching efficiency (F0-F)/F0 where F and F0 correspond to the fluorescence intensities of AuNCs in the presence and absence of Ab-AuNPs, respectively. The concentration of AuNCs was 6.0 mg/mL.

Therefore, the fluorescence enhancement efficiency (F-F0) was employed as a criterion to evaluate the best signal where F and F0 correspond to the intensities of fluorescence of AuNCs/AuNPs system in the presence and absence of *E. coli*, respectively. Hereby, 6.0 mg/mL was determined as the optimal concentration of AuNCs.

Although AuNPs concentration was previously optimized (pre optimization strategy) those nanoparticles were not conjugated with anti-*E. coli* antibodies. It is important to double check the concentration of conjugated AuNPs required to achieve an effective FRET taking in consideration the previously optimized AuNCs concentration. In this regard, conjugated AuNPs ranging from 0.31 to 4.46 ($x10^{12}$ NPs/mL) were evaluated. As observed in Figure 5.6D, 2.32 ($x10^{12}$ AuNPs/mL) allowed a 68% quenching efficiency, while higher and lower concentrations ended up with signal saturation and low quenching, respectively. It is also essential to optimize this parameter for fluorescence restoration efficiency (Figure 5.7). Therefore, this was the concentration of conjugated AuNPs selected for the next experiments.
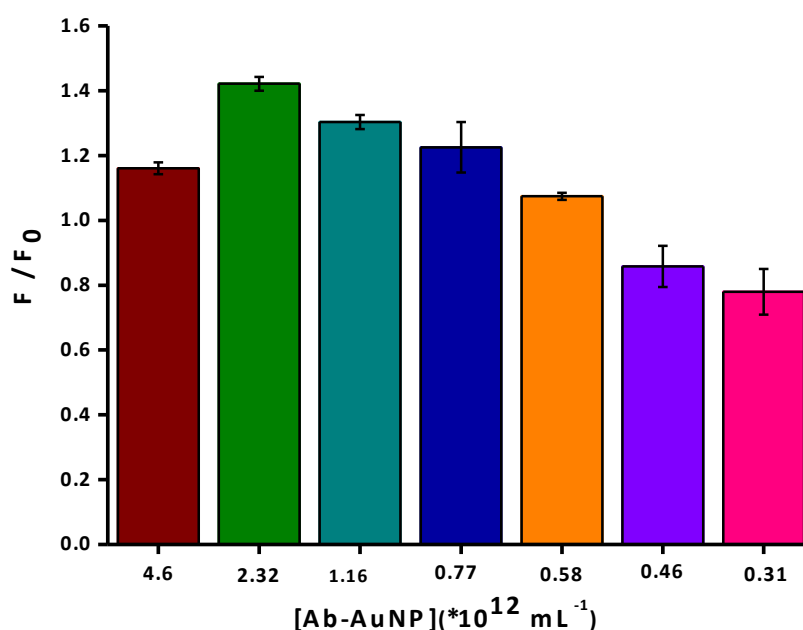
Figure 5.7. Effect of concentration of Ab-AuNPs on the photoluminescence restoration. F/F0, where F and F0 are the fluorescence intensities of AuNCs/Ab-AuNPs in the presence and absence of *E. coli*. Concentration of AuNCs and *E. coli* were 6 mg/mL and 10^5 CFU mL^{-1} respectively.

Finally, in order to better understand the response rate of our platform to *E. coli* detection, a comprehensive kinetic study was per-formed (Figure 5.8) showing that the fluorescence signal increased exponentially and reached equilibrium after 20 minutes. This reveals the assay time required before performing the final evaluation.
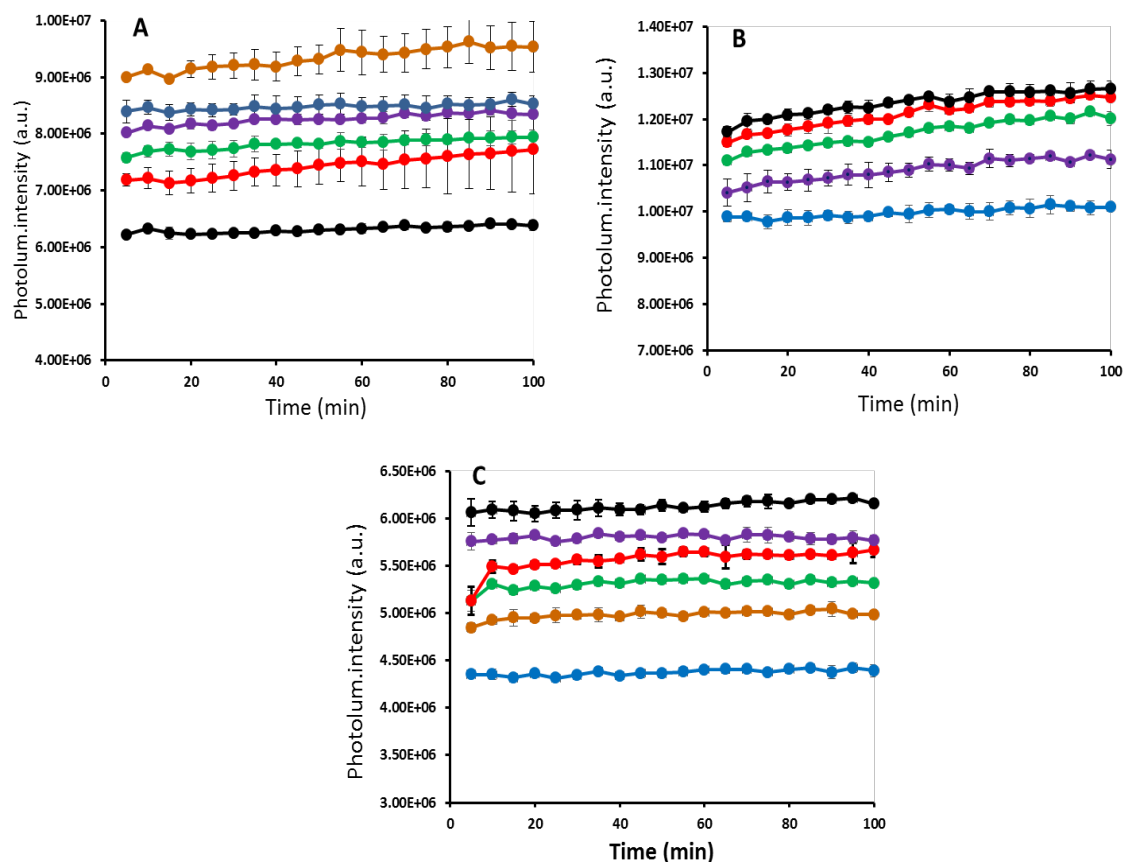

Figure 5.8. Kinetic behavior studies of AuNCs/Ab-AuNPs in the presence of various concentration of *E. coli* (A, B) from 0 to 10^5 CFU mL^{-1} and (C) from 0 to 10^4 CFU mL^{-1} with different three concentrations of Ab-AuNPs. (A) 1.16×10^{12} NPs mL^{-1}. (B) 0.77×10^{12} NPs mL^{-1}. (C) 2.32×10^{12} NPs mL^{-1}. [AuNCs]: 6 mg mL^{-1}.

5.3.4. Smartphone-based detection of E. coli.

The developed platform was firstly evaluated under optimal conditions by spiking known concentrations of *E. coli* (0 to 10^7 CFU/mL) in PBS buffer (10 mM pH 7.4) and using a spectrophotometer. As observed in Figure 5.9A, the fluorescence signal gradually increases with higher concentration of *E. coli*, with a good correlation (exponential behavior log [*E. coli*]) in the range of 0 to 10^5 CFU/mL (Figure 5.9B),

being F and F0 the fluorescence intensities at 665 nm in the presence and absence of *E. coli*, respectively. The limit of detection (LOD) was calculated as low as 1.37 CFU/mL based on 3 times "s/m" ratio, where "s" is the standard deviation of the blank fluorescence signal (three replicates) and "m" is the slope of the related calibration curve. Furthermore, the assay was evaluated with a smartphone camera, in order to get as close as possible to point-of-care conditions. In this context, a Samsung galaxy S7 smartphone was used to take a picture of the microtubes after running the assay (20 minutes incubation). The micro-tube cap was irradiated under a UV LED (Ex. 365 nm) and the smartphone was attached to a holder, the pictures were always taken in the same conditions; at ISO 100 and shooter speed 1/60 s. As illustrated in Figure 5.9C, the sample containing 0 CFU/mL of *E. coli*, defined as blank sample, is characterized by low brightness levels due to the "turn-off" FRET effect. However, with the increase of *E. coli* concentration there was a gradual in-crease in fluorescence ("turn-on" mode). In order to obtain a numerical value, the pictures were analyzed with Image J software, in which the fluorescence intensity is transformed into a value from 0 to 255 (where 0 is dark and 255 is maximum brightness). The fluorescence intensity values were normalized with the signal corresponding to absence of *E. coli* (F0). The calibration curve is observed in Figure 5.9D, which shows a power fluorescence increase. It is worth to notice a change in the mathematical function in light of the results obtained with the fluorometer and the smartphone. Graphing the values according to the function obtained with the fluorometer (log [*E. coli*]), it can be seen an exponential behavior which means that the results obtained with the smartphone follows a power function from 0 to 10^7 CFU/mL with a LOD of 4.0 CFU/mL. (Figure 5.9. D inset)
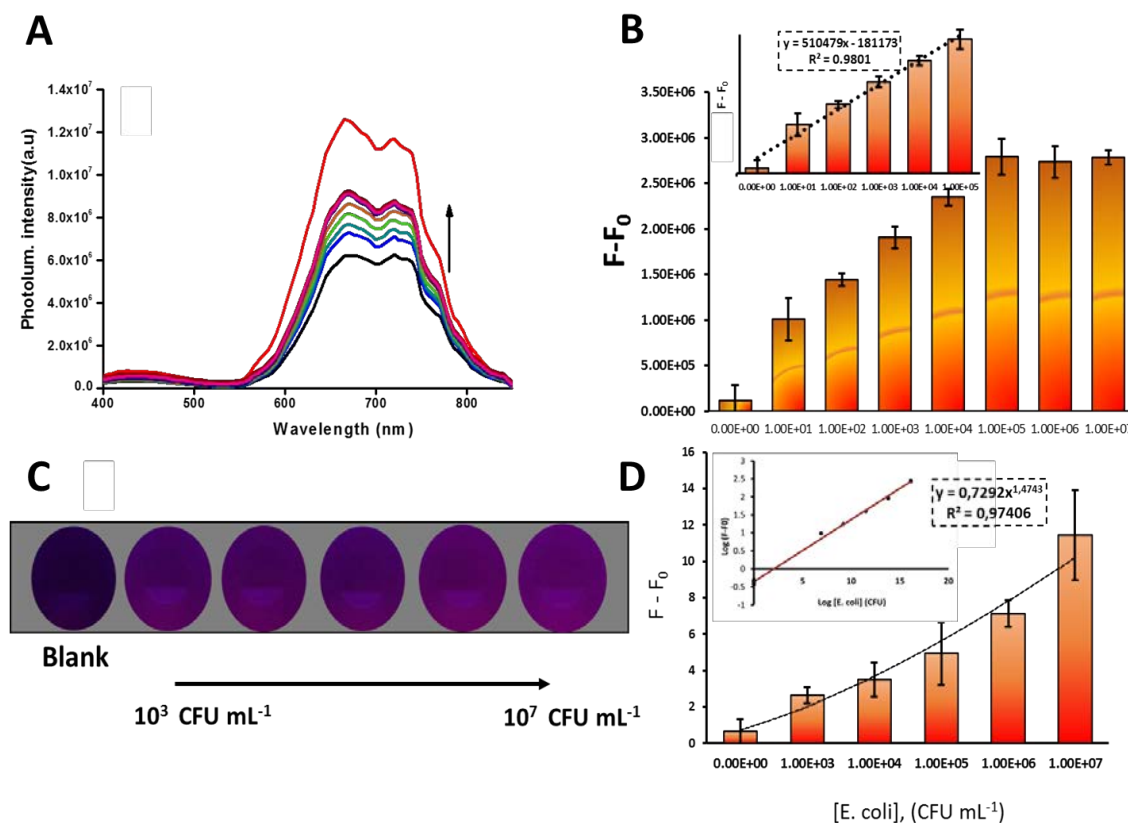
Figure 5.9. Quantification of *E. coli* O157:H7 by developed biosensor. (A) Fluorescence spectrum of AuNCs/Ab-AuNPs upon addition of different concentrations of *E. coli* from 0 to 10^7 CFU/ mL. (B) Calibration curve of the assay by using fluorimeter. (F and F0 correspond to the fluorescence intensities of AuNCs/AuNPs system in the presence and absence of *E. coli*, respectively). (C) Typical images of AuNCs/Ab-AuNPs system in the presence of various concentration of *E. coli* in the range of 0 - 10^7 CFU/mL (0, 10^3, 10^4, 10^5, 10^6 CFU/mL from left to right) captured by smartphone camera under 365 nm UV light irradiation; (D) Calibration curve resulted by processing images in the mobile phone. Error bars represent the standard deviation (n=3) inset: linear behavior of a power function.

The developed biosensor performance of *E. coli* detection was compared to some of the reported point of care sensors and summarized in Table 5.1.

Table 5.1. Comparison of the experimental and analytical performance of the present method with other point of care platforms for *E.coli* detection.

Platform	Detection method	LR (CFU mL⁻¹)	LOD (CFU mL⁻¹)	Response Time (min)	Ref.
Microfluidic chip	Electrochemical	$5\times10^1-1\times10^6$	39.0	-	[12]
Nanopaper	Photoluminescence	$10-10^5$	55.0	30	[19]
Microfluidic chip	Fluorescence	10^3-10^5	240	25	[15]
LFIA	Colorimetric	$2.08 \times 10^5-2.08 \times 10^8$	6.2×10^4	15	[9]
LFIA	Fluorescence	$10^2 - 10^5$	10.0	-	[20]
SPC electrode	Electrochemical	$10-10^4$	100	10	[7]
Lab in a tube	Fluorescence	$10-10^5$	1.37	20	Present work
Lab in a tube	Fluorescence/ Smartphone	$10^3 - 10^7$	4.0	20	Present work

LFIA: Lateral flow immunoassay, SPC electrode: screen printed carbon electrode

5.3.5. Real samples evaluation.

To further test the practicability of the biosensor, the assay was conducted by spiking known concentrations of *E. coli* (10^2 and 10^5 CFU) to tap water and river water samples collected from river Ter (Vic, Spain). The samples were evaluated following the procedure previously reported and the recoveries where calculated by comparing the results obtained in real samples (i) with the ones obtained in PBS (ii), using the following equation:

$$\text{Recovery (\%)} = 100 \times \frac{(\text{F} - \text{F0})^i}{(\text{F} - \text{F0})^{ii}}$$

The results are summarized in Table 5.2. The obtained recoveries prove that there is no drastic interference when evaluating samples with a complex matrix, thus the developed platform can be applied for the detection of *E. coli* in real samples at the point-of-care.

**Table 5.2.** Detection of *E. coli* bacteria spiked in water samples (n=3)

Sample	Spiked *E.coli* (CFU/mL)	#F-F0 in standard buffer	*F-F0 in real sample	Recovery (%)[a]
River water	10^2	1440843	1503611	103.70
	10^5	2791463	2648975	105.37
Tap water	10^2	1440843	1400975	97.23
	10^5	2783852	2740975	98.45

[a] Recovery (%) $=100 \times (\text{F-F}_0^* / \text{F-F}_0^\#)$

5.3.6. Determination of the assays specificity.

The specificity of the biosensor toward *E. coli* was assessed by evaluation samples containing *E. coli* and *Salmonella typhimurium*, which is a similar family pathogen. Dilutions of *E. coli*, Salmonella and a mixture of both bacteria where spiked in PBS. The assay was carried out following the previous procedure. As shown in Figure 5.10, the normalized fluorescence (FL) intensity increased with higher concentrations of *E. coli* (0 to 10^5 CFU/mL). Conversely, the normalized FL intensity obtained for a sample with 10^5 CFU/mL of Salmonella was similar to the one obtained for 0 CFU of *E. coli*. This result proves that the developed biosensor was only specific for *E. coli* due to the AuNPs functionalization with highly specific antibodies against *E. coli* O157:H7. This was further corroborated by evaluating solutions containing a mixture of 10^5 CFU/mL Salmonella + 10^2 CFU/mL *E. coli* and 10^5 CFU/mL *E. coli* + 10^2 CFU/mL *Salmonella*. In the first case, the obtained signal was similar to the blank (0 CFU/mL *E. coli*) and in the second case the signal was similar to the one obtained for 10^5 CFU/mL *E. coli*. Therefore, the results confirmed that the platform has a high specificity response and when applied in real samples, the achieved signal could be linked only to *E. coli* detection.
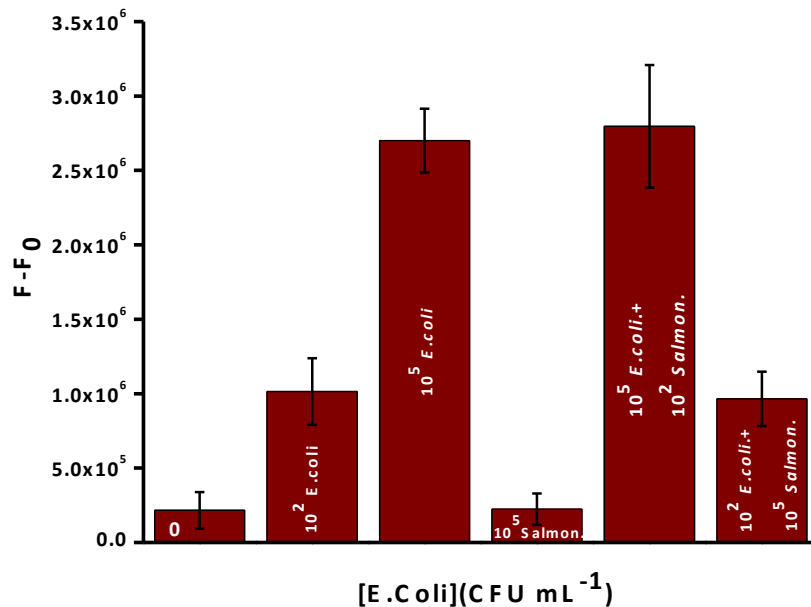
Figure 5.10. Specificity of the developed fluorescence biosensor toward *E. coli* in the presence of Salmonella as interfering bacteria. The error bars are the standard deviation of the three measurements.

5.4. Conclusion

The proposed all-in-one device combines outstanding advantage of both the glass fiber membrane as a cost-effective substrate with high loading capacity and the microtube platform as simple and portable set-up. Moreover, the detection method applied in the developed biosensor is fast (20 minutes) and doesn't require washing steps. It has proved to be highly sensitive and specific for detection of *E. coli*, although its application can be extended to other big analytes. Finally, the possibility to do smartphone-based detection empowers the developed biosensor as unique PoC tests with real applicability in resource limited settings.

5.5. References

1.   Painter, J. A. *et al.* Attribution of foodborne illnesses, hospitalizations, and deaths to food commodities by using outbreak data, United States, 1998-2008. *Emerg. Infect. Dis.* **19,** 407–415 (2013).

2.   Scallan, E., Griffin, P. M., Angulo, F. J., Tauxe, R. V. & Hoekstra, R. M. Foodborne illness acquired in the United states-Unspecified agents. *Emerg. Infect. Dis.* **17,** 16–22 (2011).

3.   Opota, O., Croxatto, A., Prod'hom, G. & Greub, G. Blood culture-based diagnosis of bacteraemia: State of the art. *Clin. Microbiol. Infect.* **21,** 313–322 (2015).

4.   Souza, R. B., Trevisol, D. J. & Schuelter-Trevisol, F. Bacterial sensitivity to fosfomycin in pregnant women with urinary infection. *Brazilian J. Infect. Dis.* **19,** 319–323 (2015).

5.   Zourob, Mohammed, Elwary, Sauna, Turner, A. P. F. *Principles of Bacterial Detection: Biosensors, Recognition Receptors and Microsystems.* (Springer Science & Business Media, 2008).

6.   Zhao, Z. *et al.* Bacteria-Activated Theranostic Nanoprobes against Methicillin-Resistant Staphylococcus aureus Infection. *ACS Nano* **11,** 4428–4438 (2017).

7.   Russo, L. *et al.* Low-Cost Strategy for the Development of a Rapid Electrochemical Assay for Bacteria Detection Based on AuAg Nanoshells. *ACS Omega* **3,** 18849–18856 (2018).

8.   Yetisen, A. K., Akram, M. S. & Lowe, C. R. Paper-based microfluidic point-of-care diagnostic devices. *Lab Chip* **13,** 2210–2251 (2013).

9.   Huang, H., Zhao, G. & Dou, W. Portable and quantitative point-of-care monitoring of Escherichia coli O157:H7 using a personal glucose meter based on immunochromatographic assay. *Biosens. Bioelectron.* **107,** 266–271 (2018).

10.   Luo, K. *et al.* Comparison of 4 label-based immunochromatographic assays for the detection of Escherichia coli O157:H7 in milk. *J. Dairy Sci.* **100,** 5176–5187 (2017).

11.   Wu, W. *et al.* A sensitive lateral flow biosensor for Escherichia coli O157: H7 detection based on aptamer mediated strand displacement amplification. *Anal. Chim. Acta* **861,** 62–68 (2015).

12. Li, Y. *et al.* An electrochemical strategy using multifunctional nanoconjugates for efficient simultaneous detection of escherichia coli O157: H7 and vibrio cholerae O1. *Theranostics* **7,** 935–944 (2017).

13. Chen, J., Alcaine, S. D., Jackson, A. A., Rotello, V. M. & Nugen, S. R. Development of Engineered Bacteriophages for Escherichia coli Detection and High-Throughput Antibiotic Resistance Determination. *ACS Sensors* **2,** 484–489 (2017).

14. Lagelly, E. T. *et al.* Integrated portable genetic analysis microsystem for pathogen/infectious disease detection. *Anal. Chem.* **76,** 3162–3170 (2004).

15. Sugino, H. *et al.* On-chip microfluidic sorting with fluorescence spectrum detection and multiway separation. *Lab Chip* **9,** 1254–1260 (2009).

16. Banerjee, T. *et al.* Multiparametric Magneto-fluorescent Nanosensors for the Ultrasensitive Detection of Escherichia coli O157:H7. *ACS Infect. Dis.* **2,** 667–673 (2016).

17. Zarei, M. Infectious pathogens meet point-of-care diagnostics. *Biosens. Bioelectron.* **106,** 193–203 (2018).

18. Nasseri, B. *et al.* Point-of-care microfluidic devices for pathogen detection. *Biosens. Bioelectron.* **117,** 112–128 (2018).

19. Cheeveewattanagul, N. *et al.* Straightforward Immunosensing Platform Based on Graphene Oxide-Decorated Nanopaper: A Highly Sensitive and Fast Biosensing Approach. *Adv. Funct. Mater.* **27,** 1–8 (2017).

20. Morales-Narváez, E., Naghdi, T., Zor, E. & Merkoçi, A. Photoluminescent Lateral-Flow Immunoassay Revealed by Graphene Oxide: Highly Sensitive Paper-Based Pathogen Detection. *Anal. Chem.* **87,** 8573–8577 (2015).

21. Qin, H., Ma, D. & Du, J. Distance dependent fluorescence quenching and enhancement of gold nanoclusters by gold nanoparticles. *Spectrochim. Acta - Part A Mol. Biomol. Spectrosc.* **189,** 161–166 (2018).

22. Chang, H. C. & Ho, J. A. A. Gold Nanocluster-Assisted Fluorescent Detection for Hydrogen Peroxide and Cholesterol Based on the Inner Filter Effect of Gold Nanoparticles. *Anal. Chem.* **87,** 10362–10367 (2015).

23. Liu, Y. *et al.* Gold nanoclusters as switch-off fluorescent probe for detection of uric acid based on the inner filter effect of hydrogen peroxide-mediated enlargement of gold nanoparticles. *Biosens. Bioelectron.* **91,** 734–740 (2017).

24. Xie, J., Zheng, Y. & Ying, J. Y. Protein-directed synthesis of highly fluorescent gold nanoclusters. *J. Am. Chem. Soc.* **131,** 888–889 (2009).

25. Bastús, N. G., Comenge, J. & Puntes, V. Kinetically controlled seeded growth synthesis of citrate-stabilized gold nanoparticles of up to 200 nm: Size focusing versus ostwald ripening. *Langmuir* **27,** 11098–11105 (2011).

26. Ambrosi, A. *et al.* Double-codified gold nanolabels for enhanced immunoanalysis. *Anal. Chem.* **79,** 5232–5240 (2007).

27. Álvarez-Diduk, R., Orozco, J. & Merkoçi, A. Paper strip-embedded graphene quantum dots: a screening device with a smartphone readout. *Sci. Rep.* **7,** 976 (2017).

28. Oyama, Y. *et al.* A glass fiber sheet-based electroosmotic lateral flow immunoassay for point-of-care testing. *Lab Chip* **12,** 5155–5159 (2012).

29. O'Farrell, B. *Lateral Flow Immunoassay Systems*. *The Immunoassay Handbook* (2013). doi:10.1016/b978-0-08-097037-0.00007-5

30. Morales-Narváez, E., Hassan, A. R. & Merkoçi, A. Graphene oxide as a pathogen-revealing agent: Sensing with a digital-like response. *Angew. Chemie - Int. Ed.* **52,** 13779–13783 (2013).

31. Chen, W. *et al.* Detection of the nanomolar level of total Cr[(III) and (VI)] by functionalized gold nanoparticles and a smartphone with the assistance of theoretical calculation models. *Nanoscale* **7,** 2042–2049 (2015).

5.6. Contributions

This work has been performed in collaboration with Dr. Niloufar Amin and Prof. Abbas Afkhami, from the Food and Drug Laboratory Research Center, Food and Drug Organization, MOH&ME (Tehran, Iran). Dr. Niloufar Amin worked on the development of the biosensor during her internship in the nanobioelectronics and biosensors group (Barcelona, Spain).

GENERAL CONCLUSIONS

Considering the exposed objectives in Chapter 2 and the obtained results in Chapters 3, 4 and 5 the following conclusion remarks are given:

- A paper-based electrophoretic bioassay (PEB) was developed.
  - The application of electrophoresis in a totally disposable paper strip was achieved using a portable smartphone-based power source.
  - The electrophoretic mobility of different QDs and AuNPs proved to be consistent with the principles of electrophoresis.
  - PEB was successfully designed for the detection of H-IgG in whole blood. The removal of the whole blood from the detection zone enabled a clean background and hence a clear visualization of TL and CL.
  - While LFAs were unable to directly handling undiluted blood samples, the signals obtained with PEB when detecting H-IgG in whole blood samples showed a correlation of 0.99 with the ones for the detection in buffer samples.
  - The future perspective is to improve the analytical sensitivity of PEB by reducing the flow rate, so that the capture bioreceptor and target analyte have more time for interaction. Reducing the voltage applied and modifying the strip architecture accordingly would decrease the flow rate. Moreover, a conjugated pad will be implemented in order to simplify the assay operation. The conjugate pad will contain the labelled antibodies in dry state, contributing to a higher stability of the reagents.

- The integration of a time-delay wax barrier in LFA enabled a simple and low-cost strategy for sensitivity and signal enhancement.
  - The results obtained supported the hypothesis that longer incubation times between the bioreceptors and analyte provide higher assay sensitivities.
  - 2.8-fold sensitivity enhancement and up to 96% signal enhancement was achieved for the detection of H-IgG.

- The assay exhibited a LoD and LoQ of 14.47 and 41.19 ng mL^{-1}, respectively, which is acceptable for this type of detection mode in LFA.

- As future perspectives, it would be worth to evaluate other working buffers able to keep the conjugate solution wet for longer time. Moreover, the assay should be validated with complex samples so as to check if the proposed strategy is compatible with this kind of samples. For instance, long retention times might favour the accumulation of protein corona in the AuNPs and nitrocellulose substrate.

- A highly sensitive, simple and low-cost platform was developed for *E.coli* detection.

  - The platform exhibited a LoD of 4 CFU mL^{-1} for *E.coli* detection, which is quite low compared to other reports.

  - Signal recoveries of 103.70 and 97.23 % were achieved in river and tap water, respectively, for the detection of *E.coli* at 10^2 CFU mL^{-1}

  - The developed assay proved to be specific for *E.coli* detection, but its application can be extended to other big analytes.

  - The future perspective is to evaluate other nanomaterials as energy donors and acceptors so as to further enhance the analytical sensitivity of the assay. Moreover it would be interesting to evaluate the capability of this platform for the detection of target analytes in more complex media such as serum or whole blood.

ANNEXES

As annexes are attached the following published review and experimental work:

Wong, XY.; Sena-Torralba, A.; Álvarez-Diduk, R.; *et al.* "Nanomaterials for Nanotheranostics: Tuning Their Properties According to Disease Needs." *ACS Nano*. 14 (3), 2585-2627 (2020).

Quesada-González, D.; Sena-Torralba, A.; Wicaksono, WP.; *et al.* "Iridium oxide (IV) nanoparticle-based lateral flow immunoassay." *Biosens. Bioelectron.* 132, 132–135 (2019).

Amin, N.; Sena-Torralba, A.; Álvarez-Diduk, R.; *et al.* "Lab in a Tube: Point-of-Care detection of *Escherichia coli*." *Anal. Chem.* 92 (6), 4209-4216 (2020).

And the posters presented at different congresses:

Quesada-González, D.; Sena-Torralba, A.; Wicaksono, W. P.; *et al.* "Iridium oxide nanoparticle-based lateral flow immunoassay" – Presented at: Transfrontier Meeting on Sensors and Biosensors, Barcelona (2018).

Sena-Torralba, A.; Toulmé, J.J.; Peyroutou, R.; *et al.* " Development of a nanodiagnostic platform for monitoring of cancer cell secreted proteins (NACANCELL)" – Presented at: Euronanomed review seminar for funded projects, Bratislava (2019). And also at: International congress on analytical Nanoscience and Nanotechnology – IX, Zaragoza (2019).